CONSTRUCTION OF CHAOTIC ATTRACTORS AND ITS APPLICATIONS

KITDAKORN KLOMKARN

A THESIS SUBMITTED IN PARTIAL FULFILLMENT

OF THE REQUIREMENT FOR THE DEGREE OF

DOCTOR OF ENGINEERING IN ELECTRICAL ENGINEERING

FACULTY OF ENGINEERING

KING MONGKUT'S INSTITUTE OF TECHNOLOGY LADKRABANG

2011

KMITL-2011-EN-D-018-031

หัวข้อวิทยานิพนธ์	การสร้างตัวดึงดูดอลวนและการประยุกต์
นักศึกษา	นายกฤดากร กล่อมการ
รหัสนักศึกษา	46060001
ปริญญา	วิศวกรรมศาสตรดุษฎีบัณฑิต
สาขาวิชา	วิศวกรรมไฟฟ้า
พ.ศ.	2554
อาจารย์ที่ปรึกษาวิทยานิพนธ์	รศ.ดร. ปิติเขต สู้รักษา

บทคัดย่อ

ในวิทยานิพนธ์ฉบับนี้ เสนอวิธีการการสร้างตัวดึงดูดอลวนแบบใหม่ 3 รูปแบบ โดยวิธีการแรกเป็นการสร้างตัวดึงดูดอลวนจากวงจรกำเนิดสัญญาณอลวนแบบผสมและแบบเอนกประสงค์ที่สามารถให้สัญญาณได้หลายรูปแบบในวงจรเดียว ในวิธีการที่สองแสดงการสร้างตัวดึงดูดอลวนจากระบบบนพื้นฐานของระบบ Lorenz ให้เป็นตัวดึงดูดอลวนแบบหลายปีกโดยใช้ฟังก์ชันไม่เป็นเชิงเส้นแบบเชิงท่อน และวิธีการรูปแบบที่สาม สร้างตัวดึงดูดอลวนจากระบบ Van der pol โดยใช้เทคนิคการต้านการควบคุมระบบอลวนหรือ Chaotification ให้เป็นตัวดึงดูดแบบใหม่มีทั้งระบบหลายสกอร์และแบบไฮเปอร์ โดยทุกรูปแบบที่นำเสนอได้ทำการศึกษาพฤติกรรมเชิงพลวัตและสร้างวงจรเพื่อยืนยันว่าตัวดึงดูดที่นำเสนอว่ามีปรากฏจริง และสุดท้ายได้สาธิตการประยุกต์ตัวดึงดูดอลวนโดยการปรับปรุงวงจร Chua เพื่อใช้ในการขับเคลื่อนหุ่นยนต์และใช้วงจรกำเนิดสัญญาณอลวนแบบเอนกประสงค์สำหรับสร้างสัญญาณสุ่มจริง

Thesis Title	**Construction of Chaotic Attractors and Its Applications**
Student	Mr. Kitdakorn Klomkarn
Student ID.	46060001
Degree	Doctor of Engineering
Program	Electrical Engineering
Year	2011
Thesis Advisor	Assoc. Prof. Dr. Pitikhate Sooraksa

Abstract

In this thesis, three novel methods for construction of chaotic attractors are presented. For the first method, the mixed –mode and the universal mode chaotic oscillator generating various patterns of chaotic signals are proposed. The second method is about construction of a multi-wing butterfly chaotic attractor derived from Lorenz-based system by using multi-segment nonlinear functions. In the last method, the multi-scroll chaotic attractor and hyper-chaotic attractors are obtained by anti-control or chaotification of the Van der Pol system. The complex dynamical behaviors of all proposed systems are investigated, and the electronic circuits are constructed to confirm that all attractors are existed. Applications of chaotic attractors are also demonstrated. We show that chaotic signals obtained from the modified Chua's circuit and the universal mode chaotic oscillator can be used for guiding the mobile robot's path and for generating a truly random number.

ACKNOWLEDGEMENTS

I would like to express my gratitude and appreciation to my advisor Assoc. Prof. Dr. Pitikhate Sooraksa for his advise, support and encouragement over my Ph.D research. I am greatly indebted to Prof. Dr. Guanrong Chen, my Co-advisor at City University of Hong Kong for loving kindness and valuable advise as well as taking care of my study time in Hong Kong. Without both of my advisors contributions and guidance this thesis would have not been possible.

Special thanks for Mr. Sakda Sakorntanon for great assisting in construction of circuit prototypes. I am thankful Mr. Narongsak Manositichai for preparing my publication in LaTeX format.

I gratefully acknowledge the scholarship from Thailand Research Fund under Grant No, RGJ-PhD 231-2547.

Finally I wish to express my deepest gratitude to my parents for their unconditional love and belief in me.

Kitdakorn Klomkarn

TABLE OF CONTENTS

TABLE OF CONTENTS (continued)

LIST OF FIGURES

LIST OF FIGURES (continued)

LIST OF FIGURES (continued)

LIST OF FIGURES (continued)

Fig. Page

LIST OF TABLES

Chapter 1

Introduction

1.1 Introduction

Exploiting chaos properties for applications in sciences is an interesting research topic in engineering community especially in various fields of electrical engineering. In electronic system, the complex noise-like property is used to improve electromagnetic interference (EMI) in power convector [1] and can be applied as testing signals both for analog and mixed-mode circuits [2,3]. In control engineering, the generated chaotic signal is utilized in path planning for mobile robots [4], enhancing the motion capability of walking micro-robots [5], and increasing efficiency of industrial liquid mixing processes [6].

In computer and information engineering, the rich variety of dynamical behaviors can be served as a random source of cryptography [7], and may be exploited for a pattern generator in chaos computing [8]. In communication engineering, synchronized property is a great source producing potential applications for radar [9] and secure communication [10]. As far as the above applications are concerned, the study of chaotic dynamics for the electrical engineering has become important and is a powerful tool to transform fundamental knowledge into chaotic products for creative economy.
In the past two decades after the invention of Chua's circuit [11], several designs of chaotic oscillators have been developed. For example, some simple chaotic oscillators were constructed from differential equations in [12], and some chaotic oscillators were constructed by combining a second-order sinusoidal oscillator with a nonlinear component [13]. For realization of chaotic oscillator circuits from the Lorenz prototype equation, Chen's attractor [14], discovered via chaotification to be a dual version to the Lorenz attractor, was constructed by analog circuitry [15]. Moreover, there is a number of papers devoted to designing complex chaotic oscillators and implementing various multi-scroll chaotic attractors [16].

To extend the aforementioned literature and to design the chaotic oscillator as major building tool boxes for the applications, in this thesis, the novel attractors and chaotic oscillators are practically

illustrated and demonstrated. A completed set of engineering aspects including modeling, design, realization, testing, and application is also presented.

1.2 Objective

The objectives of this research are as follows:

1. To find a new chaotic attractor as building boxes for applications in engineering;
2. To implement a chaotic oscillator circuit from a new chaotic system;
3. To demonstrate the new applications from the new chaotic system.

1.3 Scope of Study

Scope of this study is limited to three novel methods of construction and applications in engineering. The effectiveness of the proposed schemes are verified by computer simulation Matlab and PSpice as well as construction and tests of electronic circuits.

1.4 Thesis Outline

The organization of this thesis is as follows. Chapter 2 reviews definition of chaos and chaotic properties, including methods for construction of chaotic attractors and some example of well- known chaotic attractors. In Chapter 3, the mixed-mode and the universal mode modified from quadrature core autonomous and nonautonomous chaotic system are proposed. In Chapter 4 design and construction of the muti-wings butterfly attractor which are complex attractors modified from Lui attractor are presented. The multi-scroll chaotic attractor and a new hyper-chaotic attractor, which are realized based on chaotified basic Van der Pol are presented in Chapter 5. To utilize the findings, two applications of chaotic attractor are exploited: one is a guidance system for a mobile robot; the other is for generating truly random number shown in Chapter 6. In Chapter 7, final remarks and future works are made to conclude the work.

Chapter 2

Basic Theory

In this chapter we briefly review the chaotic attractor theory as a background leading to the thesis research. Section 2.1 gives definition about chaos and attractors. Section 2.2 explains about the well-known Lorenz attractor. Section 2.3 describes the construction of Chen attractor modified from that of Lorenz .

2.1 Definition

Chaos [17] is aperiodic long-term behavior in deterministic system that exhibits sensitive dependence on initial condition.

1. "Aperiodic long term behavior" means that there are trajectories which do not settle downs to fixed points, periodic orbit, or orbits as $t \to 0$.

2."Deterministic" means that system has no random or noisy inputs or parameters. The irregular arises from the system's nonlinearity, rather than from noisy force.

3."Sensitivity dependence on initial conditions" means that nearly trajectories separate exponentially fast, the system has a positive Lyapunov exponent.

Attractor and Chaotic attractor

An attractor is a set to which all neighboring trajectories converge. Stable fixed points and stable limit cycles are examples. We define an attractor to be a closed set A with the following properties;

1. A is an invariant set: any trajectory $x(t)$ that start in A stay in A for all time.

2. A attracts an open set of initial conditions: there is an open set U contained A such that if $x(0) \in U$, then the distance from $x(t)$ to A tends to zero as $t \to \infty$.This mean that A attracts all trajectories that start sufficiently closed to it.

3. An attractor is indecomposable.This mean that attractor cannot be split up into two nontrivial pieces.

A strange or chaotic attractor is a bounded attractor that exhibits sensitivity dependence on initial conditions (SDIC) definition: A set S exhibits sensitive dependence initial conditions if

$$\exists r > 0 \;\; such \;\; that \;\; \forall \varepsilon > 0 \;\; and \;\; \forall x \in S$$
$$\exists y \;\; such \;\; that \;\; |x(0) - y(0)| < \varepsilon, \;\; |x(t) - y(t)| > r.$$

A quantitative measurement of the sensitive dependence on the initial conditions is the Lyapunov exponent λ. It is the average of divergence (or convergence) of two neighboring trajectories in the phase space. Points are near at time 0 become exponentially far apart at time t. This can be written as

$$|x(t)| = |x(0)|e^{\lambda}. \tag{2.1}$$

Rearranging the above equation gives Lyapunov exponent

$$\lambda = \lim_{t \to \infty} \ln \frac{|x(t)|}{|x(0)|}. \tag{2.2}$$

If we consider a three-dimensional system, the relation between the signs of the Lypunov exponents and type of attractor is shown in Table 2.1.

Table 2.1 Relation of sign of Lyapunov exponents to an attractor

λ_1	λ_2	λ_3	Attractor
-	-	-	Fixed point
0	-	-	Limit cycle
0	0	-	Torus
+	0	-	Chaos

2.2 Lorenz Attractor

The Lorenz equation was published by E. Lorenz in 1963 [18] as a model for two-dimensional fluid convection. The original equation is commonly defined as three coupled ordinary differential equation like

$$\begin{aligned} x' &= -ax + ay \\ y' &= rx - y - xz \\ z' &= -bz + xy \end{aligned} \tag{2.3}$$

where x represents the velocity, y and z the temperature of the fluid and r,σ,b are positive parameters determined by the heating of the fluid, the physical properties of the fluid and the height of the layer.

To solve for the equilibrium points we set $x'=y'=z'=0$, then $y=x, z=r-1$ and $x^2=y^2=b(r-1)$ It is clear that one of those equilibrium points is $P^{\circ}=(0,0,0)$ and $P^{\pm}=(\pm\sqrt{b(r-1)},\pm\sqrt{b(r-1)},r-1)$ are equilibrium points and real when $r>1$. From equation (4), the local behavior around these equilibrium points will be given by a Jacobian matrix

$$J=\begin{bmatrix} \frac{\partial fx}{\partial x} & \frac{\partial fx}{\partial y} & \frac{\partial fx}{\partial z} \\ \frac{\partial fy}{\partial x} & \frac{\partial fy}{\partial y} & \frac{\partial fy}{\partial z} \\ \frac{\partial fz}{\partial x} & \frac{\partial fz}{\partial y} & \frac{\partial fz}{\partial z} \end{bmatrix}. \tag{2.4}$$

The Jacobi matrix for the Lorenz system J is given by

$$J=\begin{bmatrix} -a & a & 0 \\ r-z & -1 & -x \\ y & x & -b \end{bmatrix}. \tag{2.5}$$

To obtain its eigenvalues, we let $A=|J-\lambda I|$. These eigenvalues corresponding to equilibrium point (0, 0, 0) can be solved by using the characteristic equation:

$$\lambda^3+(a+b+1)\lambda^2+(a-ar+ab+b)\lambda+ab(1-r). \tag{2.6}$$

At $P^{\pm}$, the characteristic equation of J is

$$\lambda^3+(a+b+1)\lambda^2+b(a+r)\lambda+2ab(r-1). \tag{2.7}$$

Form (2.7) when $r < 1$, it is clear that all the eigenvalues are negative and the equilibrium point at the origin is stable. Let index n show number of roots on the right haft plane. For $r > 1$, the eigenvalues at the origin are one positive and two complex conjugate eigenvalves, and the system conducts unstable or saddle point index 1. Trajectories of the attractor spiral around the saddle point as they approach on the in-set surface. Thus the equilibrium points at $P^{\pm}$ exist when $r > 1$.

Let $a_1 = (a+b+1)$, $a_2 = (a+r)b$, $a_2 = (a+r)b$ $a_3 = 2ab(r-1)$.

From Routh-Hurwitz criterion, the system should be stable under condition $a_1 > 0$, $a_2 > 0$, $a_3 > 0$ or $a_1 a_2 - a_3 > 0$. And the equation can rewritten as

$$(a+b+1)(a+r)b - 2ab(r-1) > 0. \tag{2.8}$$

The equilibrium points at $P^{\pm}$ are stable if

$$r < \frac{a(a+b+3)}{a-b-1}. \tag{2.9}$$

If we set $a = 10$, $b = 8/3$ and $r > \frac{470}{19}$, the eigenvalves of $P^{\pm}$ are one negative pole and two complex conjugate eigenvalves on right haft plane, then the system is unstable or has the saddle point index 2. Trajectories of the attractor spiral around the saddle point as they approach on the in-set surface.Trajectories of the attractor spiral around the saddle point as they diverse from the saddle point.The result of numerical simulation is shown in Fig. 2.1. After short transient, the trajectory, originating from out bound of the attractor, then converges toward a set in the phase space characterized by alternating circulations look-liked random circulation around two unstable equilibrium points $P^{\pm}$. All trajectories yield strange attractors of the Lorenz equation.

To confirm that the Lorenz attractor is a bounded system, divergence of phase velocity must satisfy

$$\nabla F = \frac{\partial Fx}{\partial x} + \frac{\partial Fy}{\partial y} + \frac{\partial Fz}{\partial z} < 0 \quad . \tag{2.10}$$

Lyapunov of Lorenz system can be computed from [39] provided $\lambda_1 = 0.9, \lambda_2 = 0, \lambda_3 = -14.57$.

When a=10, b=8/3, c=28, the Lorenz system exhibits a chaotic behavior, the projections of the chaotic attractor are shown in Fig. 2.1.

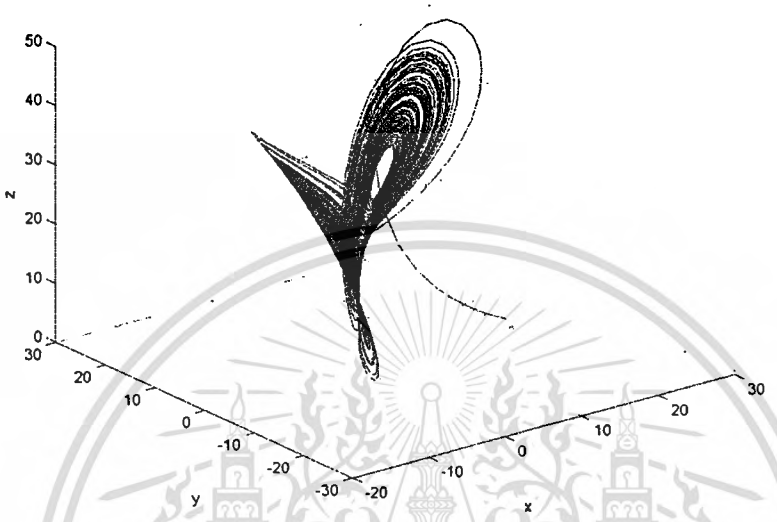

Fig. 2.1 The Lorenz attractor

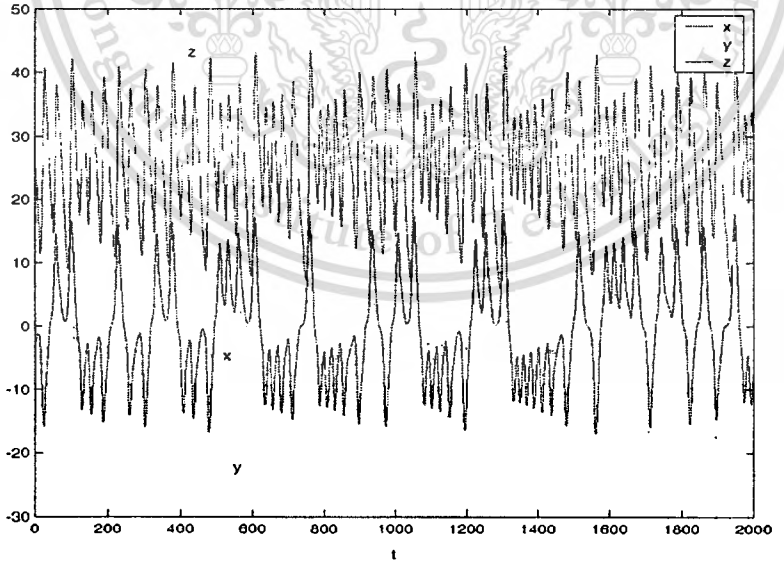

Fig. 2.2 The Lorenz attractor in time domain

2.3 Chen Attractor

Chen attractor is discovered by Chen [14], by creation of chaos with anti-control techniques. The system equations are

$$\begin{aligned} x' &= -ax + ay \\ y' &= rx - y - xz + u \\ z' &= -bz + xy \end{aligned} \qquad (2.11)$$

where a, b and c are constants, currently not in the range of chaos, and u is a linear feedback controller of the form $u = k_1 x + k_2 y + k_3 z$. To find the equilibria of the controlled Lorenz system (2.3), let $x' = y' = z' = 0$ then there exist three equilibria: The first one is at $P^{\circ} = (0,0,0)$. And the non-zero equilibria can be found by first observing that the first equation $x = y$, $z = \frac{1}{b}x^2$.

Therefore, the second equation of (2.11) leads to $x = y = \frac{1}{2}k_3 \pm \frac{1}{2}\sqrt{k^3 + 4(b + k_1 + k_2 - 11)}$, then the system's Jacobian matrix is

$$J = \begin{bmatrix} -a & a & 0 \\ c + k_1 - z & k - 1 & k_3 - x_3 \\ y & x & -b \end{bmatrix}. \qquad (2.12)$$

The Jacobian is evaluated at the zero equilibrium (0,0,0), then k_3 does not contribute to its eigenvalues. To have chaotic behavior, these two nonzero equilibria cannot be stable. That is, the Jacobian should have at least one unstable eigenvalue when it is evaluated at each of these two equilibria, $P^{\pm}$ which has eigenvalues given by the roots of the characteristic equation

$$\lambda^3 + a_1\lambda^2 + a_2\lambda + a_3 \qquad (2.13)$$

where $a_1 = (a + b - k_2 + 1)$, $a2 = (ab - ac + a + b + az + x^2 - k_1 a - k_2 a - k_2 b)$ and $a3 = (ab - abc + ax^2 + axy + abz - k_1 ab - k_2 ab)$.

From the Routh-Hurwitz condition to the system to be unstable, $k_1 = a \quad k_2 = 1 + c$ and $u = -ax + (1+c)y$ which yields the following new chaotic system:

$$\begin{aligned} x' &= -ax + ay \\ y' &= (c-a)x - ay - xz \\ z' &= -bz + xy \end{aligned} \quad . \tag{2.14}$$

For dynamical system (2.14), we can obtain

$$\nabla F = \frac{\nabla Fx}{\partial x} + \frac{Fy}{\partial y} + \frac{\partial F}{\partial z} = -a + c - b < 0 . \tag{2.15}$$

Typical parameters of Chen system are $a = 35, b = 8/3, c = 28$ and the Lyapunov of system is $\lambda_1 = 2.18, \lambda_2 = 0, \lambda_3 = -11.85$.

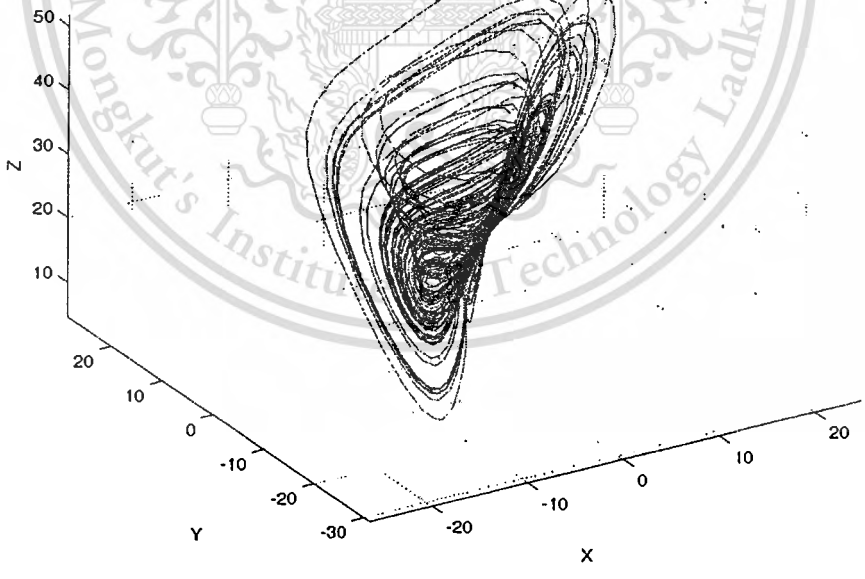

Fig. 2.3 The Chen attractor

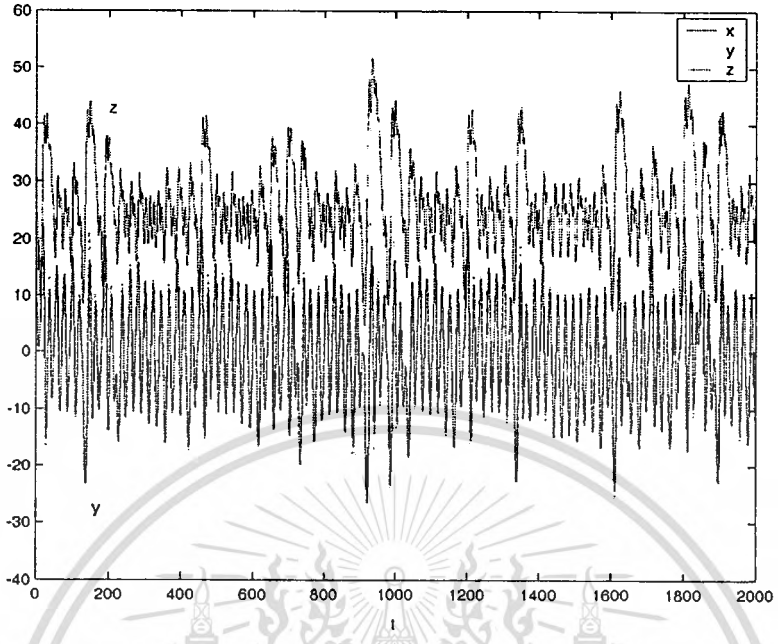

Fig. 2.4 The Chen attractor in time domain

From now on, we will use fundamental of chaos and attractors presented in this chapter for realization and circuit implementation throughout the dissertation. Basic ideas can be generated many chaotic patterns. Analytic tools and characteristics of chaotic behaviors learnt from this chapter are the prerequisite for further study as will be shown in the next chapters.

Chapter 3

Construction of Chaotic Circuits based on Two-Integrator Loop Oscillator

This chapter, we propose two types of simple chaotic oscillator circuits provided various types of chaotic signals based on the two-integrator loop oscillator. For the first type, a simple scheme for designing mixed-mode chaotic circuits using quadrature core oscillators is presented. Two mixed-mode circuits are constructed by using a few operational amplifiers in suitable combination with some autonomous/nonautonomous second/third-order chaotic circuits. For the second type, a universal mode chaotic oscillator generating a single scroll to multi-scrolls by using a programmable nonlinear function is designed and constructed.

This chapter is structured as follows. In Section 3.1, we review the basic theory of the two-integrator loop oscillator and review second-order autonomous chaotic circuit and nonautonomous chaotic circuit, as well as the third-order chaotic which are based on of the two-integrator loop oscillator circuit in Section 3.2. The proposed mixed-mode chaotic oscillators and the proposed universal-mode chaotic oscillators are explained in Sections 3.3 and 3.5 respectively. Simulation and the experiment results have verified the simplicity and effectiveness of the new design presented in Section 3.5.

3.1 Two-Integrator Loop Oscillator

In this chapter, the proposed chaotic circuits are constructed by using operational amplifiers based on the two-integrator loop techniques which consists of two types of loops. Type I has two inverting integrators with one inverting amplifier loop and Type II has one inverting integrator and one Daboo integrator in the loop.

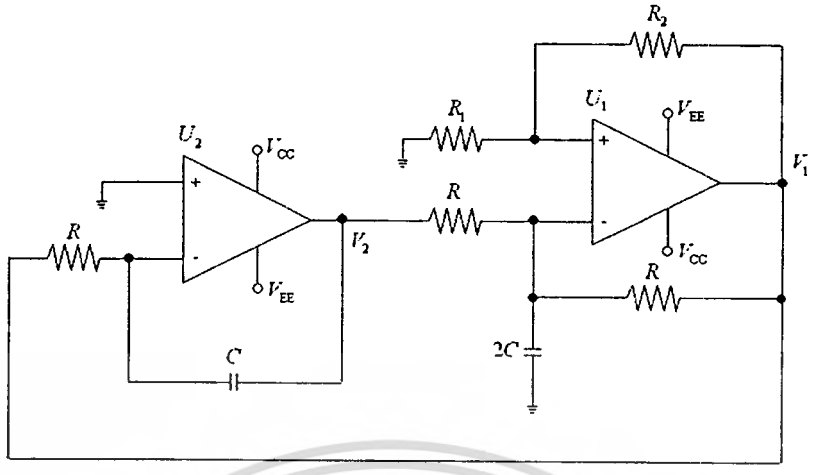

Fig. 3.1 Type I: A two-integrator loop oscillator

Fig. 3.1 shows a Type I two-integrator loop oscillator circuit, which consists of two integrators: an inverting (or Miller) integrator and a non-inverting (or Daboo) integrator [19]. The state equation of a second-order quadrature oscillator circuit is described by

$$\begin{bmatrix} \dot{v} \\ \dot{v}' \end{bmatrix} = \begin{bmatrix} \dfrac{(A-1)}{2RC} & \dfrac{(A+1)}{2RC} \\ -\dfrac{1}{RC} & 0 \end{bmatrix} \begin{bmatrix} v_1 \\ v_2 \end{bmatrix} \tag{3.1}$$

where $A = \dfrac{R_2}{R_1}$ is the amplifier gain of the Daboo integrator.

Consider the state equations (3.1) as a second-order system, which can be controlled by the controllable parameter A. When $A < 1$, a negative feedback is generated by a positive integrator, and a pair of complex conjugate eigenvalves of the system have negative real parts, resulting in poles located on the left-haft complex plane. This eventually leads system (3.1) to a damped-stable mode. Conversely, when $A > 1$, a positive feedback is provided in the positive integrator, and the complex conjugate eigenvalues of system (3.1) move to the right-haft plane. Consequently the close-loop system is in an unstable mode. To generate sine waves, a pair of the complex conjugate poles of the second-order system should stay on the imaginary axis, for which one can control the system by assigning $A = 1$, where the frequency of the oscillator is $f_0 = 1/(2\pi fC)$.

The two-integrator loop module with two inverting integrators with one inverting amplifier loop is depicted in Fig. 3.2.

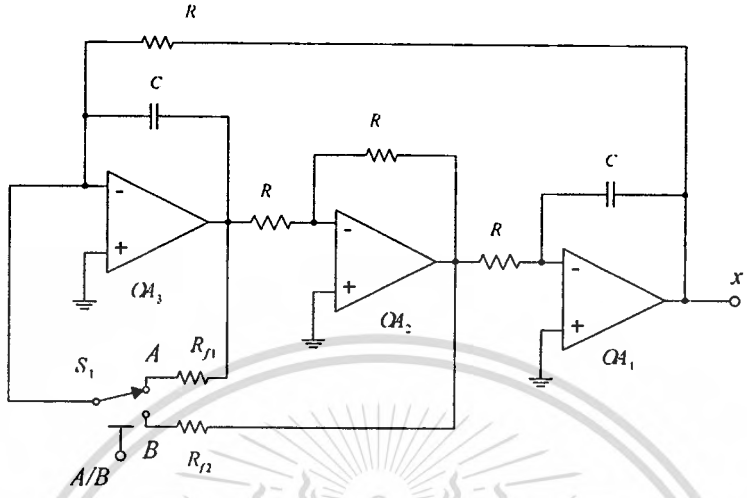

Fig. 3.2. Type II: A two-integrator loop oscillator

This circuit module consists of an inverting integrator OA1, an inverting amplifier OA2 and a summing inverting integrator OA3. It is a closed-loop second-order system, where the states x and y are outputs of OA1 and OA3. And the output of the state x is a feedback input of itself. In order to assign the complex conjugate poles moving between the LHP and the RHP, The coefficients of the output of the state y can be selected by using an analog multiplexer. The negative and positive coefficients are defined as Rf1 and Rf2 respectively. The time constant of an integrator setting frequency of the chaotic oscillator is 1/RaC. The state equation of the circuit depicted in Fig.3.2, when the switch S1 is connected to point A, can be written as inverting integrator

$$\begin{bmatrix} v'_1 \\ v'_2 \end{bmatrix} = \begin{bmatrix} 0 & \frac{1}{RC} \\ \frac{1}{RC} & -\frac{R_{f_1}}{RC} \end{bmatrix} \begin{bmatrix} v_1 \\ v_2 \end{bmatrix}. \tag{3.2}$$

And when switch S1 is connected to point B, the state equation can be written as

$$\begin{bmatrix} v'_1 \\ v'_2 \end{bmatrix} = \begin{bmatrix} 0 & \frac{1}{RC} \\ \frac{1}{RC} & \frac{R_{f_2}}{RC} \end{bmatrix} \begin{bmatrix} v_1 \\ v_2 \end{bmatrix}. \tag{3.3}$$

3.2 Chaotic Circuits based on Two-Integrator Loop Oscillator

In this section, the second-order autonomous chaotic and nonautonomqus chaotic circuits, as well as the third-order chaotic circuit, are reviewed. In order to combine these circuits into a mixed-mode circuit and rearrange to the universal mode circuit, some of these circuits are modified.

1 Second-order autonomous chaotic circuit

Consider the autonomous chaotic circuit proposed in [20], whose dynamical behaviors have been discussed in detail in [21]. This circuit is very simple, consisting of an unstable second-order linear system with feedback and a hysteresis relay, described by

$$\begin{bmatrix} x \\ y \end{bmatrix} = \begin{bmatrix} 0 & 1 \\ -1 & \alpha \end{bmatrix} \begin{bmatrix} x \\ y \end{bmatrix} + \begin{bmatrix} 0 \\ hys(x) \end{bmatrix} \tag{3.4}$$

where x and y are state variables and $hys(x)$ is a hysteresis function (see Table 3.1).

The model consists of an unstable second-order linear system with a hysteresis feedback. This linear system has complex conjugate eigenvalues on the right haft plane (RHP) with two unstable focuses on the $x-y$ plane provided stretch mechanism for the dynamic trajectory. The hysteresis element can be used as a switch or folding mechanism to excite the trajectory to another unstable plane.

In order to guarantee chaotic oscillations of the circuit (3.4), one should require $\alpha < 1$. The state equation (3.4) can be rewritten in a modified form of the quadrature core oscillator based on Type II of the two integrator loop as follows:

$$\begin{bmatrix} x \\ y \end{bmatrix} = \begin{bmatrix} a & b \\ -1 & \alpha \end{bmatrix} \begin{bmatrix} x \\ y \end{bmatrix} + \begin{bmatrix} 0 \\ k \times hys(x) \end{bmatrix}. \tag{3.5}$$

Where parameters a and b are depended on the gain of the positive integrators, and k is the hysteresis gain.

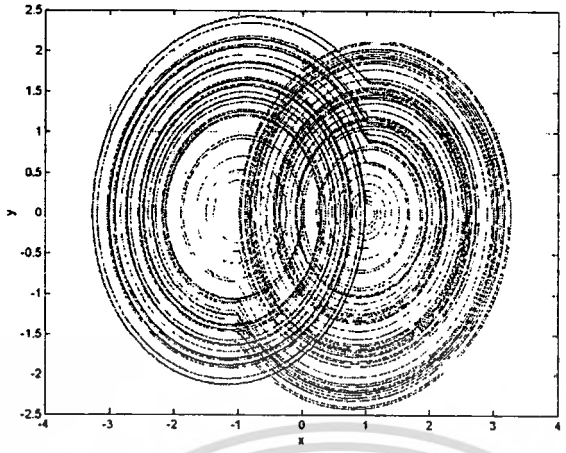

Fig. 3.3 Matlab simulation results of the system (3.4):

Table 3.1 Summary of the basic nonlinear functions

Number	Nonlinear function	Definition
1	Heaviside	$H(x)=\begin{cases}1 & x\geq 0\\ 0 & x<0\end{cases}$
2	Signum	$\mathrm{sgn}(x)=\begin{cases}1 & x\geq 0\\ -1 & x<0\end{cases}$
3	Hysteresis	$hys(x)=\begin{cases}+1, & -1<x<\infty\\ -1, & -\infty<x<1\end{cases}$
4	Saturation	$sat(x)=\begin{cases}1 & x>L\\ kx & \lvert x\rvert<L\\ -1 & x<-L\end{cases}$ where $L=\left\lvert\frac{x}{k}\right\rvert$, k is an amplifier gain.

2 Third-order autonomous chaotic circuit

Consider the third-order autonomous chaotic circuit proposed in [12] and implemented in [13] using high-frequency current-mode operational amplifiers, with the so-called double-scroll-like dynamics, described by

$$\begin{bmatrix} x' \\ y' \\ z' \end{bmatrix} = \begin{bmatrix} 0 & 1 & 0 \\ 0 & 0 & 1 \\ -1 & -1 & -\alpha \end{bmatrix} \begin{bmatrix} x \\ y \\ z \end{bmatrix} + \begin{bmatrix} 0 \\ 0 \\ f(x) \end{bmatrix}. \tag{3.6}$$

where $f(x) = \mathrm{sgn}(x)$ and α is a bifurcation parameter taking values in [0.5,0.9]. The system has negative feedback parameters in the quadrature core oscillator on the *y*-*z* plane, and is slightly modified herein as

$$\begin{bmatrix} x' \\ y' \\ z' \end{bmatrix} = \begin{bmatrix} -1 & 1 & 0 \\ 0 & 0 & 1 \\ -1 & -1 & -\alpha \end{bmatrix} \begin{bmatrix} x \\ y \\ z \end{bmatrix} + \begin{bmatrix} 0 \\ 0 \\ f(x) \end{bmatrix}. \tag{3.7}$$

where α is a bifurcation parameter taking values in between [0.1,0.3].

In order to integrate the above-reviewed circuits together, a third-order autonomous circuit is designed by extending the unstable quadrature core oscillator on the *x*-*y* plane based on the system (3.7), together with a feedback loop using a comparator in the y-state controlled by a nonlinear state-feedback with a comparator in the *z*-state. The modified circuit is described by

$$\begin{bmatrix} x' \\ y' \\ z' \end{bmatrix} = \begin{bmatrix} a & b & 0 \\ -1 & 0 & 1 \\ 0 & 0 & -\alpha \end{bmatrix} \begin{bmatrix} x \\ y \\ z \end{bmatrix} + \begin{bmatrix} 0 \\ f(x) \\ f(x) \end{bmatrix}. \tag{3.8}$$

where $f(x) = \mathrm{sgn}(x)$ and α is a bifurcation parameter taking values in [0.5-1.0].

To simplify construction of the third-order autonomous chaotic system which can be obtained a wide range of chaotic signals from a single scroll to complex scrolls by switching and adding an external driving function. The proposed model is specified by

$$\begin{bmatrix} x' \\ y' \\ z' \end{bmatrix} = \begin{bmatrix} 0 & 1 & 0 \\ -1 & \alpha & 1 \\ 0 & 0 & -1 \end{bmatrix} \begin{bmatrix} x \\ y \\ z \end{bmatrix} + \begin{bmatrix} y_p(t) \\ 0 \\ f(x) + x_p(t) \end{bmatrix}. \tag{3.9}$$

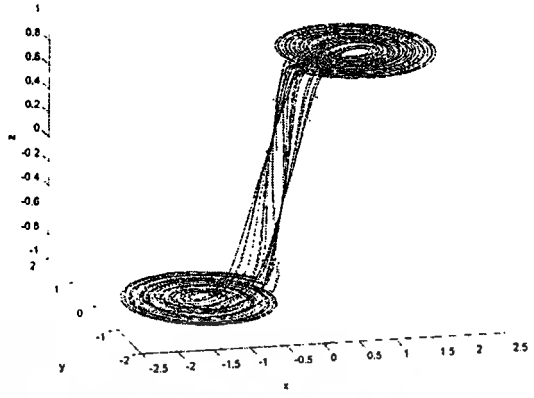

Fig.3.4 Matlab simulation results of the system (3.9) with the signum function

The system equation (3.9) consists of the third-order linear system, a nonlinear element and driving pulses. In linear system, states x and y are the second-order unstable subsystems. Adding the state z as a hyper plane, the third-order nonlinear dynamical system in Table 3.1 is dissipative, and has a negative eigenvalue and a pair of complex conjugate poles with positive real part. The equilibrium point (0,0,0) is an index-2 spiral-saddle point. Since the system is unstable on the $x-y$ plane, the trajectory scrolls are away from the equilibrium point. To fold the trajectories, nonlinear elements in Table 3.1 can be employed. In Table 3.1, the Heaviside function is applied to obtain a single scroll, while the signum function in and the hysteresis function are enforced to generate double scrolls. To assign single or double scroll, the saturation function can be used for generating chaotic signals by means of threshold control [22]. The method is as simple as adjusting the gain of the amplifier in the system. To generate multi-scroll attractors, the staircase function in equations (3.9.1a) and (3.9.1b) together with external driving pulse functions $x_p(t)$ and $y_p(t)$ are used to alter the equilibrium of the system. All nonlinear functions used herein are summarized in Table 1 and the staircase functions are:

$$f(x) = 2\{\text{sgn}(x+v_1) + \text{sgn}(x-v_1)\} \qquad (3.9.1a)$$

$$f(x) = \{\text{sgn}(x) + \text{sgn}(x+v_1) + \text{sgn}(x-v_1)\} \qquad (3.9.1b),$$

where v_1 is the referent voltage associated with creation of the new equilibrium.

3 Second-order nonautonomous chaotic circuit

To generate a chaotic attractor from a non-autonomous system, the system consists of the second-order linear circuit and a nonlinear element in the feedback loop driving by the time-varying sinusoidal signal [23]. The system is realized by a comparator as the signum function [23] implying the potential application in secure communication [24]. A different approach in realizing the system can be achieved by exploiting a saturation amplifier as a threshold controller for the nonlinear element [25]. To model the module based chaotic oscillator, the non-autonomous chaotic oscillator system is constructed by using the equation:

$$\begin{bmatrix} x \\ y \end{bmatrix} = \begin{bmatrix} 0 & 1 \\ -1 & \alpha \end{bmatrix} \begin{bmatrix} x \\ y \end{bmatrix} + \begin{bmatrix} 0 \\ f(x) + f_s(\omega t) \end{bmatrix}. \tag{3.10}$$

where α is the damping coefficient, respectively

This system can be rewritten in the Type II two-integrator-loop as

$$\begin{bmatrix} x \\ y \end{bmatrix} = \begin{bmatrix} a & b \\ -1 & \alpha \end{bmatrix} \begin{bmatrix} x \\ y \end{bmatrix} + \begin{bmatrix} 0 \\ f(x) + f_s(\omega t) \end{bmatrix}. \tag{3.11}$$

The system equation (3.10) consists of the second-order stable linear system with a sign function in the feedback loop driven by the sinusoidal signal. The system can generate a double-scroll chaotic attractor. We can also modify the system to obtain multi-scrolls by using the nonlinear function as described in equations (3.9.1a) and (3.9.1b).

In [26], the sinusoidal force is replaced by pulse excitation and can be proved that strange attractors exist in the system. This can be done by adding sign for a nonlinear transconductor. The non-autonomous chaotic system illustrated in equation (3.10) is a dissipative system and can be analyzed as the forth-order autonomous chaotic system by transforming the sinusoidal and pulse forcing functions into a second-order system.

The Matlab simulation result, applying sinusoidal driving signal and employing the nonlinear signum function, is shown in Fig.3.5. In case of using the signum function as the nonlinear element together with sinusoidal driving signal, a double-scroll attractor in Fig.3.5 is obtained. Figure 3.6

shows that of using the signum function and pulse driving signal by setting up amplitude and frequency equal to ± 0.5, 0.2 rad/s, respectively. We will see later that the simulation results obtained in this section agreed with experimental results by using the modules in the next section.

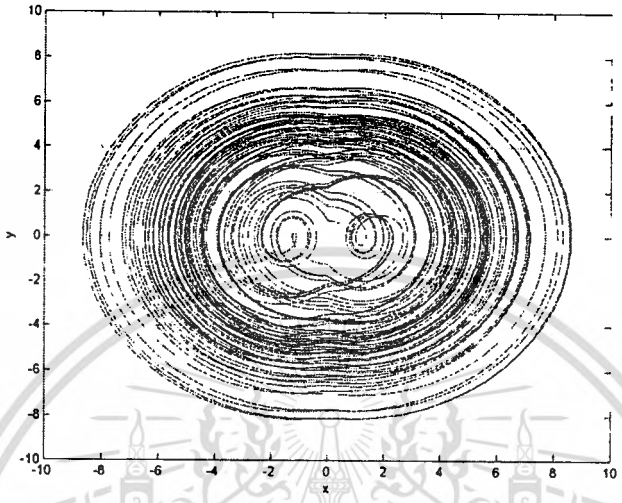

Fig.3.5 Matlab simulation results of the system (3.10) using the signum function and the sinusoidal driven signal

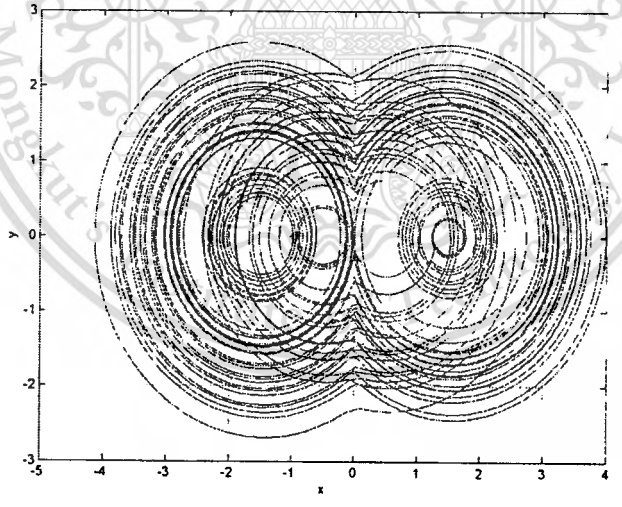

Fig.3.6 Matlab simulation results of system (3.10) using the signum function and the pulse driving signal

3.3 The Proposed Mixed-Mode Chaotic Oscillators

Two mixed-mode schemes of a chaotic circuit are now designed, based on the Type-I two-integrator loop oscillator. The first scheme of the chaotic circuit is depicted in Fig. 3.2. This circuit combines the third-order autonomous circuit (3.7) with the nonautonomous circuit (3.10). The new circuit consists of four op-amps, three analog switches, and one voltage comparator. Since the systems (3.7) and (3.10) are both damped-stable, one may assign a voltage amplifier gain of the positive integrator U1 to be unity by setting R1 = R2, and may apply negative feedback at the negative integrator U2 by connecting R3 across the capacitor.

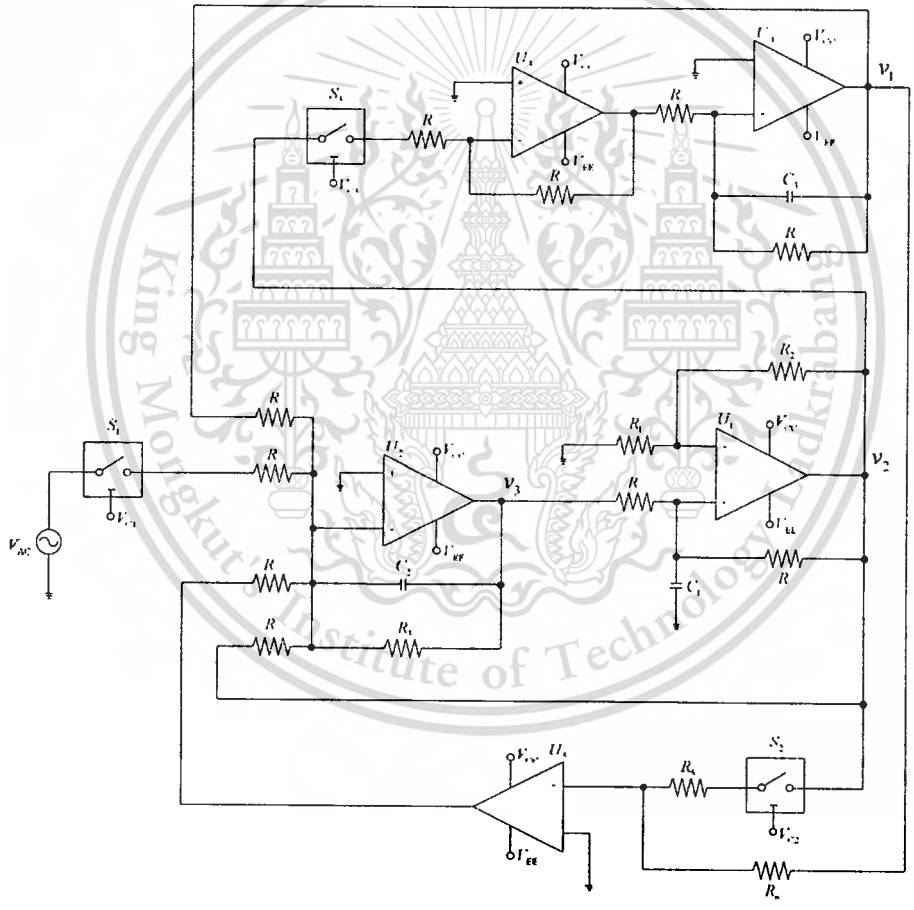

Fig. 3.7 Scheme 1: The proposed mixed-mode chaotic circuit

The mixed-mode circuit exhibits chaotic behaviors when the second-order damped system is driven by an external input. This can be done by turning on S1 to connect with the external periodic

input, turning on S2 to connect the x-state to the comparator, and turning off S3 so as to disable the third integrator. When the circuit is operated in this mode, the state equations of the circuit shown in Fig. 3.7 are expressed as

$$\begin{aligned}\frac{dv_2}{dt} &= \frac{v_3}{RC_1} \\ \frac{dv_3}{dt} &= -\frac{v_2}{RC_2} - \frac{v_3}{R_3C_2} + \frac{\mathrm{sgn}(v_2)}{R_4C_2} + \frac{v_{ac}}{RC_2}\sin(\omega t)\end{aligned}, \tag{3.11}$$

where v_{ac} is the magnitude of the ac-driven signal.

Note that in order to operate the third-order chaotic circuit, S3 must be turned on. From (3.7), the second-order damped system is operated in states y and z, and the output of the negative integrator U3 is in state x, which is connected to a comparator. To set up the autonomous configuration, S1 is turned on, but S2 is turned off to disconnect state y of the comparator.
The third-order chaotic circuit is described by

$$\begin{aligned}\frac{dv_1}{dt} &= -\frac{v_1}{RC_3} + \frac{v_2}{RC_3} \\ \frac{dv_2}{dt} &= \frac{v_3}{RC_1} \\ \frac{dv_3}{dt} &= -\frac{v_1}{RC_2} - \frac{v_2}{RC_2} - \frac{v_3}{R_3C_2} + \frac{\mathrm{sgn}(v_2)}{R_4C_2}.\end{aligned} \tag{3.12}$$

The second scheme is a three-mixed-mode chaotic circuit as shown in Fig. 3.8. The circuit contains the second-order autonomous, the second-order nonautonomous, and the third-order autonomous chaotic circuits corresponding to equations (3.5), (3.8), and (3.11), respectively. The circuit can be realized by adding only one analog switch and diodes into the first scheme discussed above. For the mixed-mode circuit, the quadrature core oscillator in the system (3.5) and that of in the system (3.8) are both unstable, but that of in (3.11) is damped-stable.

The switching of the second-order system toggled between unstable and stable modes can be controlled by either decreasing or increasing the gain A in the system (3.1). In order to control the system gain, switch S1 is operated to change the valve of the feedback resistor in a positive integrator.

When the switch is "on", the gain of the integrator U1 decreases. As a result, the system is operating in an unstable mode. In contrast, when the switch is "off", the gain of the integrator increases, leading the system to be damped-stable.

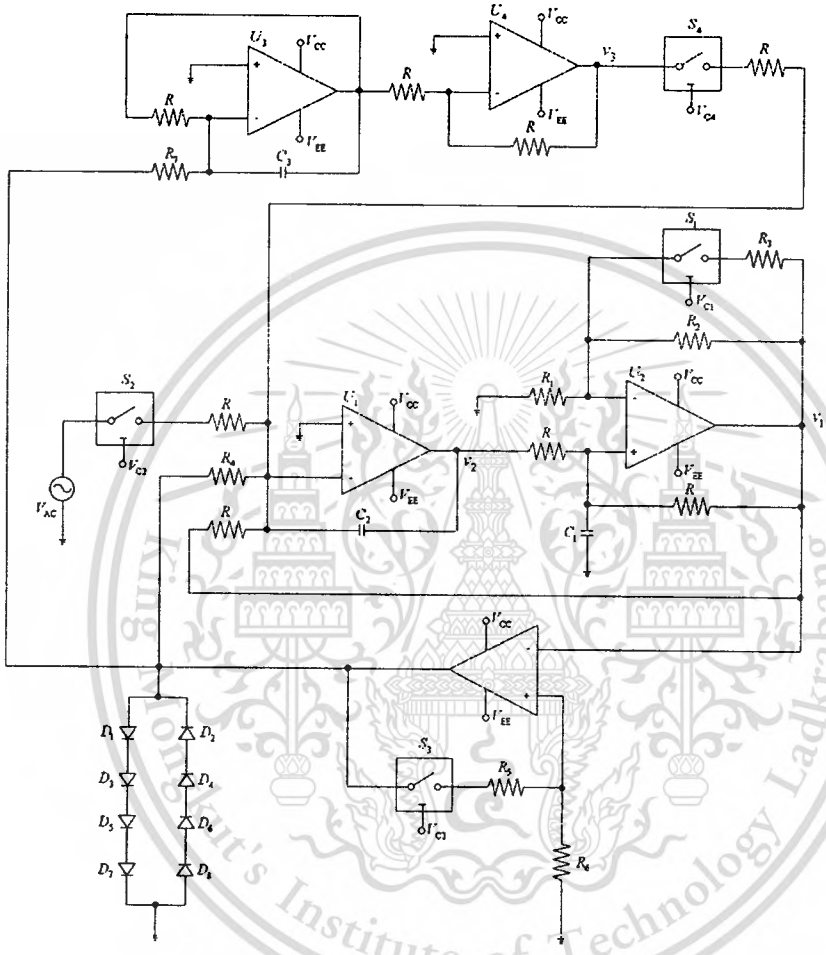

Fig. 3.8 Scheme 2: The proposed mixed-mode chaotic circuit

The mixed-mode chaotic circuit operates as a switching second-order autonomous system, which is unstable by turning on switches S1, S2 and S4, which are turned off for disconnecting external input signals and disconnecting the third integrator, respectively.

Hysteresis is provided by the nonlinear elements via turning on switch S3. Output voltage of the hysteresis-loop can be changed by adjusting diodes D1-D8. The circuit equation of this mode is

$$\begin{aligned}\frac{dv_1}{dt} &= \frac{(A-1)}{2R_1C_1}v_1 + \frac{(A+1)}{2R_1C_1}v_2 \\ \frac{dv_2}{dt} &= -\frac{v_1}{RC_2} + \frac{H(v_1)}{R_4C_2}\end{aligned} \quad . \tag{3.13}$$

To generate chaotic signals from the second-order nonautonomous system (3.11), the damped-stable second-order system is now forced by external periodic signals via turning on switches S1 and S2 while turning off switch S3. The circuit equation of this mode is

$$\begin{aligned}\frac{dv_1}{dt} &= \frac{(A-1)}{2R_1C_1}v_1 + \frac{(A+1)}{2R_1C_1}v_2 \\ \frac{dv_2}{dt} &= -\frac{v_1}{RC_2} + \frac{\mathrm{sgn}(v_1)}{R_4C_2} - \frac{v_{ac}}{R_3C_2}\sin(\omega t)\end{aligned} \quad . \tag{3.14}$$

There is one more mode of the second scheme of the chaotic circuit, which is the third-order autonomous system (3.8), where the states x and y are considered at the unstable quadrature core oscillator. The state-z is at the integrator U3. To activate this mode, all switches must be turned off except S4 (must be turned on). The circuit equation of this mode is

$$\begin{aligned}\frac{dv_1}{dt} &= \frac{(A-1)}{2R_1C_1}v_1 + \frac{(A+1)}{2R_1C_1}v_2 \\ \frac{dv_2}{dt} &= -\frac{v_1}{RC_2} + \frac{v_3}{RC_2} + \frac{\mathrm{sgn}(v_1)}{R_4C_2} \\ \frac{dv_3}{dt} &= -\frac{v_3}{R_6C_3} + \frac{\mathrm{sgn}(v_1)}{R_7C_3}\end{aligned} \quad . \tag{3.15}$$

Table 3.2 summarizes the configurations of the mixed-mode chaotic circuit, and the type of the systems, the equilibria, the behaviors of the quadrature core oscillator, and the number of active components.

Table 3.2 Characteristics of the two proposed schemes of the chaotic circuits

Mixed-mode circuit	Type of the system	Switch 'on'	Equilibria	Quadrature core
Scheme 1	Second-order nonautonomous(3.11)	S1,S2	$(\pm k,0)$	Damped-stable
	Third-order autonomous (3.12)	S3	$\left(\pm\frac{k}{2},\pm\frac{k}{2},0\right)$	Damped-stable
Scheme 2	Second-order autonomous (3.13)	S3	$\left(\pm k,\mp\frac{a}{b}\right)$	Unstable
	Second-order nonautonomous (3.14)	S1,S2	$(\pm k,ak)$	Damped-stable
	Third-order autonomous (3.15)	S3,S4	$\left(\pm\frac{k+\alpha k}{\alpha},\mp\frac{a}{b}\left(\frac{k+\alpha k}{\alpha}\right),\pm\frac{k}{\alpha}\right)$	Unstable

3.4 The Proposed Universal-Mode Chaotic Oscillators

In this section, we implement an electronic circuit united the third-order autonomous chaotic system (3.9) and the second non-autonomous chaotic system (3.10) in the same scheme, based on the Type II two-integrator loop type II. To construct the chaotic oscillator from the Type II second-order two-integrator loop, we consider chaotic systems in (3.9) and (3.10) as system composed of a linear and a nonlinear subsystem. To realize a linear system of the third-order autonomous chaotic system (3.9), we construct a first-order linear subsystem called the extended integrator circuit composed of the Type II two-integrator loop.

This extended integrator circuit is shown in dash line B. The module consists of a lossy integrator and a summing amplifier. The integrator is implemented by OA5 and a resistor *R*a and a

capacitor C used for extension of the second-order module to the third-order linear system. The summing amplifier OA6 is designed for a mixed-mode operation by adding signal from the nonlinear device and the driving signal generator.

In the nonlinear subsystem, two nonlinear circuits are constructed to chaotify the linear system to be the chaotic one. The first is the programmable nonlinear function subsystem, shown in dash line is assigned as a nonlinear function. To activate the Heaviside, the sign, the saturation and the hysteresis functions, this can be done by setting the switches 2a-2c to select the feedback resistor and the output voltage of the OA. The operational functions of the switches are shown in Table 3.3.

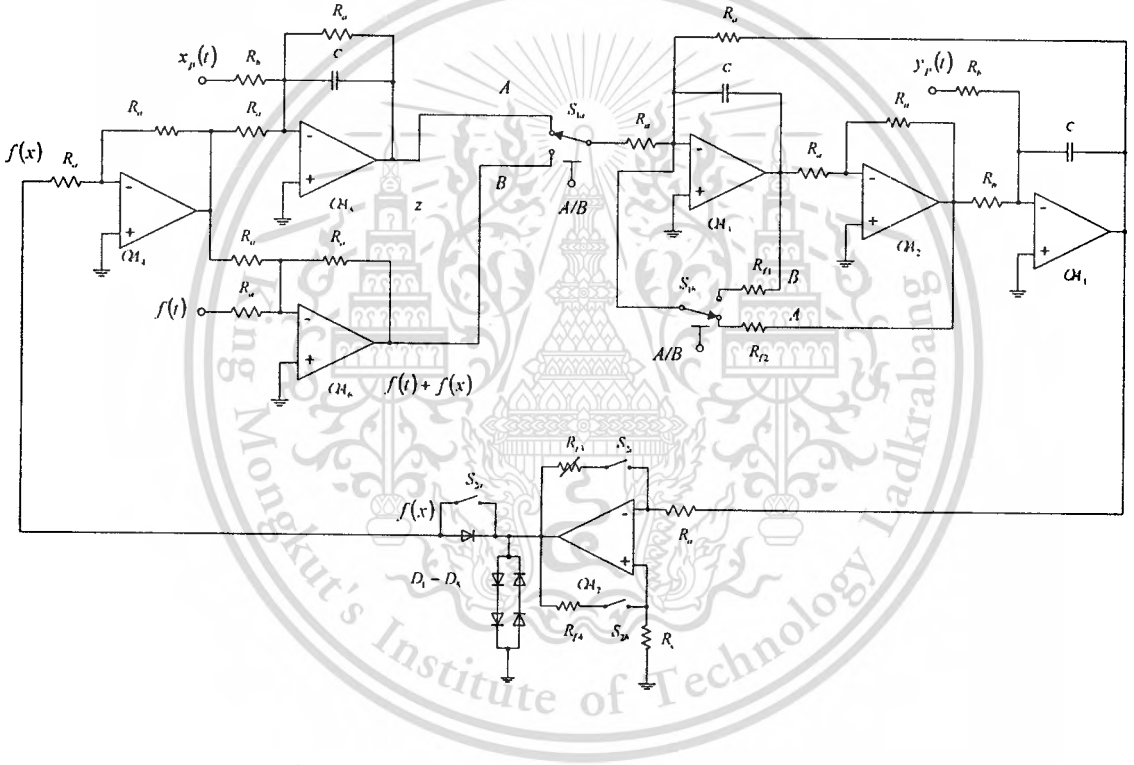

Fig. 3.9 The proposed universal-mode chaotic circuit

Table 3.3. Parameter configuration of the switches for activation of the selected function

Function	S2a	S2b	S2c
Heaviside	off	off	off
Signum	on	off	off
Saturation	on	off	on
Hysteresis	on	on	off

Because voltage bias of OA7 is in the range of ±15 V, and the saturation output is in the operational range of ± 13.5 V. Therefore, suitable diodes D1-D4 are identified as 1N914 which can be used to limit the voltage of the nonlinear function and to scale the behavior of the chaotic signals.

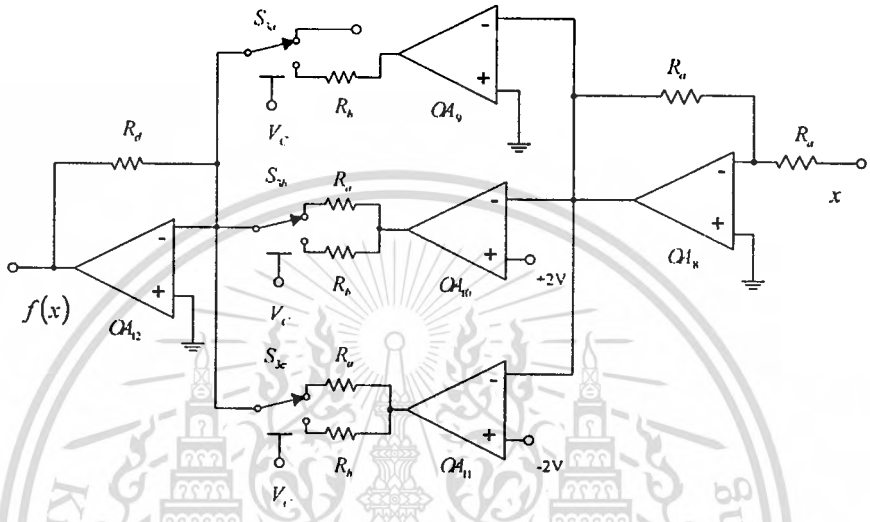

Fig. 3.10 The staircase function module

To generate a multiscroll chaotic attractor, the staircase function module shown in Fig 3.10 is employed to replace the programmable nonlinear function. The subsystem consists of operational amplifiers: OA9-OA11 realized as nonlinear functions described by equations (3.9.1a) (3.9.1b) to set the equilibria of chaotic systems of system (3.9) and (3.10). To make a module functioned using equations (3.9.1a) and equations (3.9.1b), one may set analog multiplexers S3a-S3c to connect with resistors Ra and Rb accordingly. For all functional modules, an operational amplifier LF 351 is supplied with the ± 15V supply voltage. The analog multiplexer in use is an IC CD4052 having two inputs multiplexed with the ± 12V supply voltage functioned as an automatic switch.

3.5 Simulation and Experimental Results

The proposed mixed-mode chaotic circuits have been simulated by PSpice and implemented in laboratory, thereby being confirmed and verified. In constructing the circuits shown in Fig. 3.7 and 3.8, LF 347 quad operational amplifiers were used as integrators and inverting amplifiers and

LF 351 as a comparator, along with a CD 4066 containing four analog electronic switches and a supply voltage of $\pm$ 15 V.

For the circuit scheme shown in Fig. 3.7, the valves of passive components of the first mixed-mode circuit are $R = R_1 = R_2 = 10k\Omega, R_3 = 90k\Omega$, $R_4 = 33k\Omega$, $R_5 = 100\Omega$, $C_2 = 6nF$, and $C_1 = C_3 = 3nF$. In the nonauotomous mode, the external periodic signals are set as $v_{ac} = 1V$ with $f = 5kHz$, and the controlled pulse used for toggled-switching in each mode is 2.5ms.

For the circuit scheme shown in Fig. 3.8, the values of passive components are $R = R_1 = 10k\Omega$, $R_2 = 12.5k\Omega$, $R_3 = 40k\Omega$, $R_4 = R_7 = 20k\Omega$, $R_5 = R_6 = 50k\Omega$, $C_1 = C_3 = 3nF$ and $C_2 = 6nF$. To assign the equilibria of the circuits, diodes D1-D4 are used to set the output voltages of the nonlinear function. The external periodic signal of the nonautonomous mode is $v_{ac} = 1V$ with $f = 5kHz$.

Figure 3.11 shows PSpice simulation of the voltage v_2 using the mixed-mode circuit of equations (3.11) and (3.12). In this simulation and experiment with the second circuit scheme for the three different modes, the control pulses generated for the three circuits are 5ms. As can be seen, the waveform of the voltage v_2 of the proposed scheme is shown in Fig. 3.11. The waveform of v_1 of the second circuit scheme are shown in Fig.3.12.

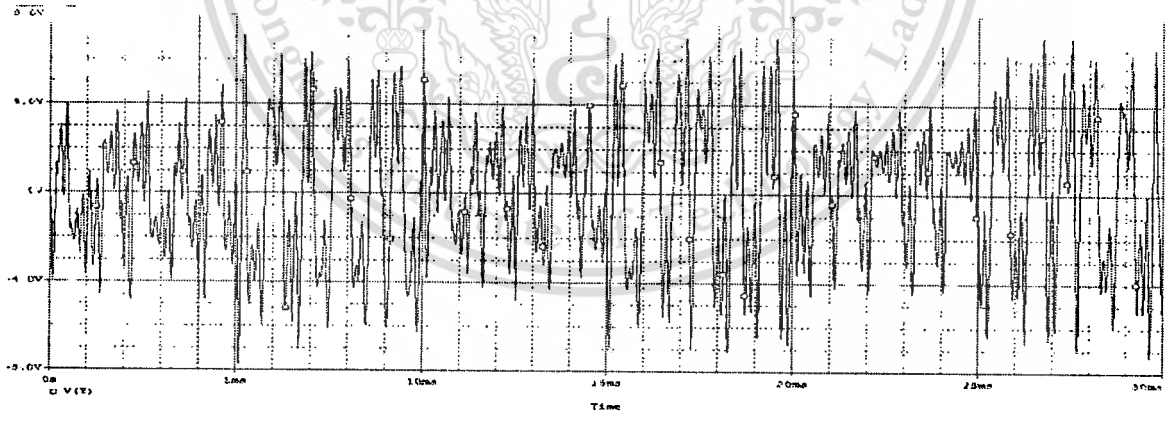

Fig. 3.11. PSpice simulation of v_2 of the mixed-mode circuit of equations (3.11) and (3.12)

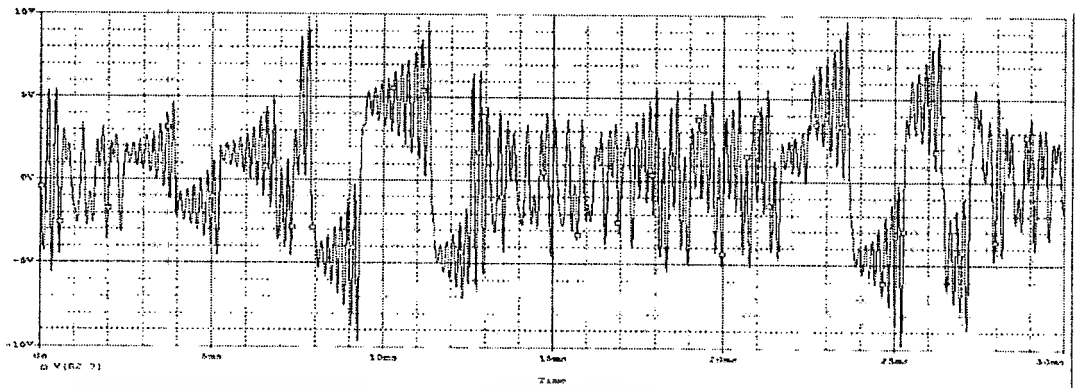

Fig. 3.12. Pspice simulation of v_1 of the mixed-mode circuit of equation (3.13),(3.14) and (3.15)

In the experiment, voltages are measured by using a digital storage and an analog oscilloscope. The upper track of the digital scope shows the waveforms of the mixed-mode v_2 and v_1 of the circuit, and the lower track of the digital scope shows the switching time of each mode. The phase portraits in each circuit, shown in Fig.3.13b are measured by an analog oscilloscope. The scales of the horizontal and vertical axes are 1/V. Figure 3.13a shows the experimental results of the first scheme of the mixed-mode chaotic circuit. The nonautonomous and autonomous modes are operated when the control voltage is high and low, respectively.

For the second scheme of the mixed-mode chaotic circuit, in the operation of the three mixed modes, the counter-3 is activated to control the electronic switches. In Fig.3.14 a-b, the nonautonomous mode is operated when the controlled voltages of the electronic switches are all high. Conversely, for the third-order autonomous circuit and the second-order autonomous circuit, the circuit is "on" whenever the control voltage is "low."

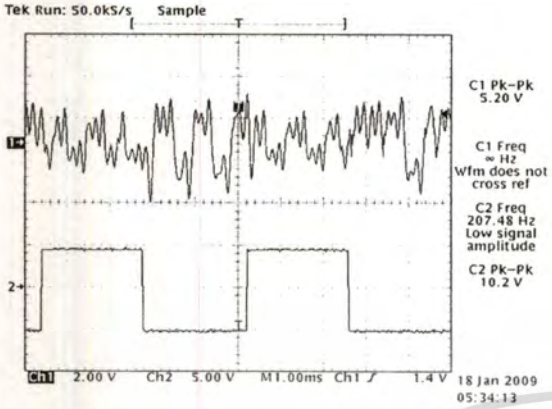

Fig. 3.13a Experimental results of Scheme 1 mixed-mode chaotic circuit for v_2

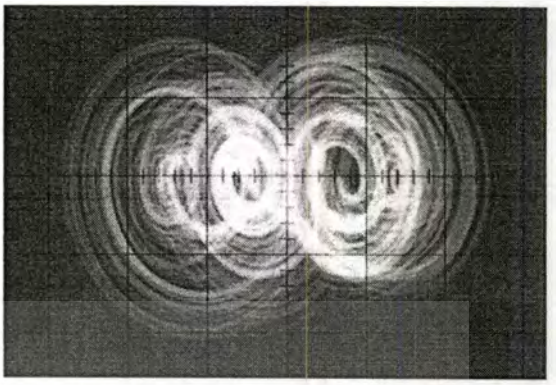

Fig 3.13b Chaotic attractors of Eqs. (3.9) and (3.10) on the $v_2 - v_3$ plane

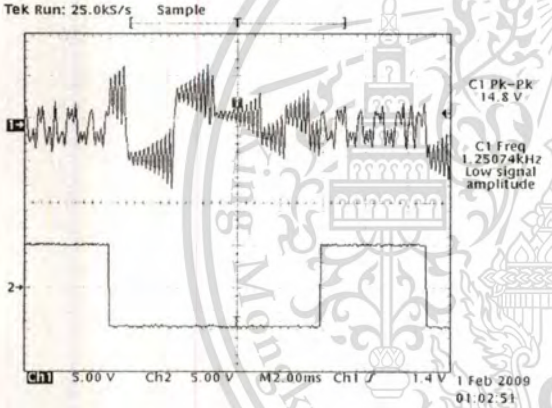

Fig. 3.14a. Experimental results of Scheme 2 mixed-mode chaotic circuit for v_1

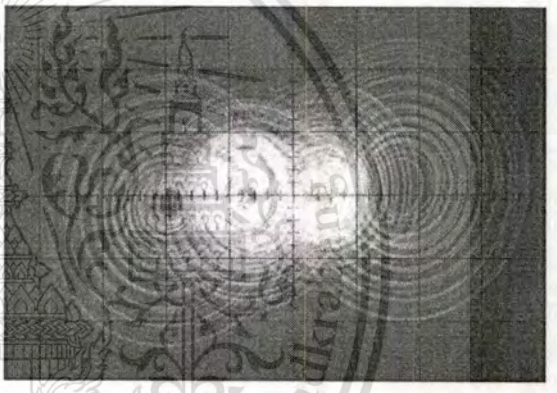

3.14b Chaotic attractors on the $v_1 - v_2$ plane

From the universal-mode chaotic circuit scheme shown in Fig. 3.9, the values of passive components of the circuit are $R_a = 10k\Omega$, $R_b = 20k\Omega$, $R_c = 50k\Omega$ $R_d = 1.5k\Omega$, $R_{f1} = 33k\Omega$, $R_{f2} = 100\Omega$, $R_{f4} = 50k\Omega$, R_{f3} (is variable resistor) $= 100k\Omega$, and $C_1 = C_2 = C_3 = 3nF$. In the nonauotomous mode with a sinusoidal source, the external periodic signals are set as $v_{ac} = 1V$ with $f = 5kHz$, with pulse driving is 2.5 ms. The external pulse signals are set as $v_{ac} = \pm 1V$ with $f = 1kHz$. In operation, the universal chaotic circuit starts operating in the third-order autonomous chaotic mode by setting the analog multiplex switch S_1 to position A. Wide ranges of scrolls are available depending on the choices of the selected programmable nonlinear functions. Those functional choices are the Heaviside, the signum, the hysteresis and the saturation functions having voltage gains 5 and 7. The Pspice simulation are shown in Fig 3.15a- 3.15e. The results of this experiment are shown in Figs 3.18a-3.18e respectively.

Replacing the programmable nonlinear function in the third-order autonomous chaotic system (3.9) by the staircase function in Fig 3.9, we obtain a three-scroll and a four-scroll attractor as shown in Fig 3.16a -b. The three-scroll and four-scroll attractor as shown in Fig 3.19a -b are generated by the system (3.9) using the nonlinear equations (3.9.1a) and (3.9.1b), respectively. Figures 3.19.c-d are two-dimensional grid scrolls which can be obtained by applying pulse signals to terminals $x_p(t)$ and $y_p(t)$.

To operate the universal circuit in the nonautonomous mode using the equation (3.10), the analog multiplex switch is set to position B. Figure 3.17 shows results of the chaotic oscillator by using Pspice simulation corresponding to the non-autonomous chaotic oscillator excited by the external pulse signal using the Heaviside or the signum functions. Meanwhile, Figures3.20a and 3.20b show results of the experiment. In Fig.3.17c, a double-scroll chaotic oscillator is obtained from the non-autonomous chaotic system using the signum function with the sinusoidal signal driving force. By using the staircase module instead, three- and four-scrolls are obtained and shown in Figs.3.20d and 3.17e, respectively. The results of the nonautomous mode using a sinusoidal driving input are shown in Fig.3.20 a-e.

In closing, the proposed schemes can be applied as educational kits for chaotic sciences and engineering education. The new patterns discovered in this dissertation can also be applied in true random number generator. Such examples will be given in Chapter 6.

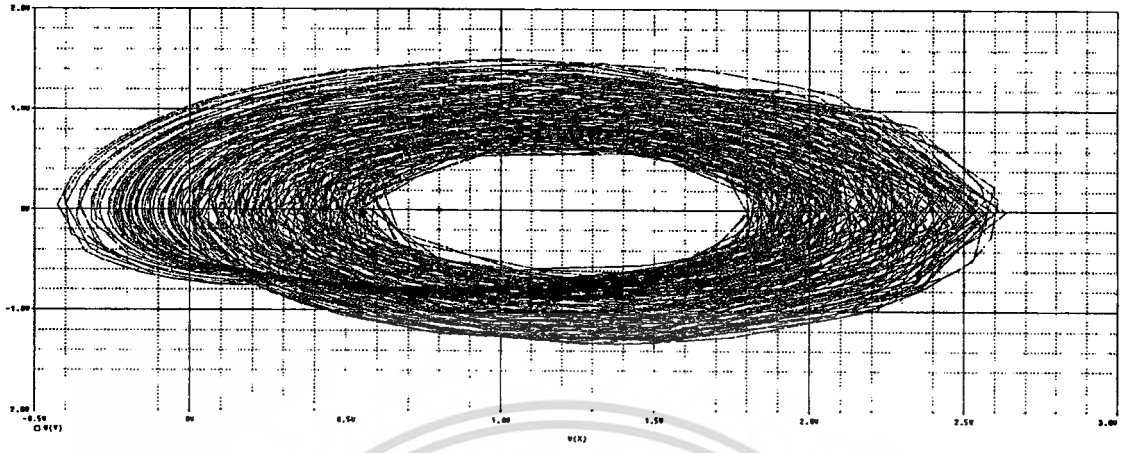

3.15(a)

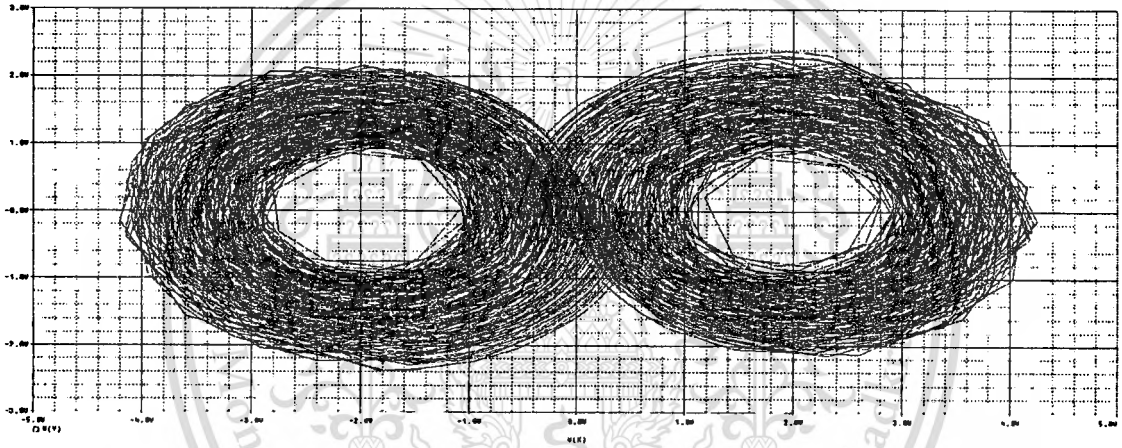

(b)

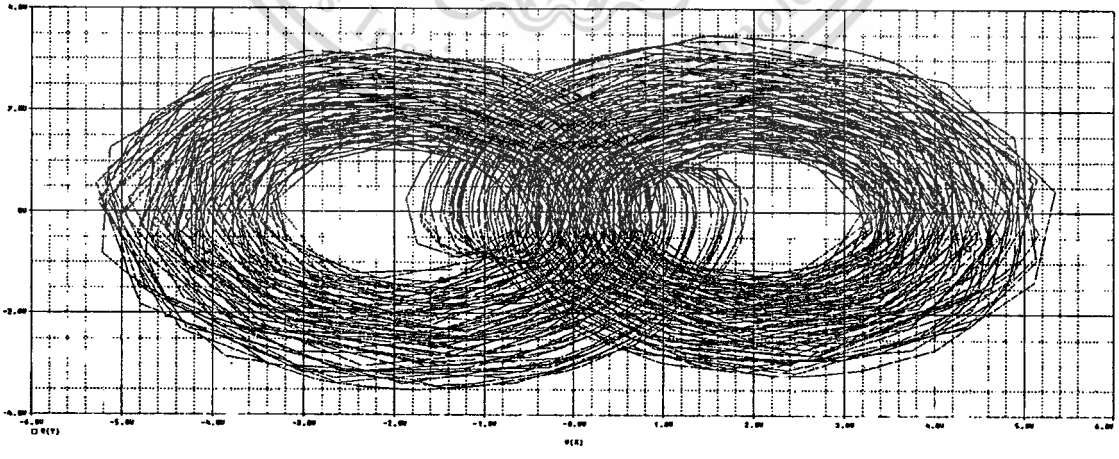

(c)

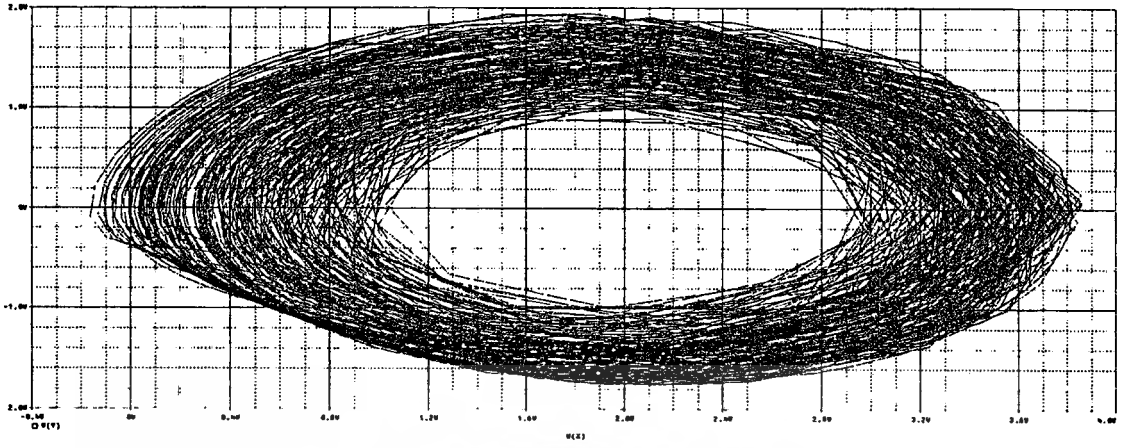

(d)

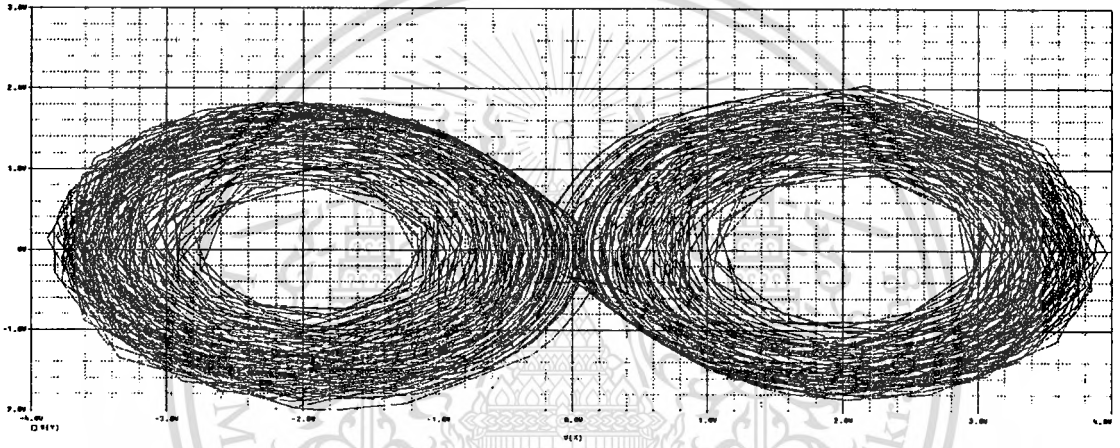

(e)

Fig 3.15 Pspice simulation results of the phase portrait on the x-y plane of the universal-mode circuit using (a) the Heaviside (b) the signum (c) the hysteresis, and (d) the saturation function with gain 5.2 and (e) the saturation function with gain 7

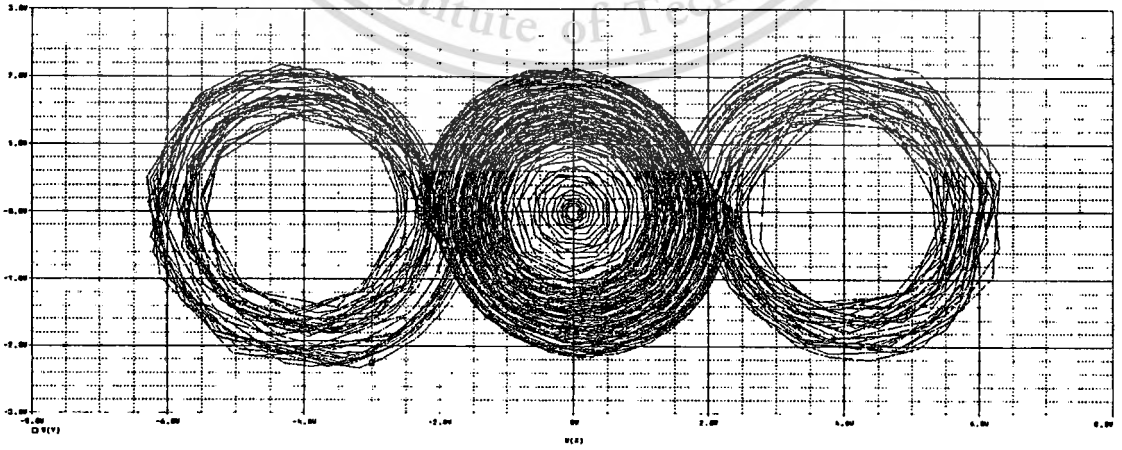

(a)

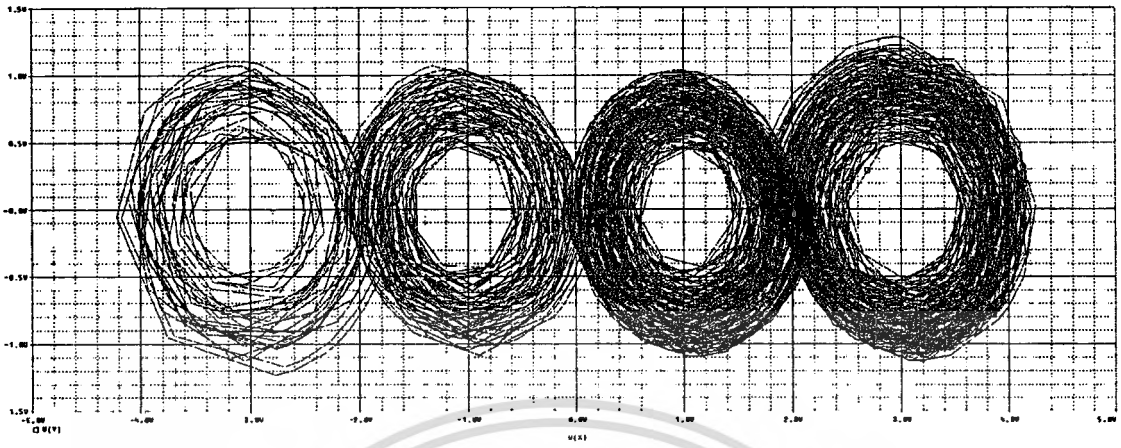

(b)

Fig 3.16 Pspice simulation results of the phase portrait on x-y plane of the universal-mode circuit with the staircase functions using Eqs.: (a) (3.10.a) (b) (3.10.b)

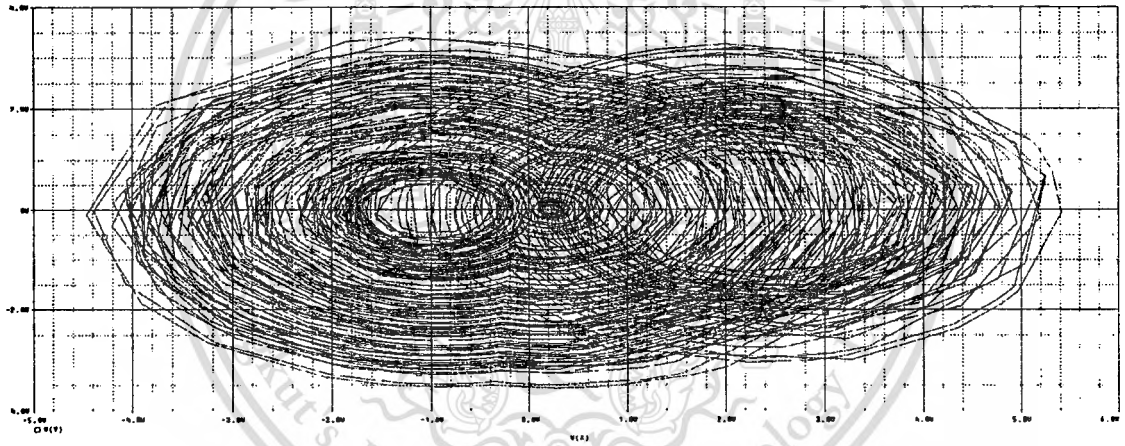

(a)

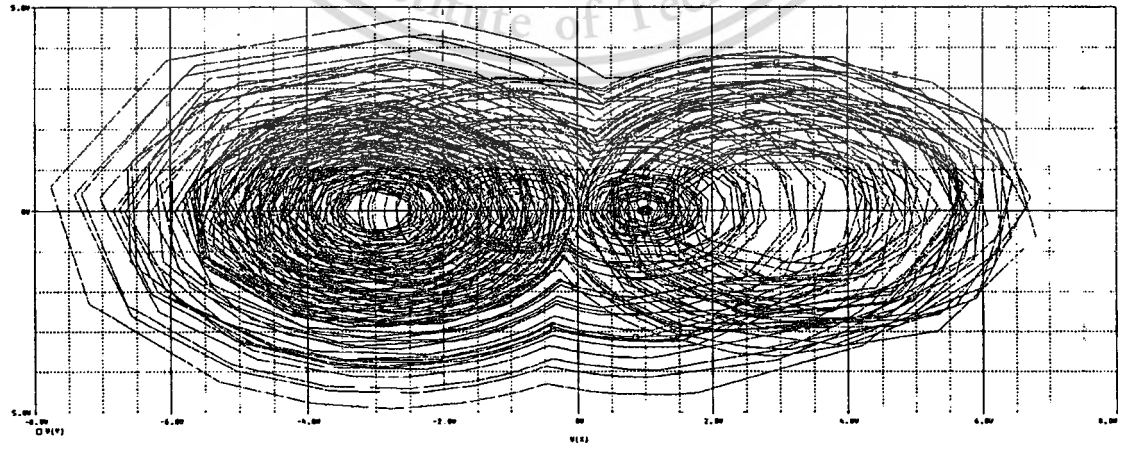

(b)

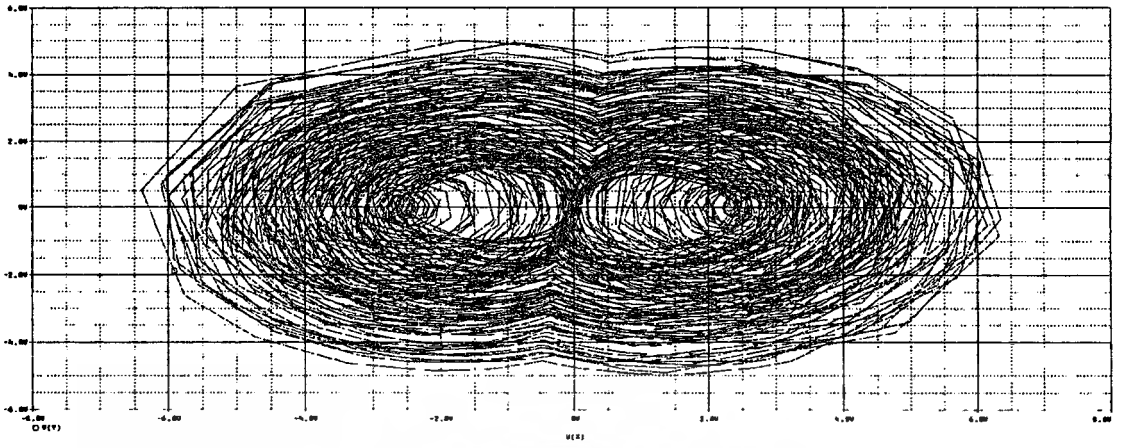

(c)

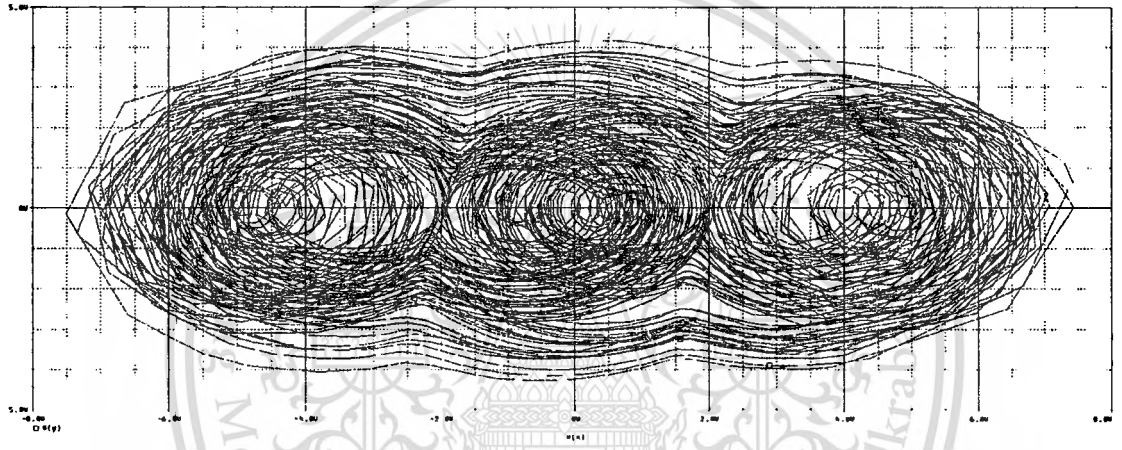

(d)

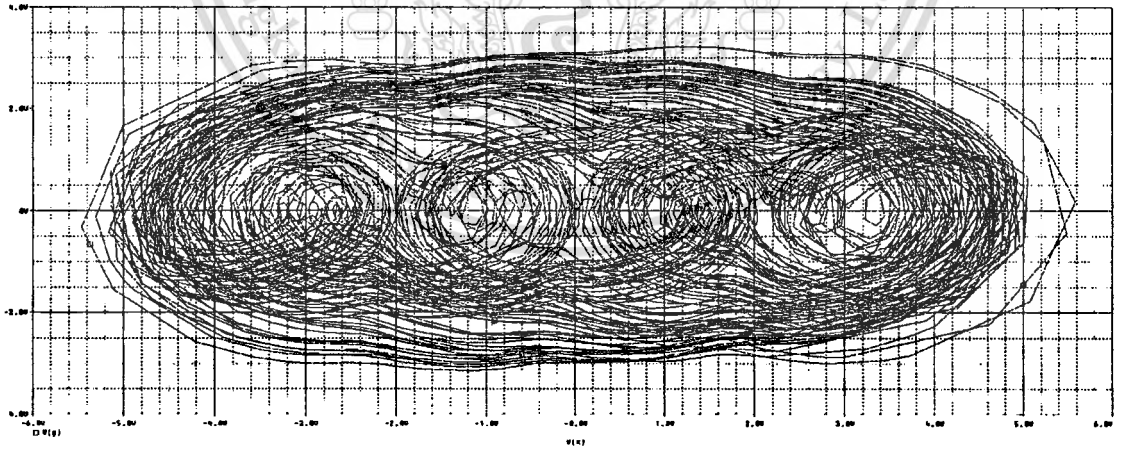

(e)

Fig 3.17 Pspice simulation results of phase portrait of the universal-mode circuit using (a) the Heaviside function (b) the signum function with the pulse drive, (c) the signum function (d) the staircase function (3.10a) (d) the staircase function (3.10b) by the sinusoidal driving on the x-y plane

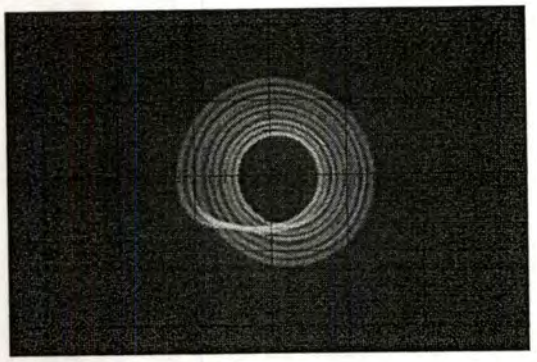

(a)

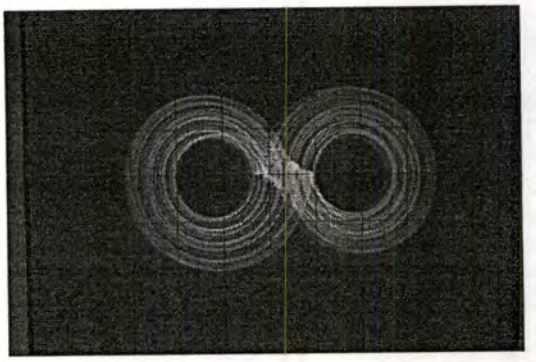

(b)

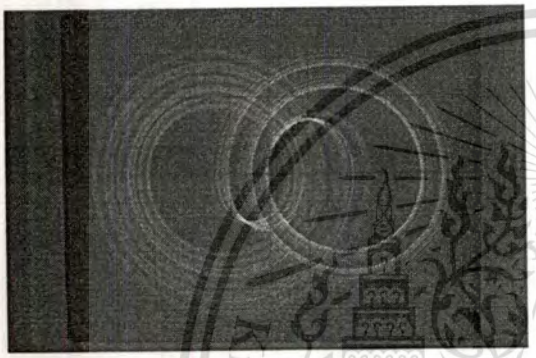

(c)

(d)

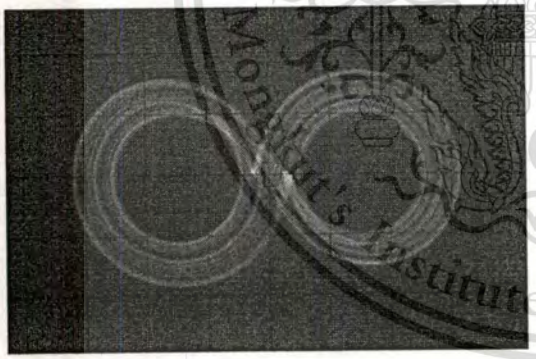

(e)

Fig. 3.18 Experiment results of the universal mode chaotic circuit in autonomous mode:
(a) using the Heaviside function
(b) using the signum function
(c) using the hysteresis function
(d) using the saturate function gain $k = 5.2$
(e) using the saturate function gain $k = 7$
Note that all subfigures are set the axes x=1V/div and y=1V/div.

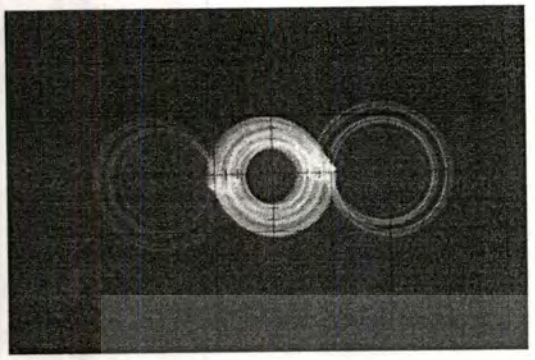

(a)

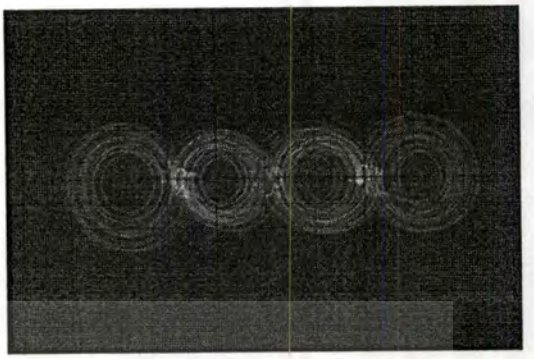

(d)

(c)

(d)

Fig. 3.19 Experiment results of universal mode chaotic circuit in multiscroll mode: (a) using the staircase function (3.9.1a) (b) using the staircase function (3.9.1b) (c) using the staircase function (3.9.1)h the $\pm 2V$ driving pulse for both $x_p(t)$ and $y_p(t)$ (d) using the staircase function (3.9.1b) with the $\pm 2V$ driving pulse both for $x_p(t), y_p(t)$ Note that: the axes of subfigures (a)-(d) are set x=2V/div and y=2V/div .

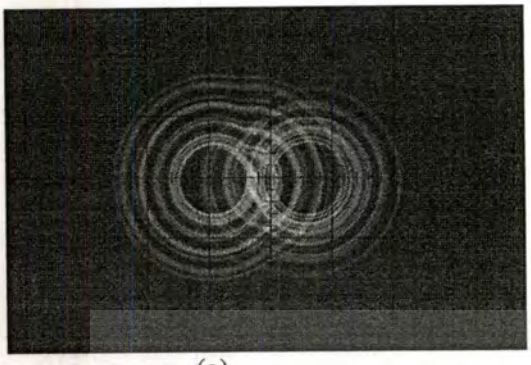

(a)

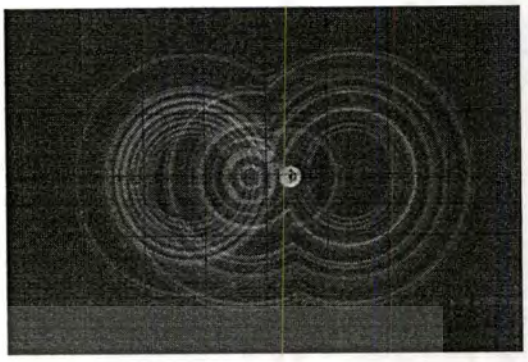

(b)

(c)

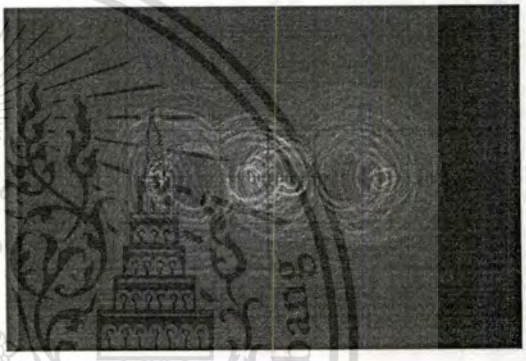

(d)

(e)

Fig. 3.20 experiment results of universal-mode chaotic circuit in non-autonomous mode:(a) using heaviside function with driving pulse signal

(b) using signum function with driving pulse signal

(c) using signum function with driving sinusoidal signal

(d) using staircase function (1.5a) with driving sinusoidal signal

(e) using staircase function (1.5b) with driving sinusoidal signal

Note that axis x=2V/div,y=2V/div.

3.6 Summary

This chapter has presented two schemes of a mixed-mode and universal-mode chaotic circuit , designed based on quadrature structures. These schemes are simple and easy to implement. In mixed-mode circuit, the first circuit scheme can realize both nonautonomous and autonomous chaotic oscillators, while the second scheme can realize one nonautonomous and two autonomous chaotic oscillators respectively. In universal mode both of nonautonomous and autonomous chaotic oscillators can be selected from programmable nonlinear function. Both simulation and experimental results have confirmed the effectiveness of the new design and the feasibility of the implementation of the mixed-mode schemes.

Chapter 4

Construction of the Multi-wing Liu Attractor

A topic of construction of complex chaotic attractors is one of interesting topics in chaotic dynamics community, because it is useful for applications in secure communication and truly random number generators. To increase complex dynamics, one may do so by increasing an equilibrium using a staircase function to increase a number of scrolls of the chaotified system as shown in Chapter 3. From Lorenz based system, the generating complex scroll is first demonstrated by [27] called proto-Lorenz system, which is a quotient of the Lorenz dynamical system and can be obtained three or four scrolls. To create of complex butterfly based on the Lorenz type, Elwalkil[28] rearranges a cross product term xz using an absolute function and a term xy using a signum function. In doing so, four-wing attractor is obtained by switching a signum function with the external pulse. The fully autonomous of the Elwalkil complex butterfly attractor is modified by embedding the state control binary switch [29]. To extend a Lorenz system as a generalized Lorenz for generating complex wings, Lu[30] proposes a three-dimensional quadratic autonomous ordinary equation which can produce two- or four-wings under control of a simple constant input. In order to increase m-wings of the Lorenz based system, Yu[31] designs a multi-segment quadratic function to replace the cross product term. In this chapter, in merit of the multi-wings butterfly attractors, we propose a new multi-wing chaotic attractor which is constructed from the butterfly type called Lui attractors.

4.1 Liu system

A Lui's chaotic attractor [32] which is a butterfly-like attractor can be described as

$$\begin{aligned} x' &= -ax + ay \\ y' &= bx - kxz \\ z' &= -cz + hx.^2 \end{aligned} \tag{4.1}$$

where x, y, z are state variables and a, b, c, h, k are constant parameters. The nonlinear terms are a cross product xz and a square x^2. The divergence of the system (4.1) is given by

$$\nabla V = \frac{\partial x'}{\partial x} + \frac{\partial y'}{\partial y} + \frac{\partial z'}{\partial z} = -(a+c). \qquad (4.2)$$

Setting parameters $a = 10, b = 40$ $c = 3, h = 4, and\ k = 1.0$, we then have $\nabla V = -13$. Since its valve is negative; therefore dynamical system (1) is dissipative. The Lyapunov exponents of this chaotic system are

$$\lambda_{L1} = 1.643, \lambda_{L2} = 0, \lambda_{L3} = -14.42.$$

Given the set of parameters above, the simulation for the system (4.1) shows the chaotic attractor in Fig 4.1.

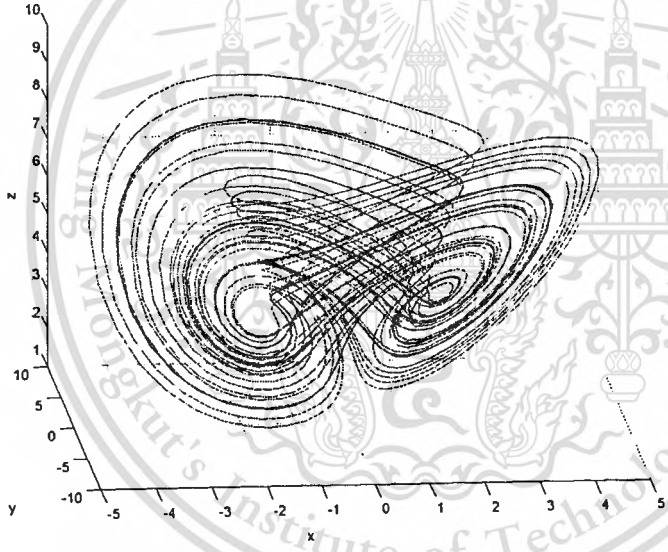

Fig 4.1. The Liu attractor

By setting $x' = 0, y' = 0, z' = 0$, the system has three equilibrium points which are described as $(0,0,0), (\pm\sqrt{\frac{bc}{hk}}, \pm\sqrt{\frac{bc}{hk}}, \frac{b}{k})$.

To investigate the characteristics of the equilibrium points, the Jacobian matrix of the system (4.1), evolved at zero equilibrium is

$$J_0 = \begin{bmatrix} -a & a & 0 \\ b & 0 & 0 \\ 0 & 0 & -c \end{bmatrix} = \begin{bmatrix} -10 & 10 & 0 \\ 40 & 0 & 0 \\ 0 & 0 & -3 \end{bmatrix} \tag{4.3}$$

The characteristic equation of J_0 is

$$|\lambda I - J| = \lambda^3 + (a+c)\lambda^2 + (ac-ab)\lambda - abc\,. \tag{4.4}$$

The eigenvalves of the Jacobain matrix are 27.839, 3.963 and 10.875. Therefore the zero equilibrium is an unstable saddle point. At non equilibrium points, P^+, P^-, the Jacobian matrix equals to

$$J^{\pm} = \begin{bmatrix} -a & a & 0 \\ b-kz & 0 & -kx \\ 2hx & 0 & -c \end{bmatrix} = \begin{bmatrix} -10 & 10 & 0 \\ 0 & 0 & -5.42 \\ 43.81 & 0 & -3 \end{bmatrix} \tag{4.5}$$

when $x = 5, y = 5, and\ z = 40$. The characteristic equation of $J^{\pm}$ is

$$|\lambda I - J| = \lambda^3 + (a+c)\lambda^2 + (ac-ab+akz)\lambda + 2ahkx^2 + ackz - abc\,. \tag{4.6}$$

The eigenvalves corresponding to nonzero equilibrium points are -18.4348 , 2.7174 $\pm$j 11.0817 which is the index-2 exhibited an unstable saddle focus.

4.2 Multi-wing Liu Attractor

From the Lorenz liked family system, the common characteristics are the following:

1. The nonlinear terms are smooth functions.

2. The number of three equilibria produce a double wing attractor.

All Lorenz-liked family systems are a symmetrical attractor and nonzero equilibrium. The system is the index-2 and location is related to a nonlinear term. In order to generate a multi-wing attractor, we increase an equilibrium point of the system in (4.1) by modifying the square term into a multi-segment nonlinear function. The four-dimensional autonomous chaotic system is described by

$$\begin{aligned} x' &= -ax + ay \\ y' &= bx - kxz \\ z' &= -cz + hf(x). \end{aligned} \quad , \tag{4.7}$$

where constant parameters a, b, c are the same parameters as those of the system (4.1) and h, k are rescaled to 7 and 10, respectively. The multi-segment nonlinear function can be expressed as

$$f(x) = m|x| - \sum_{i=1}^{n} m\left(1 + \frac{1}{2}\text{sgn}(x-i) - \frac{1}{2}\text{sgn}(x+i)\right), \tag{4.8}$$

and

$$abs(x) = \begin{cases} x & x \geq 0 \\ -x & x < 0 \end{cases},$$

and

$$\text{sgn}(x) = \begin{cases} 1 & x \geq 0 \\ -1 & x < 0. \end{cases}$$

Setting $a = 10, b = 40, c = 3, k = 10, h = 7$ and the multi-segment nonlinear function $f(x)$ for generating 4, 6 and 8 wings, when n= 1,2,3, are $f_1(x), f_2(x), and\ f_3(x)$ respectively:

$$f_1(x) = 4|x| + 2(\text{sgn}(x+2) - \text{sgn}(x-2)) - 4, \tag{4.9.1}$$

$$f_2(x) = 4|x| + 2(\text{sgn}(x+1) - \text{sgn}(x-1)) + 2(\text{sgn}(x+2) - \text{sgn}(x-2)) - 8. \tag{4.9.2}$$

$$\begin{aligned} f_3(x) = {} & 4|x| + 2(\text{sgn}(x+1) - \text{sgn}(x-1)) + 2(\text{sgn}(x+2) - \text{sgn}(x-2)) \\ & + 2(\text{sgn}(x+3) - \text{sgn}(x-3)) - 12). \end{aligned} \tag{4.9.3}$$

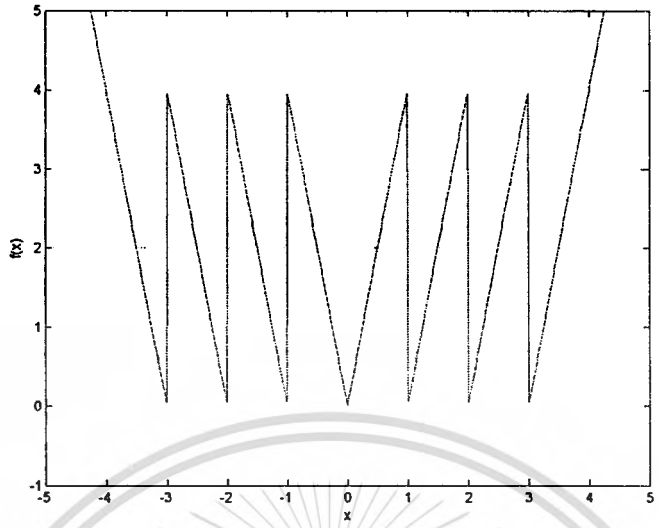

Fig. 4.2 A multi-segment nonlinear function

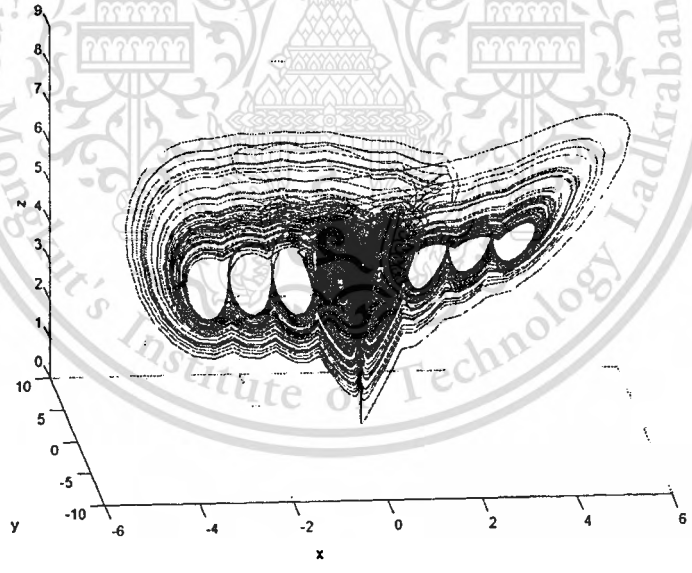

Fig. 4.3 A multi-wing Liu attractor

The numerical simulation of an 8-wing chaotic attractor using the multi-segment function $f_3(x)$ is shown in Fig. 4.3.

The zero equilibrium of the system (4.7) is (0,0,0). From equation (8), the non zero equilibrium points of the multi-wing Liu system (4.7) can be expressed $(\pm P_1, \pm P_1, \frac{b}{k})$,where $P = \frac{cb}{mkh} + i.$

The eight equilibrium points of the 8-wings chaotic attractor are:

$$Q_{\pm 1} = \pm 0.4286,\ \pm 0.4286,\ 4;$$
$$Q_{\pm 2} = \pm 1.4286,\ \pm 1.4286,\ 4;$$
$$Q_{\pm 3} = \pm 2.4286,\ \pm 2.4286,\ 4; \text{ and}$$
$$Q_{\pm 4} = \pm 3.4286,\ \pm 3.4286,\ 4.$$

The Jacobian matrix at the nonzero equilibrium is equal to

$$j = \begin{bmatrix} -a & a & 0 \\ b - kz & 0 & -kx \\ f(x)h & 0 & -c \end{bmatrix} \tag{4.10}$$

and the characteristic equation of the non zero equilibrium is

$$|\lambda I - J| = \lambda^3 + (a+c)\lambda^2 + (ac - ab - akz)\lambda + m\,\mathrm{sgn}(x)ahkx + ackz \tag{4.11}$$

The corresponding eigenvalves for each equilibrium point can be obtained as

$Q_{\pm 1}$:-15.8729, j1.4364 $\pm$ 8.5754;

$Q_{\pm 2}$:-20.8018, j3.9009 $\pm$13.3069;

$Q_{\pm 3}$:-23.7715, j5.3858 $\pm$16.0328; and

$Q_{\pm 4}$:-26.0231, j6.5116 +18.0694.

And results show that the equilibrium points are the index-2.

The system (4.7) leads to chaos with Lyapunov values shown in Table

Table 4.1 Number of wings versus Lyapunov exponents

Number of wing	Lyapunov exponents
4	$\lambda_1 = 14.931, \lambda_2 = 0, \lambda_3 = -27.203$
6	$\lambda_1 = 15.799, \lambda_2 = 0, \lambda_3 = -26.819$
8	$\lambda_1 = 14.931, \lambda_2 = 0, \lambda_3 = -27.203$

4.3 Circuitry Implementation

The dynamic behavior of the proposed chaotic attractor have been confirmed by an electronic circuit, as shown in Fig.4. In Fig. 4a, the integrator, the summing and the inverting amplifiers are realized by operational amplifiers. Multipliers are implemented by IC AD633.

The four state variables x, y, z can be obtained from each output of the integrator circuits. In order to satisfy the dynamical range of the circuit operation, the state variables are scaled by assigning v_{C1}, v_{C2} and v_{C3} as $v_{C1} = \frac{x}{10}, v_{C2} = \frac{y}{10}, v_{C3} = \frac{z}{10}$ then chaotic system is

$$\begin{aligned} \dot{v}_{C1} &= \frac{1}{R_1 C_1}\left[-\frac{R_6}{R_4} v_{C1} + \frac{R_6}{R_5} \dot{v}_{C2}\right] \\ \dot{v}_{C2} &= \frac{1}{R_2 C_2}\left[\frac{R_9}{R_7} v_{C1} - \frac{k_m R_9}{R_8} v_{C2}\right] \\ \dot{v}_{C3} &= \frac{1}{R_3 C_3}\left[\frac{R_{12}}{R_{10}} v_{C3} - \frac{R_{12}}{R_{11}} f(x)\right] \end{aligned} \tag{4.12}$$

where k_m is a scaling factor of an analog multiplier and is equal to1/10, the R_1C_1, R_2C_2, R_3C_3 are time constants of the integrator circuits. The values of electronic components are:

$R_1 = R_2 = R_3 = 100k\Omega, R_4 = R_5 = R_6 = R_7 = 10k\Omega$ $R_8 = 4k\Omega, R_9 = 40k\Omega, R_{10} = 50k\Omega,$

$R_{11} = 22k\Omega,$ $R_{12} = 15k\Omega$ and $C_1 = C_2 = C_3 = 1nF$.

To implement the nonlinear function from equation (4.8), the equation is rewritten as

$$f(x) = m|x| + \sum_{i=1}^{n} m\left(\frac{1}{2}\mathrm{sgn}(x-i) - \frac{1}{2}\mathrm{sgn}(x+i)\right) - n \times m. \tag{4.13}$$

The nonlinear function $f(x)$ is depicted in Fig. 4(b). The absolute is realized by a precision full wave rectifier and the sign function is realized by a voltage comparator. The operational amplifier is LF351 operated within ± 15 V range having saturation voltage at 13.5 V. In Fig.4.4b, the comparator blocks depend on numbers of wings of the attractor. Voltage references at each comparator is $+n$ or $-n$. And the output voltage is normalized by setting gains of differential amplifiers.

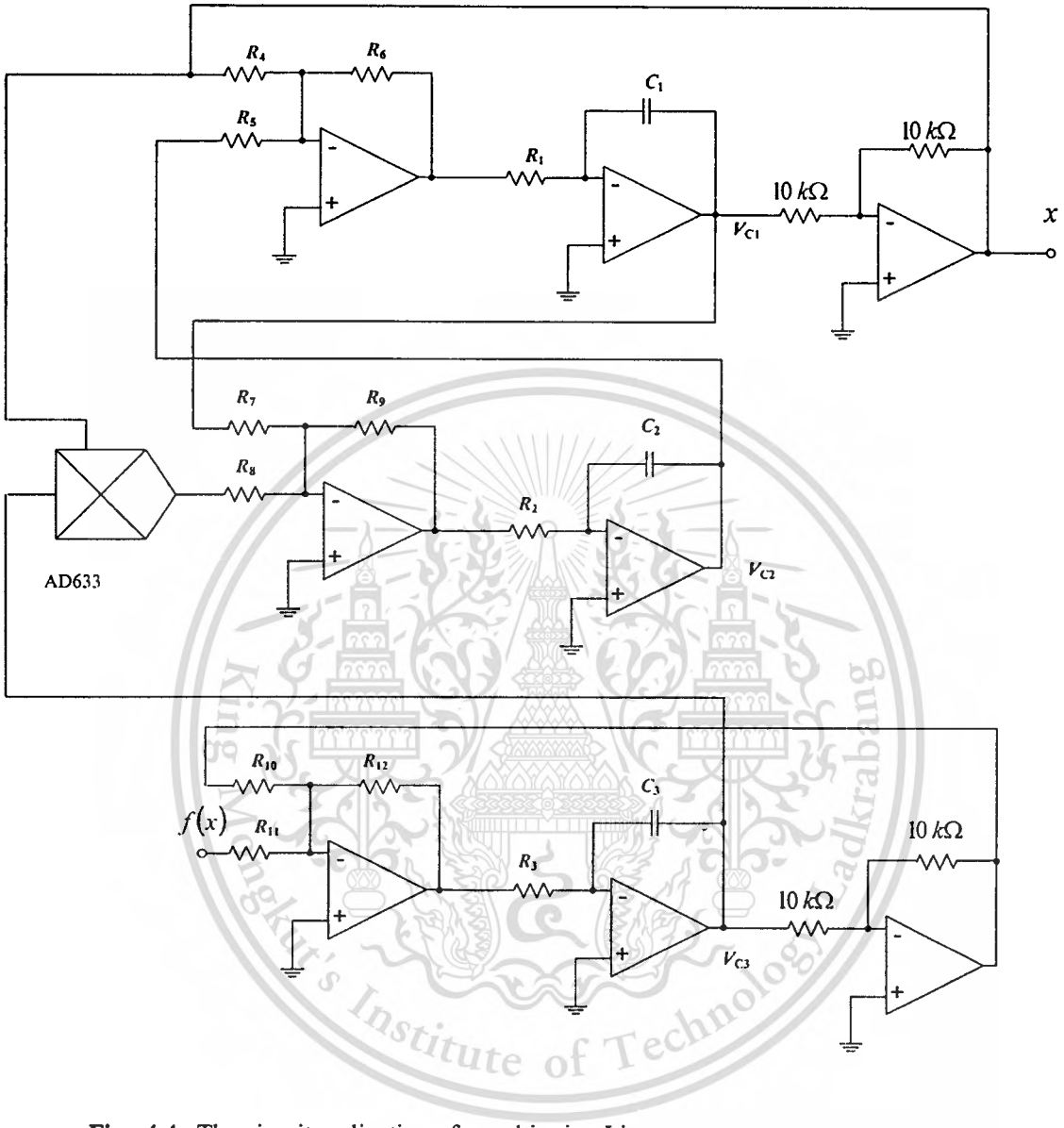

Fig . 4.4a The circuit realization of a multi-wing Liu attractor

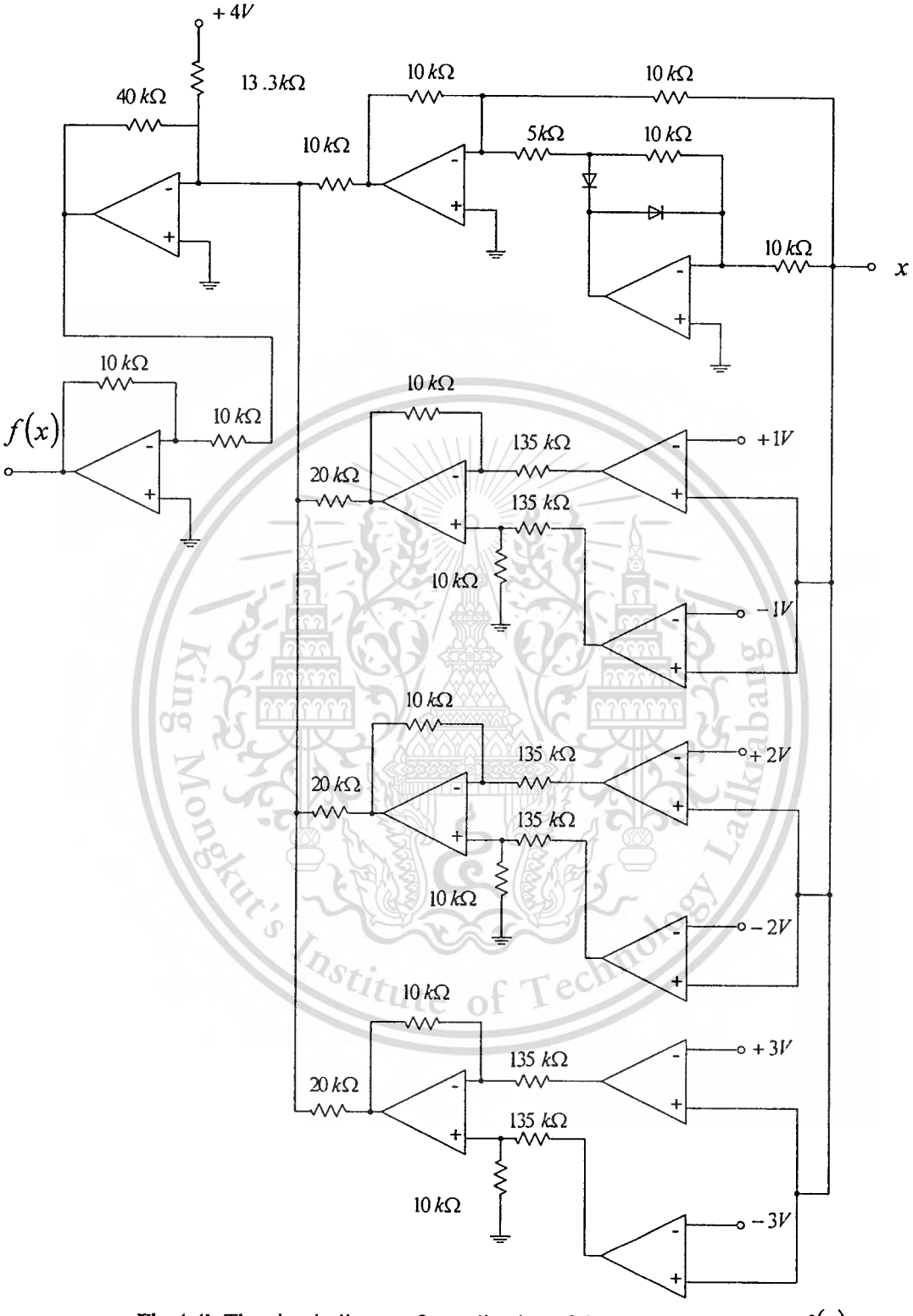

Fig 4.4b The circuit diagram for realization of the nonlinear function $f(x)$

4.4 Simulation and experiment results

The simulation results of the proposed circuit using Pspice show state x and z in Fig 4.5. Fig 4.6 show the experiment result of the multi-wing Liu attractor on the *x-z* plane. Note that the system design and implement in this chapter has been conducted the work independently and was coincidently initiated by the author contemporarily. However, the work was first published by Yu in 2008 [33]. Here we have the same results.

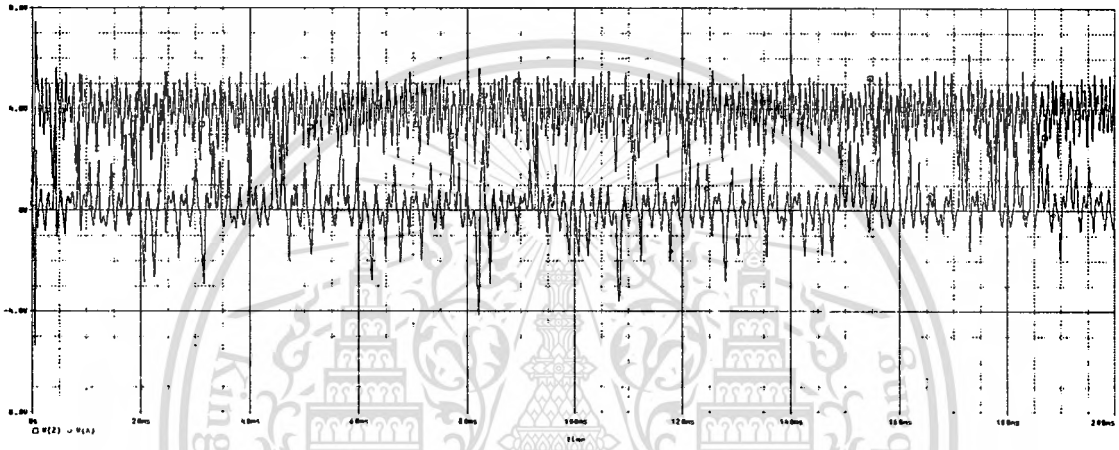

Fig 4.5 PSpice simulation of v_x and v_z of the multi-wing Liu circuit

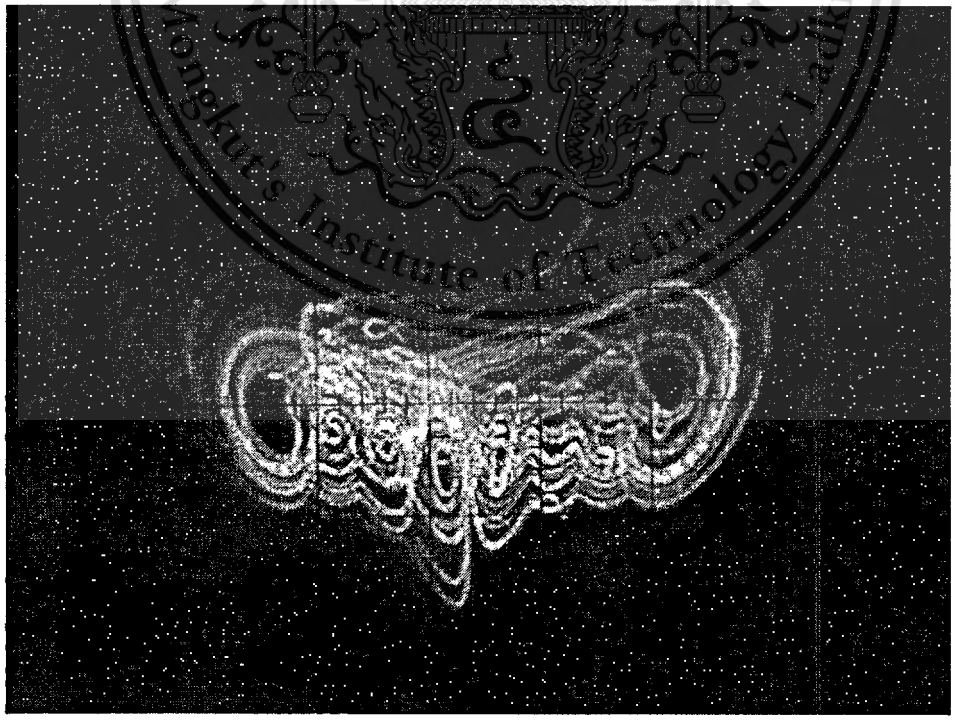

Fig. 4.6 An experiment result of the multi-wing Liu circuit

4.5 Summary

In this chapter, a multi-wing Lui attractor based on increasing equillibria of the saddle point index-2 using multi-segment nonlinear has been proposed. Numerical simulation using Matlab and PSpice for verification of the design is carried out. With rich dynamics provided by the system, this complex system may be applied for application in secure communication.

Chapter 5

Constuction of a Chaotic Attractor from the Van der Pol System

In this chapter, we propose three new chaotic attractors. Chaotification or anti- control can change a non-chaotic system into a chaotic one. The first proposed chaotic system can be considered as changing a second-order Shaw Van der Pol system to a third-order nonlinear system by adding a new state. The second proposed system can be obtained by extending the Van der Pol system to the jerk architecture. The third, we propose a novel hyper-chaotic system, which is simple to construct by modifying Van der Pol oscillator to be the forth-order system. Eventually, the stable system is turned to be an unstable one. The hyper-chaotic property is verified by calculating its Lyapunov exponent spectrum.

In the first proposed system, the variable mode chaotic system is selected between driving Shaw Van der Pol and an autonomous double scroll third-order Van der Pol chaotic system. A multiscroll chaotic attractor can be obtained from the second-proposed system by modifying a nonlinear function to be a multi-segment nonlinear function. All three proposed systems are simulated using Pspice. The experiment is also carried out to confirm the results by using electronic circuits.

5.1 The Van der Pol System

The Van der Pol system [34] as, a special case of Lienard equation, is described by the second order differential equation:

$$x'' + \mu(x^2 - 1)x' + x = 0. \qquad (5.1)$$

where μ is a damping coefficient and the equilibrium point is $(0,0)$. When $0 < \mu < 2$, the equilibrium point is an unstable focus, the system (5.1) exhibits a limit cycle.

The Shaw Van der Pol chaotic system is discovered by Shaw [35] which is a non-autonomous chaotic system, defined as follows:

$$\begin{aligned} x' &= y + A\sin wt \\ y' &= -x + y - x^2 y \end{aligned} \qquad (5.2)$$

In addition, the Van der Pol:VdP system (5.1) can be performed chaotic behaviors by driving with external force[36], coupling with Duffing oscillator[37] or using chaotification of the modified third-order system [38]. To show construction of a chaotic attractor from VdP system, we propose a new chaotic system in Sections 5.2-5.4; the circuit implementation in Section 5.5; and simulation and experimental results in Section 5.6.

5.2 Construction of Chaotic Attractor from the Extended Shaw Van der Pol System

From Shaw VdP system of Eq. (5.2), the nonlinear term of the system (5.2) is $x^2 y$. We then replace the term x^2 by an absolute function, we now have

$$\begin{aligned} x' &= y + A\sin wt \\ y' &= -x + y - f(x)y \end{aligned} \qquad (5.3)$$

where A is amplitude and w is the angular frequency. And $f(x)$ can be expressed as

$$f(x) = \begin{cases} x & x \geq 0 \\ -x & x < 0 \end{cases}. \qquad (5.4)$$

In order to obtain an autonomous chaotic attractor, we introduce a feedback controller state z. Thus the three-dimensional autonomous chaotic system is described by

$$\begin{aligned} x' &= y + az \\ y' &= -x + y - f(x)y \\ z' &= bx + cy \end{aligned} \qquad (5.5)$$

Here a, b, c are constant parameters. When $f(x)$ is an absolute function and $a = 1, b = -1$ and $c = -2$. The system in equation (5.5) exhibits a double-scroll chaotic attractor. To synthesis a multi-scroll attractor, we modify $f(x)$ to be a multi-segment nonlinear function which can be expressed as

$$f(x) = m_0|x| + \sum_{i=1}^{n} m_i(\mathrm{sgn}(x + a_i) - \mathrm{sgn}(x - a_i)) + k. \qquad (5.6)$$

The nonlinear function consists of an absolute function and a sign function

$$\operatorname{sgn}(x)=\begin{cases}1 & x\geq 0\\ -1 & x<0.\end{cases} \tag{5.7}$$

When $a=10, b=-1, and\ c=-2$, to obtain four scrolls from a multi-segment nonlinear function, we set $f(x)$ as

$$f(x)=2|x|+2(\operatorname{sgn}(x+2)-\operatorname{sgn}(x-2))-4 \tag{5.8}$$

Simulation results using Matlab for each case are shown in Figs. 5.1- 5.2.

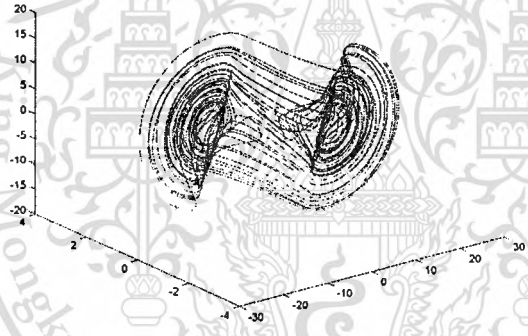

Fig. 5.1 A double-scroll attractor by means of the extended VdP system

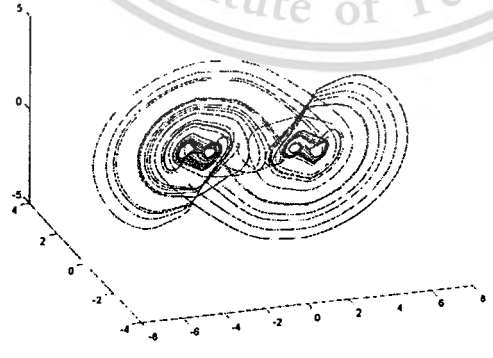

Fig. 5.2 A multi-scroll attractor by means of the extended VdP system

5.3 A New VdP-Type Multi-scroll Chaotic Circuit

In this section, another new multi-scroll VdP-type based on the VdP system is proposed. According to the VdP system in equation (5.1), we convert the form to the Jerk system as

$$x''' = x'' + \mu(x^2 - 1)x' + x \tag{5.9}$$

We set $\mu = 1$, and define $f(x)$ as a nonlinear term, the equation (5.9) can be rewritten as

$$\begin{aligned} x' &= y \\ y' &= z \\ z' &= -x + y - z - f(x)y \end{aligned} \tag{5.10}$$

To chaotify, we add the state z into the change of the state x

$$\begin{aligned} x' &= ay + bz \\ y' &= cz \\ z' &= -x + y - z - f(x)y \end{aligned} \tag{5.11}$$

where a, b, and c are bifurcation parameters, and $f(x)$ is a PWL function given by

$$f(x) = 2|x| - 4(|x+2| - |x-2|) + 5(|x+2.5| - |x-2.5|) - 9. \tag{5.12}$$

The present case focuses on generating a four-scroll attractor. There is an equilibrium point at the origin (0,0,0). To illustrate the chaotic behavior of the system, from now on throughout this paper, we set $a = 1.2, b = -2.6, c = 40$. The Lyapunov exponents of the system, LE_1, LE_2 and LE_3 are equal to 0.898078, -0.050844, and -1.847504, respectively. The sum of all LE is less than -1, implied the dissipative property of the variation of volume ∇V which can be determined by the divergence of the orbital flow:

$$\nabla V = \frac{\partial x'}{\partial x} + \frac{\partial y'}{\partial y} + \frac{\partial z'}{\partial z} < -1 \tag{5.13}$$

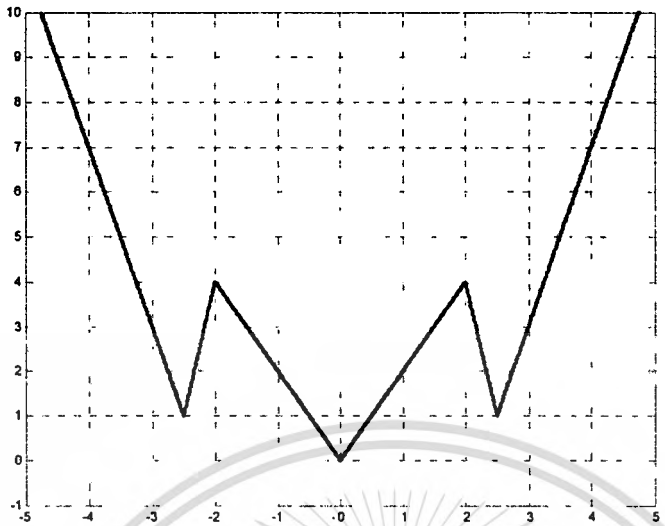

Fig 5.3 The PWL function used for the new VdP multi-scroll system

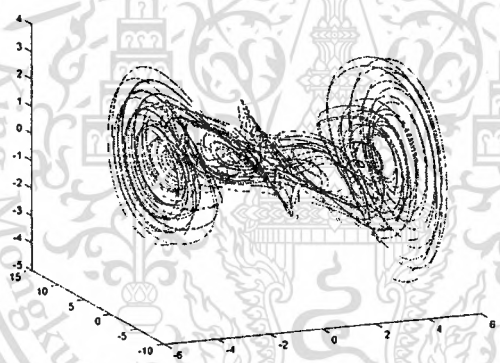

Fig. 5.4 A multi-scroll attractor by chaotifying VdP system

5.4. The Modified Hyper Van der Pol System

In order to generate a hyper-chaotic attractor, a dynamic system requires the minimum number of the coupled first-order autonomous ordinary differential equations to be four. We convert the Van der Pol system into the fourth order hyper-jerk equation as

$$x'''' = x''' + x'' + \mu(x^2 - 1)x' + x. \qquad (5.14)$$

By setting $\mu = 1$, modifying x^2 to be $|x|$, changing new variables $x' = y, x'' = z, x''' = w$, the hyperjerk Van der Pol equation can be transformed into the fourth-variable first-order system equation:

$$\begin{aligned} x' &= y \\ y' &= z \\ z' &= w \\ w' &= -x + y - z - w - |x|y. \end{aligned} \tag{5.15}$$

To create hyper-chaotic behaviors, we chaotify system (5.15) by modifying two terms and adding three more terms to the system, we now have

$$\begin{aligned} x' &= ay + bz + cw \\ y' &= dz + w \\ z' &= w \\ w' &= -x + y - z - w - |x|y. \end{aligned} \tag{5.16}$$

The system (5.16) has only one equilibrium point $E_0 = (0,0,0,0)$. Linearizing the system (5.16) at the equilibrium yields the Jacobian matrix

$$j = \begin{bmatrix} 0 & a & b & c \\ 0 & 0 & d & 1 \\ 0 & 0 & 0 & 1 \\ -(1+\operatorname{sgn}(x)y) & (1-|x|) & -1 & -1 \end{bmatrix}. \tag{5.17}$$

The eigenvalues of the matrix are obtained by solving the characteristic equation

$$\lambda^4 + \lambda^3 + c\lambda^2 + (a + b - d)\lambda + ad = 0. \tag{5.18}$$

To generate chaotic behavior, the system (5.16) should be unstable or eigenvalves of the system stay on the right half of the complex plane. According to Routh-Hurwitz criteria, the real part of eigenvalues must be positive, when $c < 0, and\ a + b < d$. We choose $a = 1.2, b = -1.5, d = 1$ and

c is the tuning parameter. Note that, to confirm the chaotic behavior, LE characterizing the stability properties is computed by the algorithm in [39]. For a chaotic system, there are one positive, one zero, and two negative Lypunov exponents. For hyper-chaotic system, there are two positive values in four Lyapunov exponents. The computational results of the system (5.16) are shown in Table 5.1.

Table 5.1 Lyapunov values of the systems

c	LE_1	LE_2	LE_3	LE_4	State
-0.1	0.0583	0.0461	0	-0.9727	Hyper-chaos
-0.2	0.1573	-0.0352	0	-0.9853	Chaos
-0.3	0.2016	0.0027	0	-0.9923	Hyper-chaos
-0.4	0.2324	0.0185	0	-0.9932	Hyper-chaos
-0.5	0.2563	0.0098	0	-0.9899	Hyper-chaos
-0.6	0.2676	0.0272	0	-0.9852	Hyper-chaos
-0.7	0.2562	0.2222	0	-1.0212	Hyper-chaos
-0.8	0.312	0.3007	0	-1.0654	Hyper-chaos

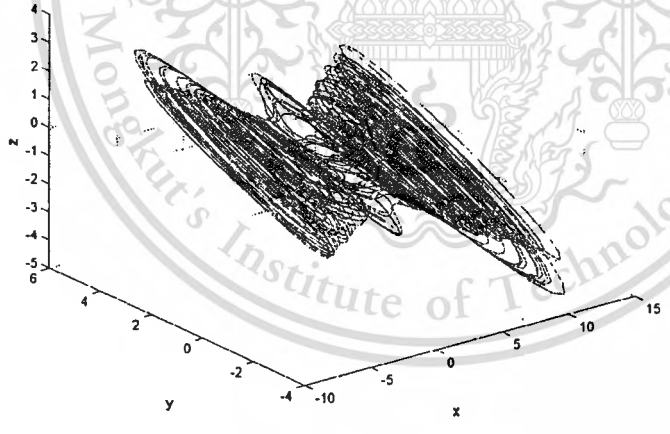

Fig. 5.5a Phase portrait of the Hyper Van der Pol chaotic attractor in the x-y-z space

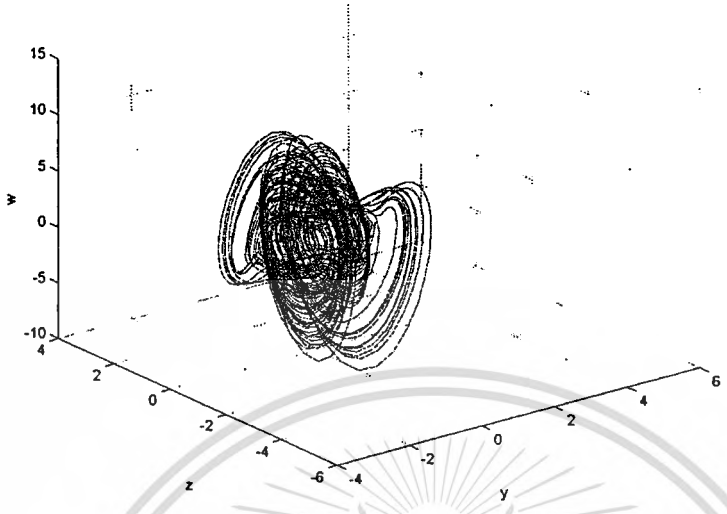

Fig. 5.5b Phase portrait of the Hyper Van der Pol chaotic attractor in the *z-w-y* space

5.5 Circuitry implementation

In this section, we explain the realization of the chaotic circuit in Sections 5.2-5.4. The electrical implementation of the Shaw Van der Pol and the extended chaotic systems described in equations (5.3) and (5.5) can be divided into two parts which are the main circuit and the sub-nonlinear circuit. The main circuit shown in Fig. 5.6a serves for integration and feedback coefficients. The state variables *x,y* and the extended z are obtained from the output of operational amplifiers *OA1-OA3*. The sub-nonlinear depicted in Fig.5.6b and 5.6c are an absolute function and a multi-segment nonlinear function, respectively. The absolute function is realized by precision a full wave rectifier. The multi-segment nonlinear function is consisted of a precision full wave rectifier and a sign function, which implements by a comparator circuit.

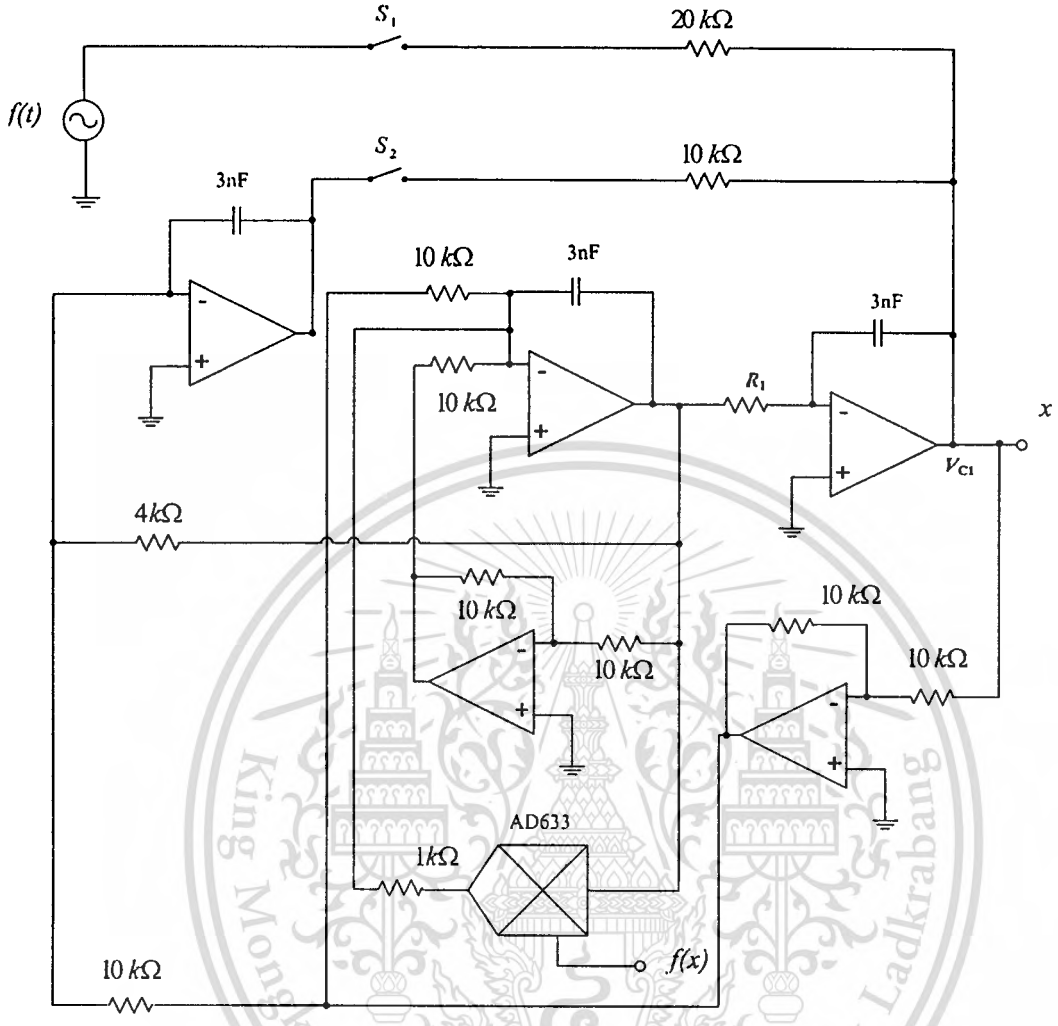

Fig. 5.6a The Shaw VDP circuit and the main circuit for the extended VdP system

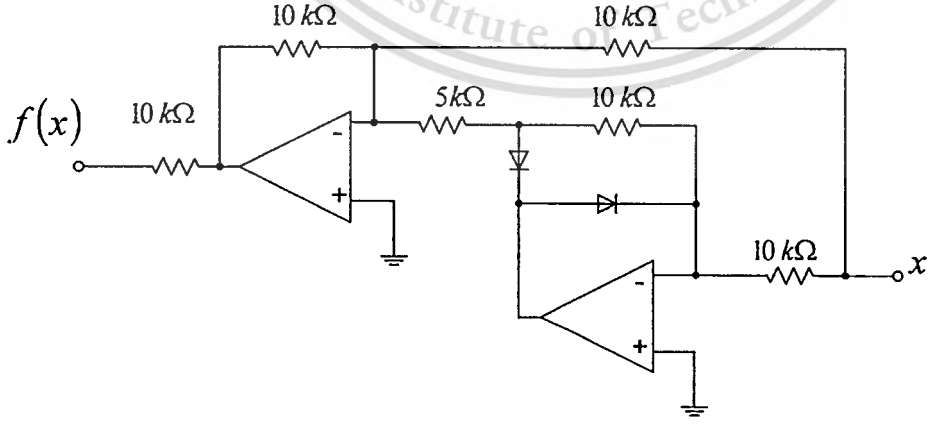

Fig. 5.6b The full wave rectifier circuit

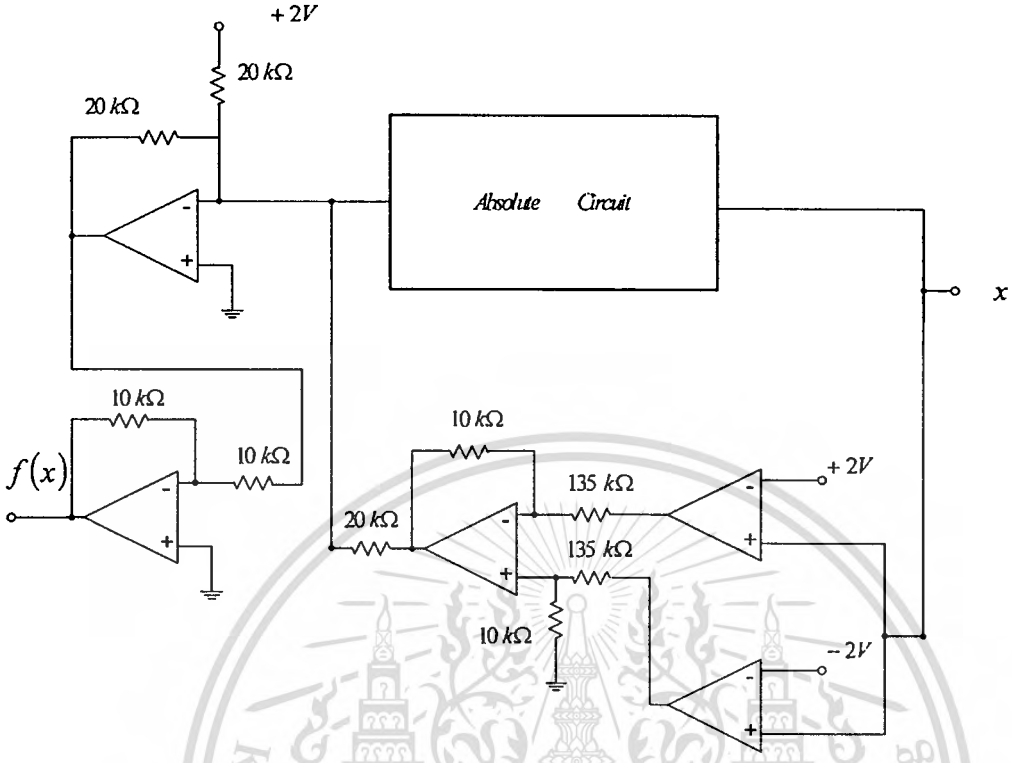

Fig. 5.6c The multi-segment nonlinear function scheme

To achieve the modified Shaw Van der Pol chaotic circuit in equation (5.3), the electronic switch S_1 in the main circuit is turned "on" to connect driven sinusoidal wave with the system; and a sub-nonlinear feedback circuit is a full wave rectifier. The state equation of the circuit realized from equation (5.3) are expressed as

$$\frac{dv_{C1}}{dt} = \frac{1}{C_1}\left[\frac{v_{C2}}{R_1} + \frac{v_{ac}}{R_{15}}\sin(wt)\right]$$
$$\frac{dv_{C2}}{dt} = \frac{1}{C_2}\left[\frac{v_{C1}}{R_3} + \frac{v_{C2}}{R_2} - \frac{f(x)v_{C2}}{R_{10}}\right] \qquad (5.17)$$

where v_{ac} is the magnitude of the ac driven circuit.

The double-scroll chaotic circuit employing an extended Van der Pol system can be obtained by turning on the electronic switch S_2 to connect the extended state z with the state y. In order to achieve a multi-scroll chaotic circuit by using an extended Van der Pol system, the electronic switch

S_2 is turned-on and a multi-segment nonlinear function is used for the nonlinear feedback. The third-order circuit of equation (5.5) are described by

$$\begin{aligned}
\frac{dv_{C1}}{dt} &= \frac{1}{C_1}\left[\frac{v_{C2}}{R_1} + \frac{v_{C3}}{R_{13}}\right] \\
\frac{dv_{C2}}{dt} &= \frac{1}{C_2}\left[\frac{v_{C1}}{R_3} + \frac{v_{C2}}{R_2} - \frac{f(x)v_{C2}}{R_{10}}\right] \\
\frac{dv_{C3}}{dt} &= \frac{1}{C_3}\left[\frac{v_{C1}}{R_{12}} + \frac{v_{C2}}{R_{11}}\right]
\end{aligned} \tag{5.18}$$

The second circuit diagram is a new multi-scroll VdP chaotic system (5.11) shown in Figs. 5.7 a-b, where Fig. 5.7a depicts the integrators and multipliers and Fig. 5.7 b shows the PWL function. In practice, the integrator circuit is realized by using an inverting integrator, whereas the multiplier circuit is realized by an IC AD633. The adjustment for parameters a, b and c can be performed by tuning R_1, R_7, and R_2, respectively. For the PWL function, the circuit is realized by half-wave rectifiers, where the slope of each piece shown in Fig. 5.7 b corresponds to each half-wave rectify circuit. The slopes can be adjusted by manipulating the gains of the op-amps. For example, the slope of magnitude can be adjusted by summing 2 and -6 together. Similarly, the slop of magnitude 5 is the result of summing 11 and -6.

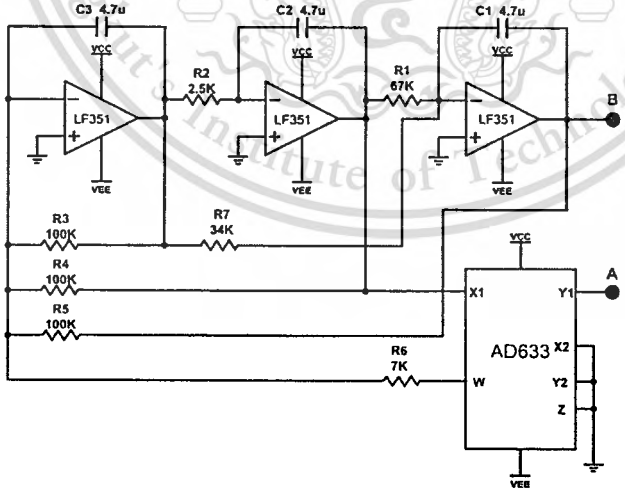

Fig. 5.7a The proposed-chaotified VdP circuit scheme

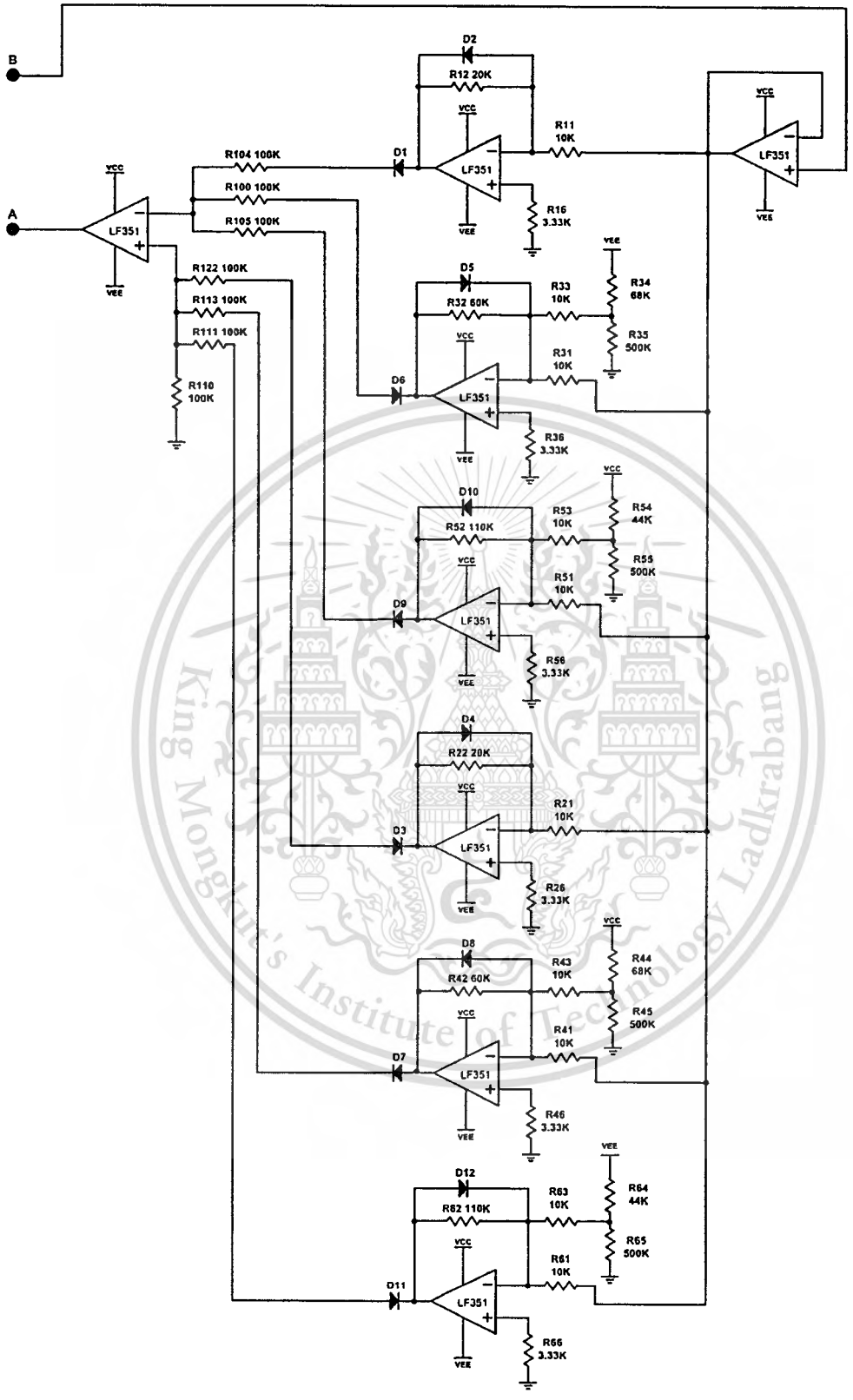

Fig. 5.7b The nonlinear circuit of equation (5.10)

The electronic circuit is designed to realize the proposed hyper-chaotic system. In Fig. 5.8, the circuit consists of four inverting integrators and a nonlinear function $|x|y$. From the state variables defined in the system (5.16), the integrator U_1, U_2, U_3 and U_5 correspond to the integration of the state variables $x, -y$, and z respectively. The nonlinear function consists of analog four-quadrant multipliers and an absolute circuit. In implementation, all operational amplifiers in use are ICs LF351. The multiplier is implemented by an IC AD633 with ±15 V voltage supply. The absolute function is realized by a precision full-wave rectifier circuit shown in dash line. By applying standard node analysis techniques to the circuit, the state equations of the circuit are expressed by:

$$\begin{aligned}
\frac{d}{dt}x &= \frac{1}{C_1}\left[\frac{1}{R_a}y - \frac{1}{R_b}z - \frac{1}{R_c}w\right] \\
\frac{d}{dt}y &= \frac{1}{C_2}\left[\frac{1}{R_d}z + \frac{1}{R}w\right] \\
\frac{d}{dt}z &= \frac{1}{C_3 R}w \\
\frac{d}{dt}w &= \frac{1}{C_4}\left[-\frac{1}{R}x + \frac{1}{R}y - \frac{1}{R}z - \frac{1}{R}w - \frac{1}{R_m}|x|y\right],
\end{aligned} \tag{5.19}$$

where $R_a.R_b, R_c$ and R_d are employed to scale a, b, c and d respectively. The values of the components are $R = R_d = 100k\Omega, R_a = 83k\Omega$, $R_b = 67k\Omega$ and $R_c = 10\,k\Omega$ (a variable resistor). The analog multiplier has the function in the form $W = 0.1(X_1 - X_2)(Y_1 - Y_2) + Z$. In the summing integrator U_5 , we use $R_m = 10k\Omega$, and $R = 100k\Omega$ for scaling x, y, z and w . The values of the capacitors are $C_1 = C_2 = C_3 = C_4 = 0.1\mu F$.

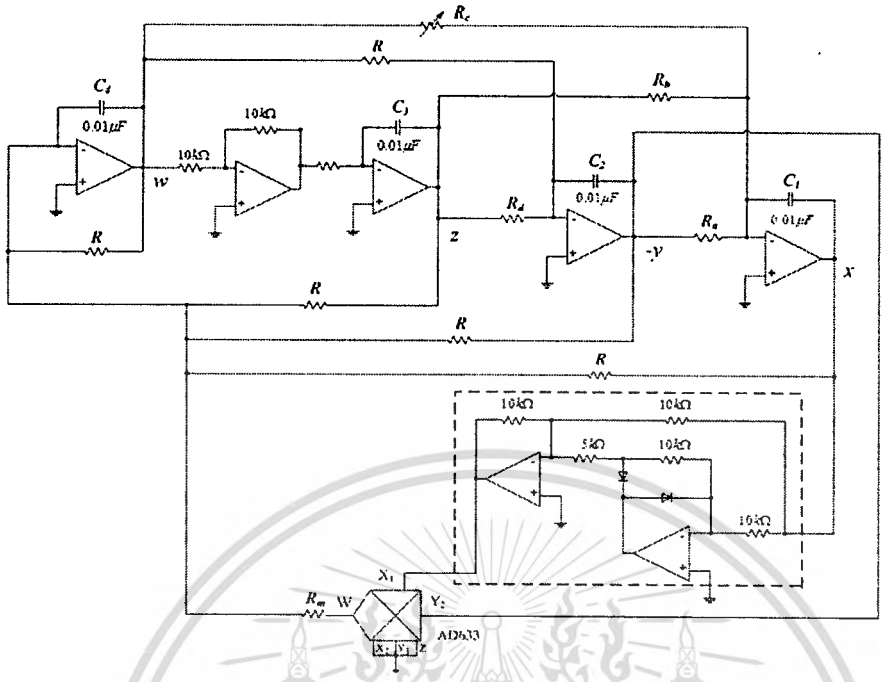

Fig. 5.8 Circuit realization of the hyper –chaotic VdP system

5.6 Simulation and Experiment Results

In this section, to verify all proposed circuit, we use PSpice to simulate and verify by experimental circuits. From Shaw VdP circuit shown in Fig 5.6a, simulation result is shown in Fig 5.9a. When the circuit in Fig 5.6a operated in the extended Shaw VdP chaotic oscillator mode, the simulation and experimental results of implemented circuit are shown in Fig.5.9b and Fig 5.10a respectively.

To present a multi-scroll attractor, we connect the main extended Shaw VdP circuit in Fig.5.6a with the multi-segment nonlinear function circuit in Fig. 5.6c, the simulation and experimental results of implemented circuit are shown in Fig.5.9c and Fig 5.10b, respectively.

From a new multi-scroll VdP circuit in Fig. 5.8, the simulation is performed by PSpice using the parameters as a = 1.2, b = -2.6, and c = 40, PSpice simulation and the experimental result from implementation of the real circuit for a four-scroll chaotic attractor are shown in Figs. 5.11 and 5.12. In the last simulation and experimental results from the hyper VdP chaotic circuit, the waveforms v_{C1} and v_{C2} are simulated by PSpice with $R_c = 142k\Omega$ as shown in Figs 5.13a, 5.13b and 5.13d. The

phase portraits measured from circuit on the x-y , the x-z and the w-z planes are shown in Figs. 5.14a ,5.14b and 5.14c, respectively.

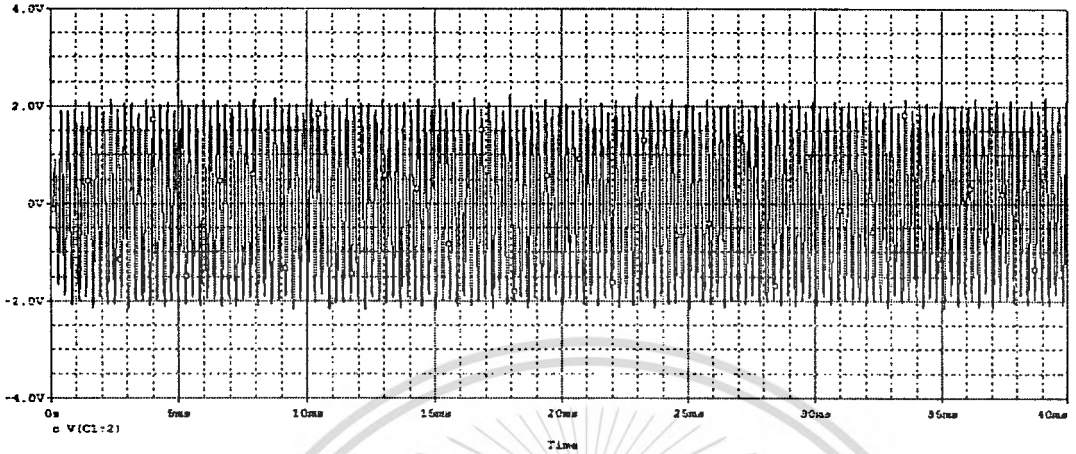

Fig. 5.9a PSpice simulation of the v_{C1} of the Shaw VdP mode

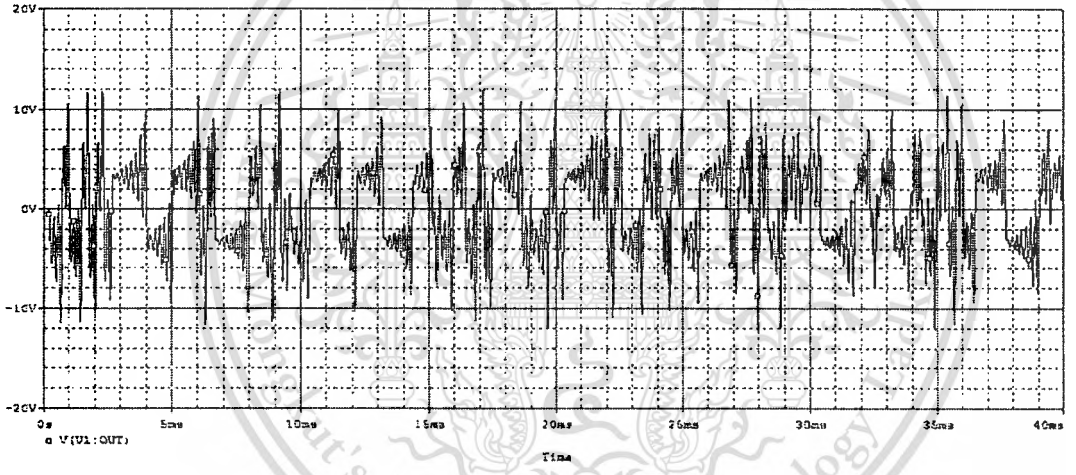

Fig 5.9b PSpice simulation of the v_{C1} of the extended VdP chaotic circuit with an absolute function

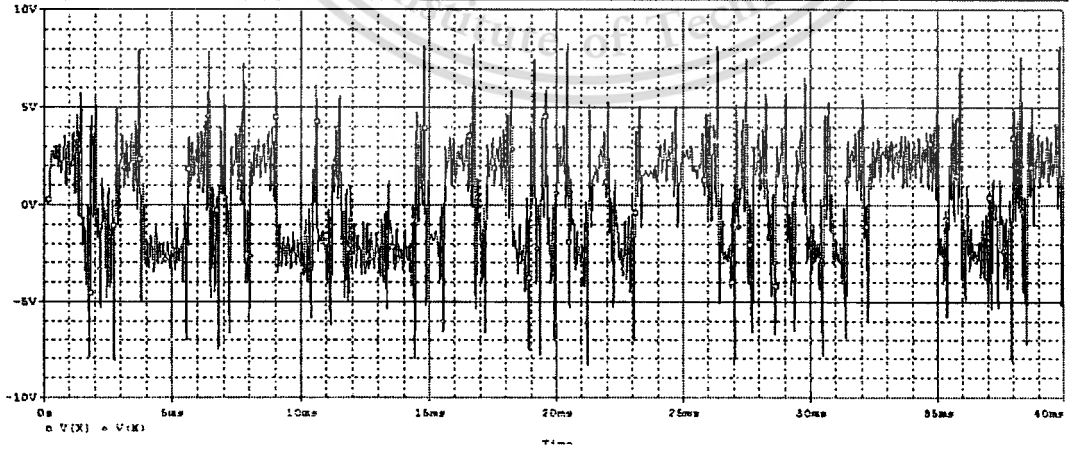

Fig 5.9c Pspice simulation of the v_{C1} of the multi-scroll extended VdP chaotic circuit

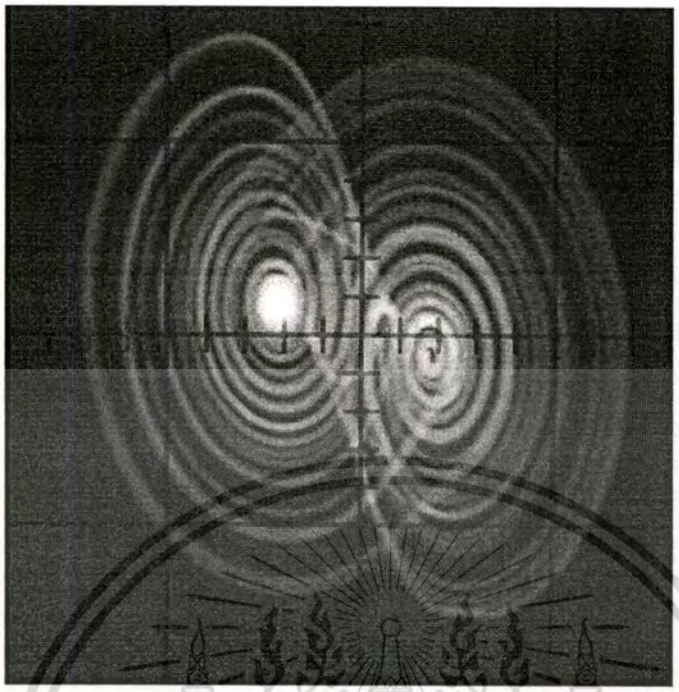

Fig 5.10a Experimental measurement of the double-scroll extended ShawVdP chaotic attractor on the x-z plane

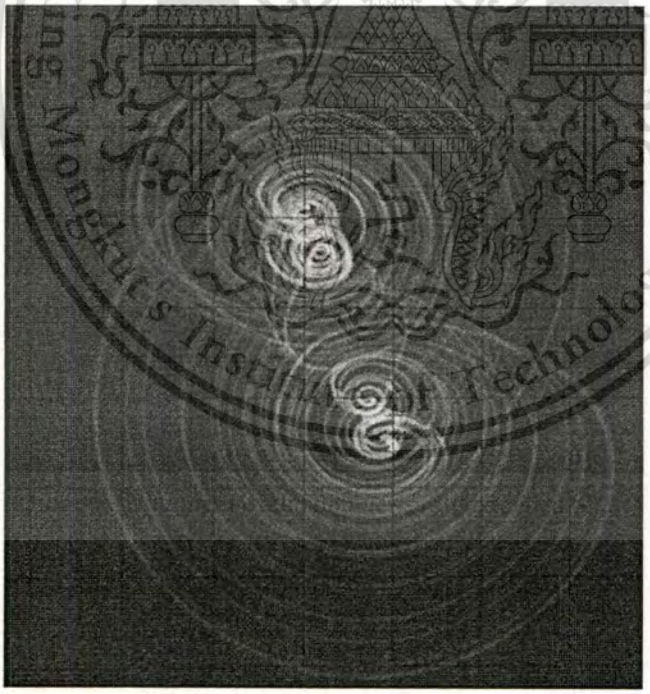

Fig 5.10b Experimental measurement of the multi-scroll extend Shaw VdP on the x-z plane

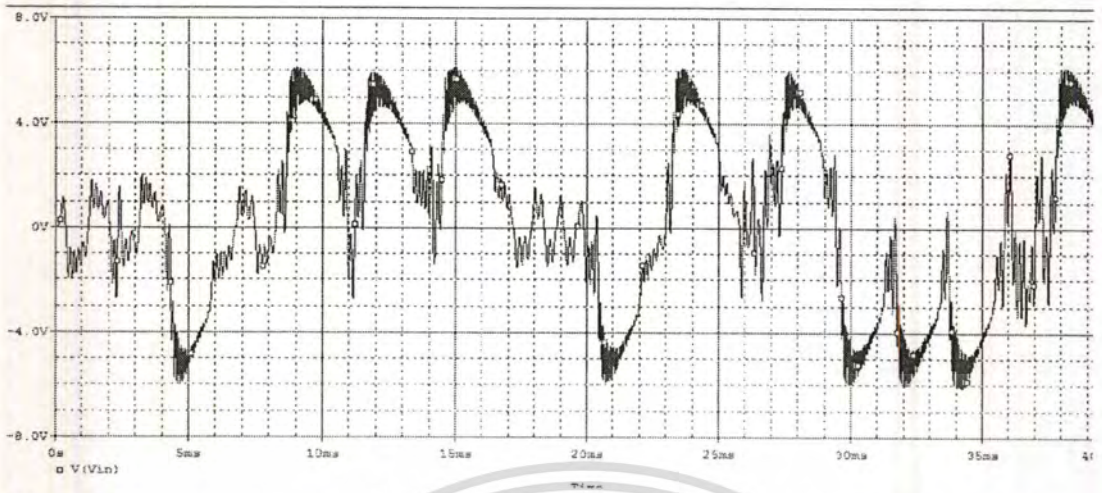

Fig. 5.11 PSpice simulation results of the v_{C1} of the new VdP-type multi-scroll chaotic circuit

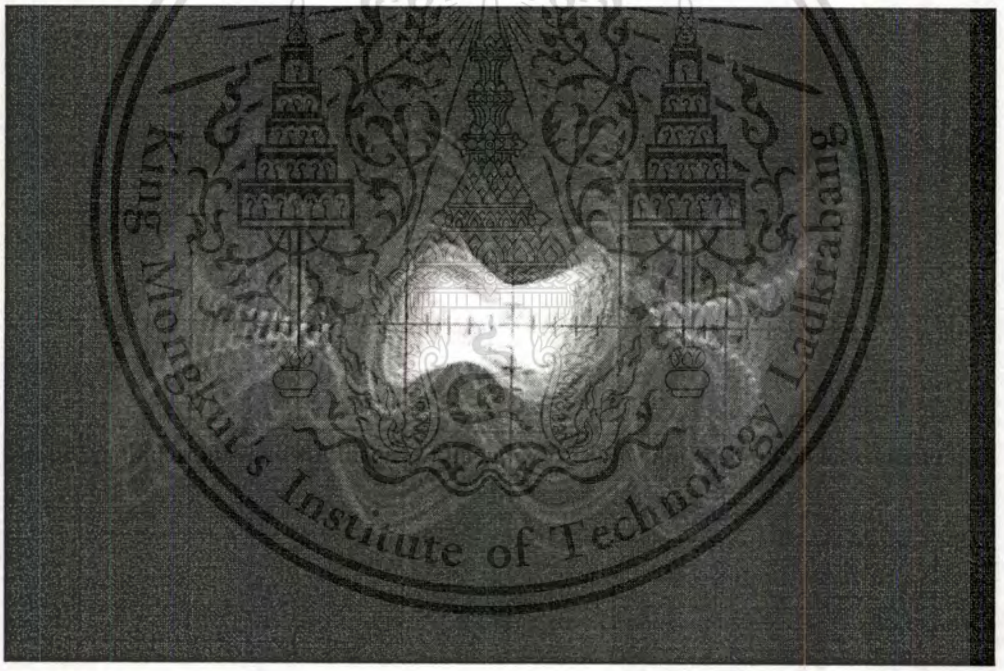

Fig. 5.12 Experimental measurement of the VdP on the xz plane

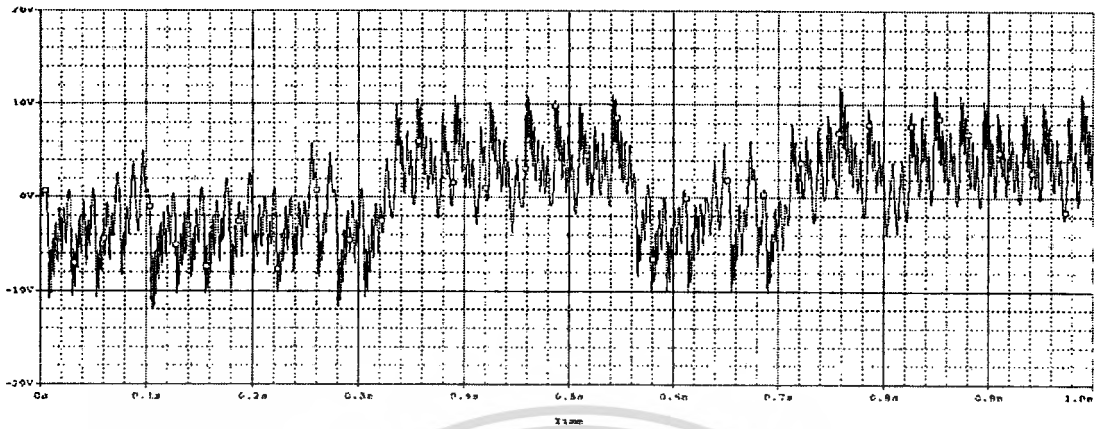

Fig. 5.13a PSpice simulation of the v_{C1} of the hyper-chaotic VdP system

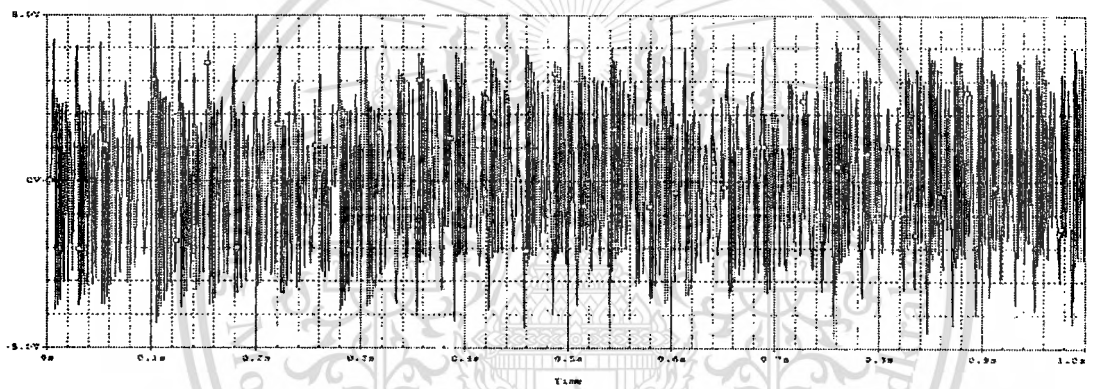

Fig. 5.13b PSpice simulation of the v_{C2} of the hyper-chaotic VdP system

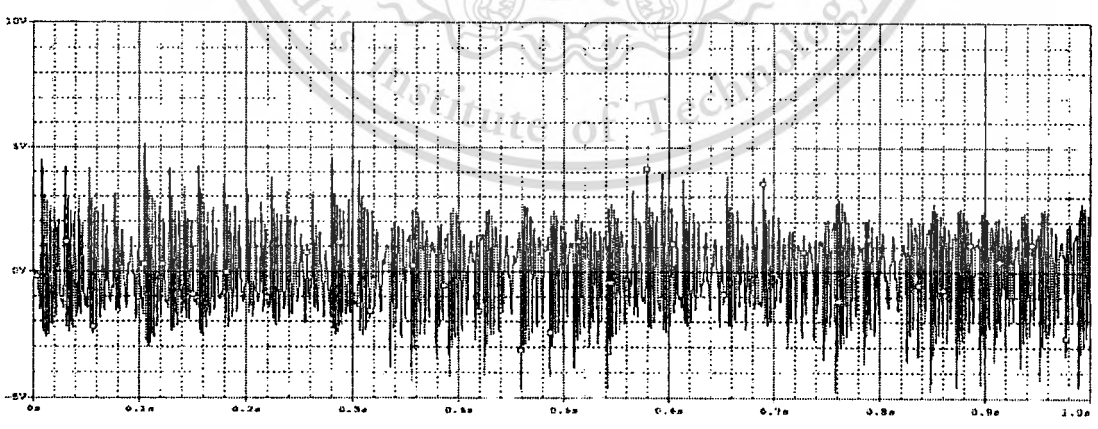

Fig. 5.13c PSpice simulation of the v_{C3} of the hyper-chaotic VdP system

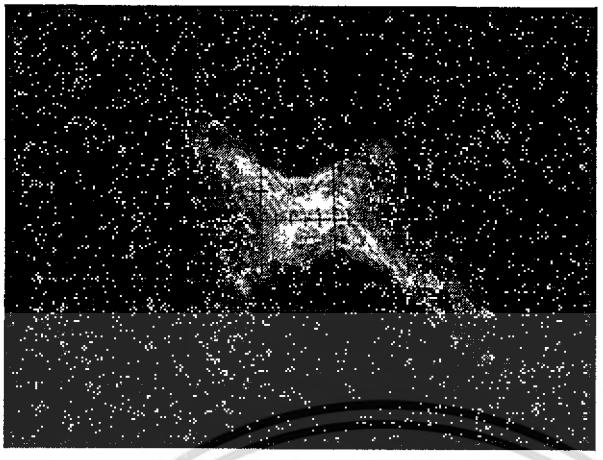

Fig. 5.14a The phase portrait of the hyper-chaotic VdP system on the x-y plane

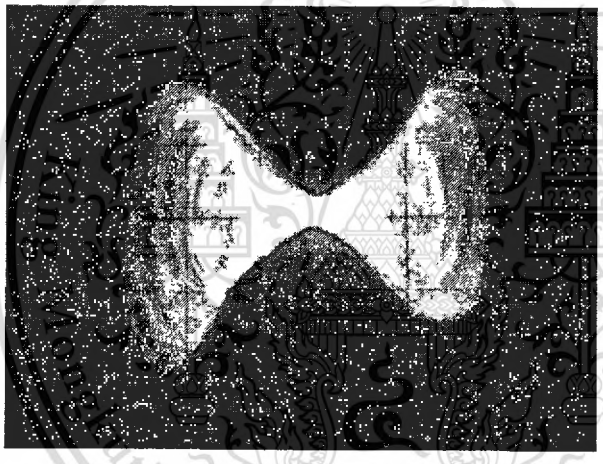

Fig. 5.14b The phase portrait of the hyper-chaotic VdP system on the x-w plane

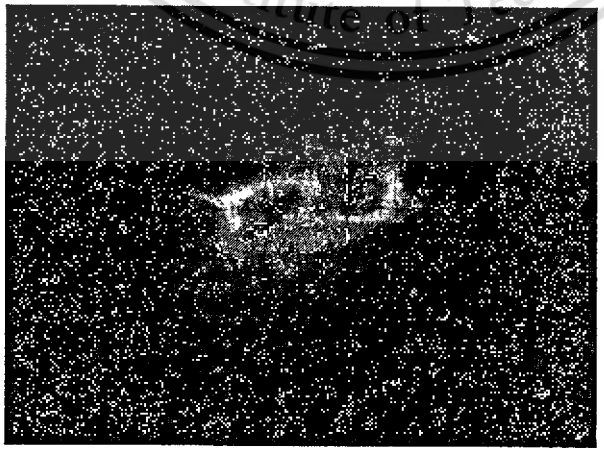

Fig. 5.14c The phase portrait of the hyper-chaotic VdP system on the w-z plane

5.7 Summary

This chapter presents a new kind of chaotic attractors modified from the Van der Pol system. The variable mode and the multi-scroll chaotic circuits can be obtained from modifying Shaw VdP. A new multi-scroll and a hyper-chaotic attractor can be obtained from chaotification of the VdP system. The proposed hyper-chaotic attractor is suitable for chaos based communication in secure communication. All proposed systems can be realized by using simple electronic circuits. The dynamic behaviors of the proposed system obtained from the simulation have been confirmed by electronic circuit construction and the experiment results.

Chapter 6

Applications of Chaotic Attractors

In this chapter, we propose two applications of chaos in engineering. First, we exploit attractor's trajectory as guiding signals for a mobile robot. Second, we demonstrate that a chaotic attractor may be employed for generating truly random signals.

In robotics, the first chaotic mobile robot is proposed by Nakamura [4], where Arnold's equation is used to generate chaotic motion. The advantage of exploiting chaotic signals in an autonomous mobile is to navigate throughout the unknown terrain for various tasks such as demining, cleaning and patrolling. However, these implementations need the high performance arithmetic CPU for pattern generators. In this chapter, instead of using a microcontroller or a CPU, we propose a chaotic mobile robot which is directly controlled by a simple autonomous chaotic circuit. The chaotic motion generator is implemented by using a low frequency coupled Chua's circuit (LFCC). In this chapter, a lab-scale two-wheel mobile robot is constructed. The two wheels are controlled independently by DC motors, which are driven by the LFCC circuit described in Sections 6.1-6.3.

In secure communication, a true random number generator (TRNG) in which outputs are a sequence of statistically independent and unbiased binary digits are widely used in cryptography[41], statistical simulation and build-in self-test digital system.. In this chapter, we show an application of chaotic attractors from Chapter 3 for generating true random binary sequences. This will be shown in Sections 6.4-6.5.

6.1 Chaotic Mobile Robot

In this chapter, a chaotic robot, consisted of a trajectory generator circuit, a motor control circuit and DC motors, is designed and analyzed. The robot has one free wheel and two fix wheels controlled by DC motors. In order to obtain the navigation path, we apply chaotic signals into a motor control circuit for changing speed on either wheel of the robot. The kinematical scheme of mobile robot can be shown in Fig. 6.1, where V is linear velocity of the robot. V_L is the velocity of

the left wheel, V_R is the velocity of the right wheel, L is the distance between two wheels, and ω is the angular velocity, where $\omega = \frac{V_R - V_L}{2}$. The motion of the robot in the rectangular coordinate can be described by

$$\begin{bmatrix} \dot{x} \\ \dot{y} \\ \dot{\theta} \end{bmatrix} = \begin{bmatrix} \cos\theta & 0 \\ \sin\theta & 0 \\ 0 & 1 \end{bmatrix} \begin{bmatrix} V \\ \omega \end{bmatrix}. \tag{6.1}$$

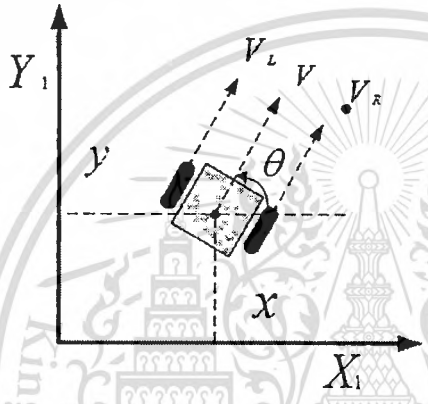

Fig. 6.1 Kinematical scheme of the two-wheel mobile robot

6.2 The Low Frequency Coupled Chua's Circuit: LFCC Circuit

Chua's circuit [42] is shown in Fig. 6.2a. It is a simple oscillator which can exhibit a rich variety of bifurcations and chaotic behaviors. The circuit consists of one inductor, two capacitors, one linear resistor, and one piecewise-linear resistor. The dynamic equation of Chua's circuit is described by three differential equations:

$$\begin{aligned} C_1 \frac{dvc_1}{dt} &= \frac{1}{R}(vc_2 - vc_1) - f(vc_1) \\ C_2 \frac{dvc_2}{dt} &= \frac{1}{R}(vc_1 - vc_2) + i_L \\ L \frac{di_3}{dt} &= -vc_2 \end{aligned} \tag{6.2}$$

where i is the current through the inductor L, Vc_1 and Vc_2 are voltage across capacitor C_1 and C_2 respectively, where $f(\ )$ is the function of three-segment piecewise-linear of the nonlinear resistor. Characteristics shown in Fig. 6.2b is defined by

$$f(v_R) = G_b V_R + \frac{1}{2}(G_a - G_b)\left(|v_R + B_p| - |v_R - B_p|\right) . \tag{6.3}$$

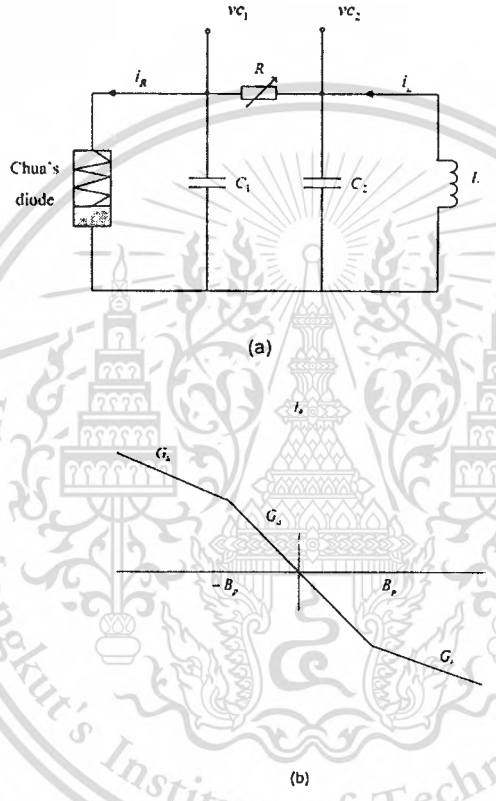

Fig 6.2 (a) Chua's circuit, (b) Three segment piecewise-linear characteristics of the nonlinear resistor

where G_a and G_b are the slopes in the inner and outer regions respectively, and B_p denotes break points of the piecewise-linear curve shown in Fig. 6.2b. For simplicity, we use the dimensionless state equation to represent the equation (6.2) by changing the variables:

$$
\begin{aligned}
&x \equiv \frac{Vc_1}{B_p}, y \equiv \frac{Vc_2}{B_p}, z \equiv \frac{i_L R}{B_p} \\
&\alpha \equiv \frac{C_2}{C_1}, \beta \equiv \frac{R^2 C_2}{L}, \tau \equiv \frac{t}{RC_2} \\
&a \equiv RG_a, b \equiv RG_b
\end{aligned}
\quad . \tag{6.4}
$$

Thus, general equations of Chua's circuit are

$$
\begin{aligned}
\frac{dx}{d\tau} &= \alpha(y - x - f(x)) \\
\frac{dy}{d\tau} &= x - y + z \\
\frac{dz}{d\tau} &= -\beta y
\end{aligned}
\tag{6.5}
$$

where

$$
f(x) = bx + \frac{1}{2}(a-b)\left[|x+1| - |x-1|\right] . \tag{6.6}
$$

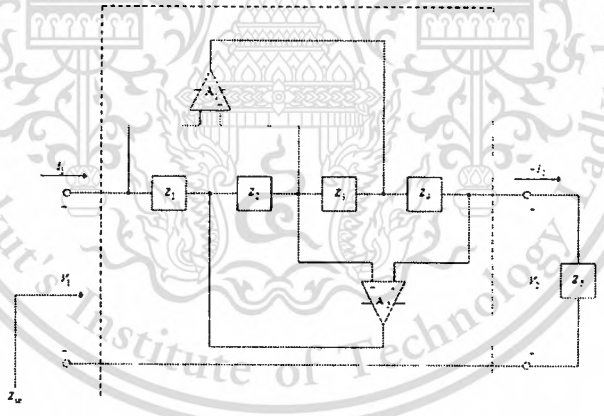

Fig. 6.3 Antoniou's General immitance converter

In this chapter, we use a very low frequency of chaotic circuit to drive DC motors. The high value of the inductor can be realized by the Antoniou's general immitance converter (GIC) structure [43] having input impedance Z_{in} shown in Fig. 6.3. The equivalent inductance can also be realized by using $Z_4 = 1/sc$ and $Z_1 = R_1, Z_2 = R_2, Z_3 = R_3 = Z_5 = R_5$ and is computed by using

$$
L_{eq} = \frac{R_1 R_3 R_5 C}{R_2} . \tag{6.7}
$$

In order to increase complicated chaotic behaviour, we use mutually coupled between the identical autonomous oscillator technique. The two low frequency Chua's circuits are coupled by linear resistor via electronic switches, which are controlled by pseudo-random binary sequence: PRBS signal [44] with polynomial $X^4 + X + 1$.

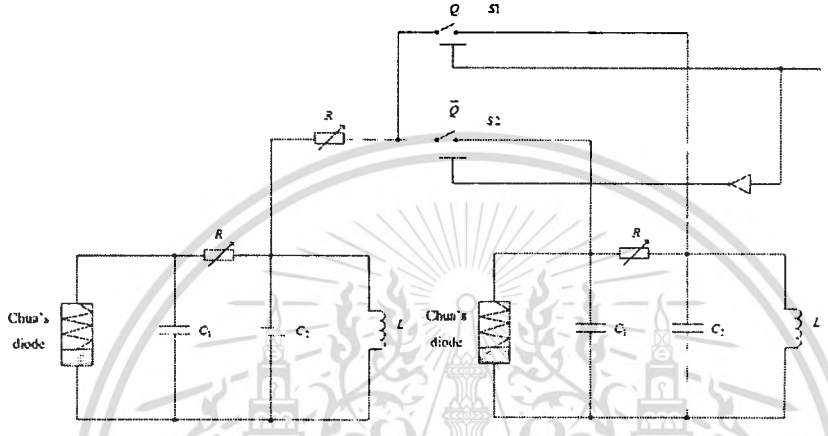

Fig. 6.4 Low frequency coupled Chua's circuit

$$
\begin{aligned}
\frac{dx_1}{d\tau} &= \alpha\left(y_1 - x_1 - f(x_1)\right) \\
\frac{dy_1}{d\tau} &= x_1 - y_1 + z_1 + k\left(y_2 - y_1\right) \\
\frac{dz_1}{d\tau} &= -\beta y_1 \\
\frac{dx_2}{d\tau} &= \alpha\left(y_2 - x_2 - f(x_2)\right) \\
\frac{dy_2}{d\tau} &= x_2 - y_2 + z_2 + k\left(y_1 - y_2\right) \\
\frac{dz_2}{d\tau} &= -\beta y_2
\end{aligned}
\tag{6.8}
$$

, where $k = R/R_c$.

On the other hand, when the states of the switches are in the other way around, namely S2 is ON and S1 is OFF, one has a coupled Chua's circuit which is coupled between state y and state x

on the left side and the right side of Fig. 6.4, respectively. In this case, the state equation of the coupled circuit is given by equation (6.9).

$$\begin{aligned}
\frac{dx_1}{d\tau} &= \alpha\left(y_1 - x_1 - f(x_1)\right) + k(x_2 - x_1) \\
\frac{dy_1}{d\tau} &= x_1 - y_1 + z_1 \\
\frac{dz_1}{d\tau} &= -\beta y_1 \\
\frac{dx_2}{d\tau} &= \alpha\left(y_2 - x_2 - f(x_2)\right) + k(x_1 - x_2) \\
\frac{dy_2}{d\tau} &= x_2 - y_2 + z_2 \\
\frac{dz_2}{d\tau} &= -\beta y_2
\end{aligned} \qquad (6.9)$$

6.3 Experimental Results

Simulation results in [45], for which more than a hundred chaotic patterns and more than a ten thousand run times have been tested, suggest that the Chua's circuit is the best pattern yet simple for implementation in the sake of path diversity and area coverage. For Chua's circuit in this experiment, the parameters of the circuit in Fig. 6.2 are as follows: G_1 =0.76 mS, G_2 =-0.41mS $\pm B_p$ =1V, R =1.8K, C_1 =23.5 μF C_2 =235 μF and L=45 H. From equation (6) we use $R_1 = R_2 = R_3 = R_5 = 1K, R_5 = 1.8K$ and $Z_4 = 1/sc$, C =23.5 μF.

The LFCC circuit included PRBS with polynomial are driven by the 0.5 Hz clock signal as the robot's driver shown in Fig. 6.6. For the path record, the robot has a mark pen which can plot a trajectory on the map. An area of 20x20 blocks divided on the plain paper, which each block is 10x10 cm, is set up for working areas in the experiment. In this experiment, the robot starts at a corner of the working areas. In the moving, when the robot approaches the wall, its reflected path is set exactly the same as the law of inflection — the reflected angle is equal to the incident one.

To emulate the situation in de-mining tasks, ten marked indicated in red in Fig. 6.6 are randomly selected to be assumed as buried location of each personal killing M14 bomb. The time is recorded on the map whenever the robot can find the bomb, which implies by time that the robot can find the red mark on the map. According to our experiment, after 30 minutes, the robot can cover 289

blocks, which is accounted for 72.25% of the whole area, and is be able to find all bombs given randomly.

Fig. 6.5 A prototype of "No-CPU" chaotic robot

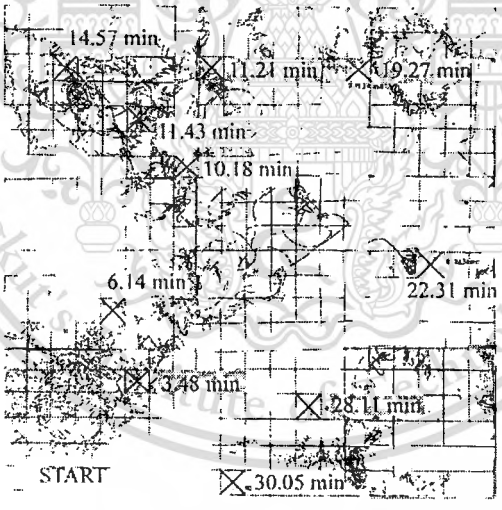

Fig. 6.6 Trajectories of the chaotic mobile in the experiment

6.4 TRNG based on Chaotic Attractors

Practically, a sequence from a true random number generator should have maximum entropy or it should have the following properties:

1. A random sequence of bits must be unpredictable or the entropy of a random sequence must be at its maximum.

2. The number of ones should approach number of zeros as the length of the sequence tends to infinity.

3. A long sequence of random bits should not be lossless compressible by any known or unknown technique.

To achieve these properties, the proposed TRNG which is shown in Fig.6.7 consisted of a chaotic attractor, a random bit generator and a bit corrector or a de-screwing circuit. The chaotic attractor circuit is used as a random source. Conversion of random signal from the chaotic circuit into digital sequences is quantized by a random bit generator. The goal of the de-screwing process which is implemented by Von Neumann technique to uniform bit stream outputs. The output of de-screwing is used for producing a true random binary sequence.

Fig. 6.7 The block diagram of the proposed true random number generator

To generate random sequence number, we consider chaotic signal from the chaotic system (3.9) with a signum function. All trajectories of the system (3.9) swing between nonzero equilibrium located on $(\pm 1,0,\pm 1)$ are extracted into digital binary valves. Figure 6.8 shows chaotic signal of the system (3.9) at state x, we use two comparator circuits to set up threshold for extracting binary values. The first comparator is set threshold at $+1$ and the second comparator is set threshold at -1. In Fig. 6.9, when the chaotic signal passes $+1$ through the maximum value, the output of the first comparator obtains output as 1. In contrast, when chaotic signal passes -1 through the minimum value, the output of the second comparator obtains output as 1.

The goal of the de-screwing is to uniformly distribute the bit stream and eliminate the correlation in output of a random bit generator. We use the Von Neumann extractor [46] which is implemented by software to achieve this proposes. The extractor takes pairs of consecutive bits as inputs, and output bits can be mapped as in Table 6.1below:

Table 6.1 – Von Neumann corrector

Input bits	Output bits
0,0	none
0,1	1
1,0	0
1,1	none

The corrector removes any bias either 1 or 0 to be over represented in an uncorrected bit stream. In Fig 6.9 the input sequence 1100000110001111111 from the random bit generator are ---10----.

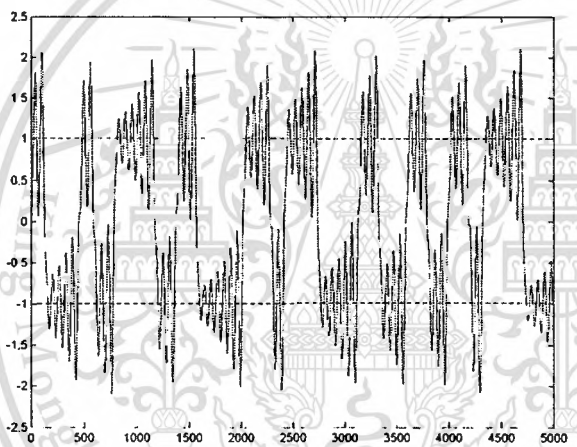

Fig.6.8 The chaotic signal at state x of the system (3.9)

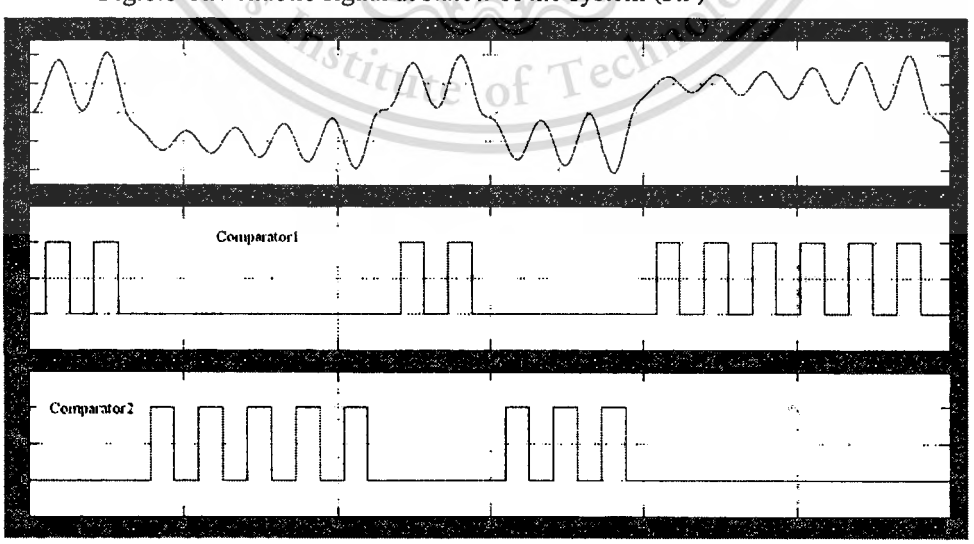

Fig.6.9 The binary value extracted from the chaotic attractor

6.5 Statistical Evaluation and Experimental Result

In order to verify the randomness property of proposed bit streams of the TRNG, we use the FIPS-140-2 [47] issued by National Institute of Standard and Technology (NIST) to test the sequences. The FIPS includes four tests that are determined sequences of 20,000 bits. If there is any failure in the test means the TRNG fails the test. The test procedures are as follows:

1. Mono bit test: the test is carried out to indicate whether the number of 0's and 1's are in the bit stream are approximately the same. The test passes, if number of ones is within the range (9,654-10,346)

2. Poker test: A sequence of 20,000 bits is divided into 5,000 consecutive 4-bit segments. Denote $f(i)$ as the number of each 4 bit value i, where $0 < i < 15$. Then evaluate the following:

$$X = \frac{16}{5000}\sum_{i=1}^{n}[f(i)]^2 - 5000 \tag{6.10}$$

The poker test is passed or each segment appears at the same expected rate, if $2.16 < X < 46.17$.

3. Run test: the test indicates whether the number of block (runs of 1's) and the gaps (runs of 0's) of various lengths occur at the expected frequency for 20,000 bit stream.

The test is passed, if the length of each run is fallen into the required interval in Table 6.2.

Table 6. 2 – Run test specification

Length of Run	Required Interval
1	2,315-2,685
2	1,114-1,386
3	524-723
4	240-384
5	103-209
6+	103-209

4. Long run test: The long run test is accepted if there are no runs of length 26 or more.

In the experiment, the random binary sequences from A/D converter connect to a computer via the parallel port. The results of unbiased sequences corrected by Von Neumann technique is passed standard which is tested by FIPS is shown in table 6.3.

Table 6.3 Results of FIPS 140-2 tests

Monobit test	Poker test	Runs test	Long run test
9,998	11.18	Length 1=2,423 Length 2=1,146 Length 3 = 357 Length 4 = 120 Length 5 = 111 Length 6+ = 88	No long run

6.6 Summary

In this chapter, for the first application, the chaotic robot using LFCC circuit is built and can be recognized as a "no-CPU" robotic architecture. Experimental result reveals effectiveness of the chaotic trajectory in finding randomly given spots representing the equivalent bomb's buried location in the land mine field.

The second application has shown a technique for construction of a TRNG by the proposed chaotic source. According to the experiment, the chaotic attractor which is an autonomous dynamical system can use as the random source. In the future, the TRNG bit rate can be improved by using high frequency operation amplifiers. Other statistical tests for verification of the effectiveness of the proposed TRNG should be investigated.

Chapter 7

Conclusions

In this thesis, the construction chaotic attractor and application are presented. To construct simple chaotic oscillator, the mixed-mode and universal-mode chaotic circuits, which can be obtained both of nonautonomous and autonomous modes, are proposed. The universal scheme is simply laid out as a block-like architecture. The universal mode is a generalized version, as its name implied, of the mixed mod circuits. In the mixed-mode circuit, both proposed circuit schemes are simple, which use only a quad op-amp, an analog electronic switch IC, and an op-amp for implementing the nonlinear function. It can be used as motion-based application such as chaotic mixing.

The universal mode chaotic oscillator is designed on concept of modular design. It is cost-effective and is easy-to-implement by using only a few op-amps. Therefore it is effectively suitable to use as an education tool for electronic engineering. To exploited the chaotic attractor for secure communication, the complex multi-wing butterfly attractor which is modified from Lui attractor is realized by using a piecewise linear function. In addition to synthesis another complex chaotic attractor for the same purpose, the chaotification technique is applied to the Van der Pol system. The variable mode, multi-scroll and hyper-chaotic attractor can be obtained from this anti-control chaos method.

To utilize the above findings, two applications are demonstrated: one is for application in a mobile robot and the other is for truly random generator. Modified Chua's circuit is employed for generating guiding signals for a mobile robot. Meanwhile, the designed universal mode chaotic oscillator is adopted for generating a truly random number generator.

Note that all proposed chaotic oscillators are implemented by the voltage mode operational amplifiers. To further improve the high-frequency operations, current-mode op-amps or special op-amps may be used, which will be verified in further studies.

References

[1] Hong, L., Zhong, L., Zhang, B., Wang, F., Tan, N. & Halang, W.A. [2010] "Design of Analogue Chaotic PWM for EMI Suppression," *IEEE Trans. EMC* **52**, pp. 1001-1007.

[2] Ma, H.G., Zhua, X.F., Xua, J.F. & Ai, M.S. [2008] "Circuit state analysis using chaotic signal excitation," *J. the Franklin Inst.* **345**, pp. 75-86.

[3] Addabbo, T., Fort, A., Rocchi, S. & Vignoli, V. [2010] "Exploiting Chaotic Dynamics for A-D Converter Testing," *Int. J .Bifurc. and Chaos* **20**, pp. 1099-1118.

[4] Nakamura, Y. & Sekiguchi, A. [2001] "Chaotic mobile robot," *IEEE Trans. on Robotic and Automation*, vol. 17, pp. 898-904.

[5] Buscarino, A., Fortuna, L., Frasca, M., & Muscato, G. [2007] "Chaos does help motion control," *Int. J. Bifurc. and Chaos* **17**, pp. 3577-3582.

[6] Zhang, Z. & Chen, G. [2007] "Chaotic liquid shaker: design, implement and application," *Int. J. Bifurc. and Chaos* **17**, pp. 4443–4451.

[7] Yalcın, M.E., Suykens, J.A.K. & Vandewalle, J. [2004] "True random bit generation from a double-scroll attractor," *IEEE Trans. Circuits. Syst.-I* **51**, pp. 1395–1404.

[8] Ditto, W.L., Murali, K. & Sinha, S. [2008] "Chaos computing: ideas and implementations" *Phil. Trans. R. Soc. A* **366**, pp. 653-664.

[9] Liu, Z., Zhu, X.H., Hu, W. & Fei, J. [2007] "Principles of chaotic signal radar," *Int. J. Bifurc. and Chaos* **17**, pp. 1735-1339.

[10] Tam, W.M., Lau, F.C.M. & Tse, C.K. [2006] *Digital Communications with Chaos: Multiple Access Techniques and Performanc* , Elsevier, Amsterdam.

[11] Madan, (Ed.), [1993] *Chua's Circuit: A Paradigm for Chaos*, World Scientific, Singapore.

[12] Sprott, J.C [2000] "Simple chaotic systems and circuits," *Amer. J. Phys*. vol. 68, pp. 758 -763.

[13] Ewakil, A.S. & Kennedy, M.P. [2001] "Construction of classes of circuit independent chaotic oscillators using passive-only non-linear devices," *IEEE Trans. Circ. Syst.-I*, vol. 48, pp. 289–30.

[14] Chen, G. and Ueta, T. [1999] "Yet another chaotic attractor." *Int. J. Bifur. Chaos* 9, pp. 1465–1466.

[15] Zhong, G. and Tang, W.K.S. [2001] "Circuitry implementation and synchronization of Chen's attractor," *Int. J. Bifur. Chaos* 12, pp. 1423-1427.

[16] Lü, J.H. and. Chen, G. [2006] "Generating multiscroll chaotic attractors: Theories, methods and applications," *Int. J. of Bifur. Chaos*16, pp. 775-858.

[17] Strogatz, S.H. [1994], Nonlinear Dynamics and Chaos: with Applications to Physics, Biology, Chemistry, And Engineering, Addison-Wesley, Reading, MA.

[18] Lorenz, E.N. [1963], "Deterministic nonperiodic flow," *J Atmos Sci* **20**, pp. 130–141.

[19] Sergio, F. [2002] *Design with Operational Amplifiers and Analog Integrated Circuits*, (3rd Ed.), McGraw-Hill, New York.

[20] Cook, P.A. [1985] "Simple feedback systems with chaotic behavior," *Syst. Contr. Lett.*, vol. 6, pp. 223–227.

[21] Moreno, U.F., Peres, P.L.D. & Bonatti, I.S. [2001] "Analysis of piecewise-linear oscillators," *IEEE Trans. Circuits Syst.-I* **50**, pp. 1120-1124.

[22] Lü, J.H., Murali, K., Sinha, S., Leung, H. & Aziz-Alaoui, M.A. [2008] "Generating multi-scroll chaotic attractors by thresholding," *Physics Letters A* **372**, pp. 3234-3239.

[23] Mykolaitis, A., Tamasevicius, A., Namajunas, A., Cenys, A. & Anagnostopoulos, A. [2000] "Non-autonomous 2nd order chaotic circuit with comparator," *IEE Proc. G Circuits, Devices Syst.***147**, pp. 291 – 292.

[24] Milioua, A.N., Antoniadesa, I.P., Stavrinides, S.G. & Anagnostopoulos. A.N. [2007] "Secure communication by chaotic synchronization: Robustness under noisy conditions,"*Nonlinear Anal: Real World Appl.* 8, pp. 1003–1012.

[25] Mohamed, I.R., Murali, K., Sinha, S. & Lindberg, E. [2010] "Design of Threshold Controller Based Chaotic Circuits" *Int. J. Bifurc. and Chaos* **20**, pp. 2185-2191.

[26] Ozoguz, S & Elwakil, A.S. [2004] "On the realization of circuit-independent nonautonomous pulse-excited chaotic oscillator circuits," *IEEE Trans. Circuits Syst.-II,* **51**, pp. 552-556.

[27] Miranda, R. & Stone, E. [1993] "The proto-Lorenz system," *Physics Letters A178*, pp. 105–113.

[28] Elwakil A.S., Özoguz, S. & Kennedy, M.P. [2002] "Creation of a complex butterfly attractor using a novel Lorenz-type system," *IEEE Trans. Circuits and Syst. I* 49, pp. 527–530.

[29] Elwakil, A.M., Özoguz, S. & Kennedy, M.P. [2003] "A Four-Wing Butterfly Attractor from a Fully Autonomous System," *Int. J. of Bifur. Chaos* 13, pp.3093-3098.

[30] Lu, J.H., Chen, G. & Cheng, D. [2004] "A new chaotic system and beyond: the generalized Lorenz-like system," *Int. J. of Bifur. Chaos* 14, pp. 1507-1537.

[31] Yu, S.M., Tang, K.S., Lü J.H. & Chen G. [2010] "Generating 2n-wing attractors from Lorenz-like systems," *Int. J. Circuit Theory and Applications*, 38(3), pp-243–258.

[32] Liu, T. Liu, L. & Liu, K. [2004] "A new chaotic attractor," *Chaos, Solitons & Fractals*. vol. 22, pp-1031–1038.

[33] Van der Pol B. [1922] "On relaxation oscillations," *Philos Mag* **2**, pp. 978–992.

[34] Shaw, R. [1981] "Strange attractor chaotic behavior, and information flow," Zeitschrift fur Naturforschung, 36a, pp. 80-112.

[35] Guckenheimer, J., Hoffman, K. & Weckesser, W. [2003] "The forced Van der Pol equation I: Slow flow and its bifurcation," *SIAM J. Appl. Dynamical Syst.*, vol.2, pp. 1-35.

[36] Chedjou, J.C., Fotsin, H.B., Woafo, P. & Domngang, S. [2001] "Analog simulation of the dynamics of a Van der Pol oscillator coupled to a Duffing oscillator," *IEEE Trans Circuits Syst. I* 48, no.6, pp.748–757.

[37] S. Bentez, S., Acho, L. & Guerra, R. [2006] "Chaotification of the Van der Pol system using jerk architecture," *IEICE Trans. on Fundamentals*, vol. E89-A, pp. 1088-1091.

[38] Wolf A, Swift J.B, Wwinney, H.L, Vastano, J.A. [1985] "Determining Lyapunov exponents from a time series," Physica D-16, pp.285–317.

[39] Sprott, J.C. [2003] *Chaos and Time-Series Analysis*, Oxford University Press, New York.

[40] Madan, R.N. [1993] Chua's Circuit: A Paradigm for Chaos, World Scientific series on nonlinear science, Singapore.

[41] Antoniou, A., [1969] "Realization of gyrators using operation amplifiers," *IEE Proc.* **116**(11) (19), pp. 1838-1850.

[42] Yamorik, V.N. & Demidenko, S.N. [1988] "Generation and Application of Pseudorandom Sequences for random testing," John Willy & Sons, New York.

[43] Jansri, A., Klomkarn, K. & Sooraksa, P. [2004] " Further investigation on trajectory of chaotic guiding signals for robotics systems," ***Proc***.Intl. Symp. on Communications and Information Technology, pp. 1166-1170.

[44] Menezes, A. J., Oorschot, P. V., & Vanstone, S.A. eds.[1997] *Handbook of Applied Cryptography*, CRC press, Boca Raton, FL.

[45] Neumann, J. V, [1963], ***Jon Von Neumann*** *Collected Works*, MacMillan.

[46] NIST. 1999 Federal Information Processing Standard Publication FIPS PUB 140-2: Security requirements for cryptographic modules.

Related Publications

1. **Klomkarn, K.**, Payakkawan, P., Sooraksa, P., "Generating hyper-chaotic attractor from Van der Pol system, Proc. of the 9th *International Symposium on Communications and Information Technology(ISCIT2009)*, InCheon Korea, pp.1492-1495, Sept. 2009.
2. **Klomkarn, K.** & Sooraksa, P., "Some Construction Chaotic attractor from Van der Pol System,"*Proc of the 3rd International Conference on Dynamics, Vibration and Control (ICDVC-2010)*, Hangzhou, China, May 2010.
3. Sooraksa, P. & **Klomkarn, K.**, ""No-CPU "Chaotic Robots: From Classroom to Commerce," *IEEE CAS magazine*, vol.10, pp.46-53, First Quarter 2010.
4. **Klomkarn, K., Sooraksa, P.**, & Chen, G., "New Construction of Mixed-mode Chaotic Circuits, " *International Journal of Bifurcation and Chaos* , Vol. 20, no.5 pp. 1485-1497, 2010.
5. **Klomkarn, K. & Sooraksa, P.**, "Simple Self instructional modules based chaotic oscillators: A few blocks generating many patterns," Accepted for Publication in International Journal of Bifurcation and Chaos.

Author Biography

Kitdakorn Klomkarn was born in Nan, Thailand, on July 19, 1963. He received B.Ind (computer technology) and M.Eng (electrical engineering) from King Mongkut's Institute of Technology Ladkrabang. He has served as faculty member of faculty of engineering since 1993. Mr. Klomkarn received RGJ-PhD scholarship from 2005-2008, the Thailand Research Fund research award in 2008. His main research interests are in chaos engineering and applications.